Control of endosomal Toll-like receptor (TLR) signaling by nanoparticles and applications in cancer therapy

Helen C. Chen

A dissertation

submitted in partial fulfillment of the

requirements for the degree of

Doctor of Philosophy

University of Washington

2014

Reading Committee:

Hong Shen, Chair

David Hockenbery

Samson Jenekhe

Chris Ramsborg

Program Authorized to Offer Degree:

Chemical Engineering

Table of Contents

Page

Acknowledgments i

Abstract ii

List of Abbreviations iv

Introduction

1. Pathogen recognition receptors 1
2. Toll-like receptors 3 and 9 recognize nucleic acids 1
3. Two distinct signaling pathways arise from TLRs
   - 3.1 The NF-κB pathway 1
   - 3.2 The IRF-7 pathway 2
   - 3.3 Potential role of controlled TLR activation in cancer 2
4. Specific Aims 3
5. References 4

Chapter 1: The effects of particle size on toll-like receptor 9-mediated cytokine profiles

1.1 Abstract 6
1.2 Introduction 6
1.3 Materials and Methods
- *1.3.1* Cell Culture 9
- *1.3.2* Preparation and characterization of ODN-coated PS particles (ODN-PLL-PS) 9
- *1.3.3* Quantification of the surface density of ODNs on ODN-PLL-PS particles 11
- *1.3.4* Regulation and measurement of endosomal pH 11
- *1.3.5* Stimulation of DCs with ODN-PLL-PS 12
- *1.3.6* Measurement of cytokine concentrations 12
- *1.3.7* Statistical analysis 13

1.4 Results and Discussion
- *1.4.1* Characterization of ODN-PLL-PS 13
- *1.4.2* Differential cytokine profiles induced by CpG ODNs 15
- *1.4.3* The effect of endosomal pH on cytokine profiles induced by CpG ODNs 17

1.5 Conclusion 22
1.6 References 22

Chapter 2: Selectively targeting the TLR9 – IRF7 signaling pathway by polymer blend particles

2.1 Abstract 27
2.2 Introduction 27
2.3 Materials and Methods
2.3.1 Cell culture 29
2.3.2 Reagents 29
2.3.3 Synthesis of pH-sensitive polymers 30
2.3.4 Fabrication of polymer blend particles 31
2.3.5 Characterization of blend particles 31
2.3.6 Quantification of the polymer composition and the loading of CpG 2216 in blend particles 32
2.3.7 Quantification of FITC-CpG 2216 released from particles at 37 °C at different pHs 33
33
2.3.8 Preparation and characterization of CpG 2216-adsorbed particles 33
2.3.9 Stimulation of cells by CpG 2216 34
2.3.10 Measurement of endosomal pH 35
2.3.11 Measurement of cytokine concentrations 35
2.3.12 Immunocytochemistry 36
2.3.13 Confocal microscopy and image analysis 37
2.3.14 Statistical analysis 37
2.4 Results and Discussion
2.4.1 Characterization of pH-sensitive copolymers 37
2.4.2 Composition, size, morphology, and surface charge of polymer blend particles 38
2.4.3 Cytokine profiles induced by CpG2216-containing polymer blend particles 42
2.4.4 Impaired translocation of NF-κB by Terpolymer-CpG 44
2.4.5 Mechanisms of selectively targeting the IRF-7 pathway by Terpolymer-CpG 45
2.5 Conclusion 50
2.6 References 50

Chapter 3: Characterization of breast cancer cell responsiveness to Terpolymer particles

3.1 Abstract 54
3.2 Introduction 54
3.3 Materials and Methods
3.3.1 Cell culture 61
3.3.2 Preparation and characterization of polymer blend particles 62
3.3.3 Quantification of polyIC loading in blend particles 62
3.3.4 Quantification of polyIC released from particles at 37°C at different pHs 63
3.3.5 MTT assay 63
3.3.6 Flow cytometry 64
3.3.7 Measurement of cytokine concentrations 65
3.3.8 In vitro scratch assay 66
3.3.9 Statistical analysis 66

3.4 Results and Discussion
3.4.1 Characterization of Ter-polyIC particles 66
3.4.2 Cytokine secretion profile induced by Ter-polyIC from mouse splenocytes 70
3.4.3 The cytotoxicity of Ter-polyIC is dependent on the type of triple negative breast cancer cell line 71
3.4.4 Ter-polyIC induces cell death of a subpopulation of BT-20 cells 76
3.4.5 The effect of polymer blend particles on the cytokine profiles of triple negative breast cancer cell lines 77
3.4.6 The effect of polymer blend particles on the *in vitro* migration of BT-20 cells 78
3.5 Conclusion 89
3.6 References 89

Supplemental Work

Supplemental 1. Supplemental information for Chapter 1 93
Supplemental 2. Supplemental information for Chapter 2 97
Supplemental 3. The rescue of IL-6 secretion following Ter-CpG 2216 treatment 98
Supplemental 4. Ter-CpG 1826 and Ter-CpG 2216 induce distinct cytokine secretion profiles 100
Supplemental 5. TLR9 signaling regulates the intracellular trafficking of nanoparticles 102
Supplemental 6. The effect of polymer blend particles on the cytokine profile of THP1 cells 109
Supplemental 7. The effect of polymer blend particles on MDA-MB-231 cells 111
Supplemental 8. The effect of polymer blend particles on purified BT-20 cell subpopulations 115
Supplemental 9. The effect of pH on the release of polyIC from Ter-polyIC 120
Supplemental 10. The method of analysis of BT-20 cells by flow cytometry 122
Supplemental 11. The method of analysis of hydrodynamic size measurements of polymer blend particles by dynamic light scattering 132
References 137

List of Figures

Chapter 1
Figure 1. Characterization of ODN-PLL-PS 15
Figure 2. The effect of particle size on the production of IL-6 and IFN-α 16
Figure 3. The change in the pH of endosomes by the addition of NH_4Cl 18
Figure 4. The effect of endosomal pH on the production of cytokines 19

Chapter 2
Figure 1. Chemical structure of PLGA, Terpolymer, Dipolymer 1:1 and Dipolymer 3:1 38
Figure 2. Size, surface charge, and morphology of polymer blend particles 41
Figure 3. Effect of the composition of pH-sensitive polymer on the cytokine secretions of cells 43

Figure 4. Effect of Terpolymer-CpG on the nuclear translocation of transcription factors 45
Figure 5. Mechanisms of selectively targeting IRF-7 pathway by Terpolymer-CpG particles 47

Chapter 3
Figure 1. Characterization of Ter-polyIC, Ter-adsorb polyIC high, Ter-adsorb polyIC low and Ter-GpC particles 68
Figure 2. SEM and TEM images of Ter-polyIC, Ter-adsorb polyIC and Ter-GpC particles 68
Figure 3. Size measurements of Ter-polyIC, Ter-adsorb polyIC and Ter-GpC particles by SEM images 69
Figure 4. Relative uptake levels of polymer blend particles by BT-20 cells 70
Figure 5. Cytokine secretion profile from mouse splenocytes induced by Ter-polyIC 72
Figure 6. Effect of Ter-polyIC on MDA-MB-231 and BT-20 cell proliferation 73
Figure 7. Dose-responsiveness of BT-20 cells to Ter-polyIC and soluble polyIC 74
Figure 8. Effect of adsorbed polyIC amount on BT-20 cell viability 75
Figure 9. Effect of polymer blend particles on the percentage of total cells that are live and dead 79
Figure 10. CD44 subpopulation analysis of live cells after treatment with polymer blend particles 80
Figure 11. CD44 subpopulation analysis of dead cells after treatment with polymer blend particles 81
Figure 12. Analysis of CD44 medium cell subpopulation viability after treatment with polymer blend particles 82
Figure 13. Analysis of CD44 high cell subpopulation viability after treatment with polymer blend particles 83
Figure 14. IL-6 secretion from BT-20 cells treated with polymer blend particles 84
Figure 15. Type I IFN secretion from BT-20 cells treated with polymer blend particles 85
Figure 16. Effect of polymer blend particles on cytokine secretion from MDA-MB- 231 cells 86
Figure 17. BT-20 cell uptake of polymer blend particles 87
Figure 18. Effect of polymer blend particles on the *in vitro* migration distance of BT-20 cells 88

Supplemental Work
Figure S1. Characterization of PLL-PS 93
Figure S2. Levels of IFN-α in response to CpG ODN 1826 93
Figure S3. Relative levels of cellular uptake of 2216-PLL-PS in the presence of NH_4Cl 94
Figure S4. Colocalization of microparticles with early endosomes 94
Figure S5. Confirmation of the composition of blend particles by 500 MHz ^1H NMR 97

Figure S6. Levels of IL-6 and IFN-α induced by Terpolymer-CpG particles that contain CpG 2216 that is not fluorescently tagged 98
Figure S7. The rescue of IL-6 secretion following Ter-CpG 2216 treatment of BC-1 cells 100
Figure S8. Ter-CpG 1826 and Ter-CpG 2216 induce distinct cytokine secretion profiles 101
Figure S9. Intracellular distributions of ODN-PLL-S relative to the microtubule-organizing center 106
Figure S10. CpG 2216-ODN-PLL-PS traffics to the perinuclear region within 30 min particle uptake 106
Figure S11. Differences in the mode of particle transport between 1826-PLL-PS and 2216-PLL-PS 107
Figure S12. The effect of the type of CpG on the mobility of nanoparticles 108
Figure S13. Effect of polymer blend particles on the cytokine secretion profile from THP1 cells 110
Figure S14. Standard curves used for the quantification of the type I IFN concentration in THP1 cell supernatants 111
Figure S15. Effect of Ter-CpG on MDA-MB-231 cell viability 112
Figure S16. Effect of Ter-CpG on MDA-MB-231 cell proliferation 113
Figure S17. IL-6 secretion from MDA-MB-231 cells treated with Ter-CpG 114
Figure S18. Dose-dependent IL-6 secretion from MDA-MB-231 cells treated with camptothecin 115
Figure S19. Effect of polyIC on the secretion of IL-6 from BT-20 cell subpopulations 117
Figure S20. Effect of IL-6 and type I IFN signaling on BT-20 cell subpopulations 118
Figure S21. Effect of the mode of presentation of polyIC by polymer blend particles on the viability of BT-20 cell subpopulations 120
Figure S22. Effect of pH on the release of polyIC from Ter-polyIC particles at 37°C 121
Figure S23. Flow cytometry plots of polymer blend particles stained with anti-CD44, AnnexinV, and 7-AAD 123
Figure S24. Flow cytometry plots of BT-20 cells pulsed with polymer blend particles and analyzed after 1 day 124
Figure S25. Flow cytometry plots of gated BT-20 cells pulsed with polymer blend particles and analyzed after 1 day 125
Figure S26. Flow cytometry histograms of gated BT-20 cells pulsed with polymer blend particles and analyzed after 1 day 126
Figure S27. Flow cytometry plots of live and dead BT-20 cells pulsed with Ter-GpC and analyzed after 1 day 128
Figure S28. Flow cytometry plots of live and dead BT-20 cells pulsed with Ter-polyIC and analyzed after 1 day 129
Figure S29. Flow cytometry plots of live and dead BT-20 cells incubated with type I IFN and analyzed after 1 day 130
Figure S30. Flow cytometry plots of live and dead BT-20 cells incubated with cell culture medium and analyzed after 1 day 131

Figure S31. Hydrodynamic size and surface charge measurements of Ter-adsorb polyIC low by dynamic light scattering 134
Figure S32. Hydrodynamic size and surface charge measurements of Ter-adsorb polyIC high by dynamic light scattering 136

List of Tables

Chapter 2
Table 1. The polymer compositions and CpG 2216 in blend particles 39

Chapter 3
Table 1. Type I IFN in anticancer treatment 55
Table 2. Constitutive TLR9 expression in various tumor cells and tumor tissues 58
Table 3. The polyIC loading in Ter-polyIC and Ter-adsorb polyIC 69

Acknowledgements

I would like to express my sincere gratitude to several people without whom I could not have completed this work.

First, I would like to thank Professor Hong Shen for giving me the opportunity to do my Ph.D. work in her lab. I thank her for her ideas and guidance which made this work possible.

I thank Dr. David Hockenbery, Professor Samson Jenekhe, Dr. Chris Ramsborg, Professor David Castner, and Professor Rachel Wong for their support, evaluation of my work, and feedback. I am grateful for the willingness of Dr. David Hockenbery to provide insight into my work and for helpful discussions regarding the breast cancer project.

Thanks to all of the members of the Shen Lab for their help and for creating a nice working atmosphere. Thanks to Melanie J. Coyne and Siri Machiraju for their commitment to the analyses of images for the breast cancer cell migration project. Thanks to Tim Sakanashi for performing DLS measurements for the particle aggregation project. Thanks to Xi Zhan for the synthesis of copolymers, for the fabrication of polymer blend particles, for acquiring SEM and TEM images, and for NMR analysis of polymer blend particles. Thanks to Dr. Bingbing Sun for acquiring the SEM images of polystyrene particles. Thanks to Prof. Hong Shen for phenotyping breast cancer cells, and examining the expression of TLRs of breast cancer cells. Thanks to Dr. Hai Nguyen for conducting cell sorting to purify breast cancer cells.

Finally, I want to express my sincere gratitude to my mom, dad, and brother for their unrelenting support and encouragement throughout my graduate studies.

University of Washington

Abstract

Control of endosomal Toll-like receptor (TLR) signaling by nanoparticles and applications in cancer therapy

Helen C. Chen

Chair of Supervisory Committee:
Professor Hong Shen
Chemical Engineering

Toll-like receptors (TLRs) play critical roles in the activation of innate and adaptive immune responses. TLRs 3 and 9 are expressed in endosomal and lysosomal compartments and recognize nucleic acids. The activation of TLRs 3 and 9 leads to two distinct signaling pathways resulting in the nuclear translocation of nuclear factor kappa B (NF-κB) and interferon regulatory factor 7 (IRF-7). The NF-κB and IRF-7 pathways induce pro-inflammatory cytokines (such as IL-6) and type I interferons (IFNs such as IFN-α), respectively. Pro-inflammatory cytokines are associated with tumorigenesis, whereas type I IFNs can induce anticancer effects.

In this work, the effects of biomaterial size and composition on the cytokine secretion profile of cells were studied. The effect of biomaterial size was evaluated by adsorbing TLR9 ligands onto micro- and sub-micro polystyrene particles. The cytokine profile was correlated with the pH of endosomes and lysosomes that internalized particles of different sizes were exposed to. The effect of biomaterial composition was evaluated by incorporating TLR3 and TLR9 ligands into polymer blend nanoparticles of precise polymer compositions. The polymer composition could be tuned to induce distinct cytokine profiles. Interestingly, the terpolymer blend was able to present TLR ligands in a manner that resulted in IFN-α induction only. Such control of TLR signaling provided the motivation for applications in breast cancer therapy.

The efficacy of terpolymer blend particles containing TLR ligands was assessed for triple negative breast cancer cell lines. The treatment efficacy was determined by effects on cell proliferation, cell death, cell migration, and cell expression of CD44, a marker for a metastastic phenotype. TLR9 ligands encapsulated in terpolymer particles were not an effective treatment for both MDA-MB-231 and BT-20 cell lines. TLR3 ligands encapsulated in terpolymer particles were the most effective treatment for BT-20 cells, but were ineffective for MDA-MB-231 cells. The treatment efficacy was correlated with the level of type I IFNs.

List of Abbreviations

7-AAD	7-aminoactinomycin D
AIBN	2-(dimethylamino)ethyl methacrylate, 2,2’-azobis(2-methylpropionitrile)
BMA	butyl methacrylate
CD24	cluster of differentiation 24
CD44	cluster of differentiation 44
CFSE	carboxyfluorescein succinimidyl ester
DAPI	4',6-diamidino-2-phenylindole
DCM	dichloromethane
DCs	dendritic cells
DLS	dynamic light scattering
DMAEMA	(dimethylamino)ethyl methacrylate
DMEM	Dulbecco's Modified Eagle Medium
DOTAP	1,2-dioleoyl-3-trimethylammonium-propane
DPBS	Dulbecco's Phosphate-Buffered Saline
dsRNA	double-stranded ribonucleic acid
EEA-1	early endosome antigen 1
ELISA	enzyme-linked immunosorbent assay
FACS	fluorescence-activated cell sorting
FBS	fetal bovine serum
FITC	fluorescein isothiocyanate
GM-CSF	granulocyte-macrophage colony-stimulating factor
gMFI	geometric mean fluorescent intensity
HEPES	4-(2-Hydroxyethyl)piperazine-1-ethanesulfonic acid
Hsp	heat shock protein
IFN	type I interferon
IFNAR	interferon-alpha/beta receptor
IHC	immunohistochemistry
IL-12	interleukin 12
IL-6	interleukin 6
IMDM	Iscove's Modified Dulbecco's Medium
IRF-7	interferon regulatory factor 7
LAMP-2	lysosomal associated membrane protein 2
LPS	lipopolysaccharide
mRNA	messenger ribonucleic acid
NF-κB	nuclear factor kappa-light-chain-enhancer of activated B cells
NK cells	natural killer cells
NMR	nuclear magnetic resonance
ODN	oligodeoxynucleotide

p65	transcription factor p65
PAA	2-propylacrylic acid
PAMP	pathogen associated molecular pattern
PARP	poly adenosine diphosphate-ribose polymerase
PDL	poly-D-lysine
PLGA	Poly(lactic-co-glycolic acid)
PLL	poly-L-lysine
polyIC	polyinosinic:polycytidylic acid
PRR	pathogen recognition receptor
PS	polystyrene
PVA	polyvinyl alcohol
RPMI medium	Roswell Park Memorial Institute medium
RT-PCR	real-time polymerase chain reaction
SEM	scanning electron microscopy
ssDNA	single-stranded deoxyribonucleic acid
TEM	transmission electron microscopy
THF	tetrahydrofuran
TLR	toll-like receptor
TNBC	triple negative breast cancer
TNF-α	tumor necrosis factor alpha
VSV-GFP	Vesicular Stomatitis Virus-green fluorescent protein
ZP	zeta potential

Introduction

1. Pathogen recognition receptors

Our body's immune system comprises the innate immune system and the adaptive immune system. The innate immune system relies on a defined set of pathogen recognition receptors to distinguish foreign agents from self. In contrast, our adaptive immune system acquires receptors during our lifetime. One of the largest families of innate immune receptors are the Toll-like receptors, which are transmembrane proteins situated on the plasma membrane and on endosomal and lysosomal membranes.

2. Toll-like receptors 3 and 9 recognize nucleic acids

Toll-like receptors 3 and 9 (TLR3, TLR9) play critical roles in the activation of innate and adaptive immune responses, and as mediators for cancer therapy. TLR3 recognizes double-stranded RNA (dsRNA), and polyIC is a synthetic form of dsRNA that is used to activate TLR3. TLR9 recognizes CpG motifs of single-stranded DNA. CpG oligonucleotides (ODNs) are single strands of ~ 20 nucleotides containing one or more immunostimulatory C-G dinucleotides. In resting cells, TLR3 and TLR9 reside in the endoplasmic reticulum. Upon stimulation by polyIC or CpG ODNs, respectively, TLR3 and TLR9 are recruited to endosomes where they bind to their ligand, resulting in TLR signaling [1]. The stimulation of TLR3 and TLR9 leads to two signaling pathways through NF-κB and IRF-7 activation and the induction of pro-inflammatory cytokines (such as interleukin-6, IL-6) and type I interferons (IFNs), respectively.

3. Two distinct signaling pathways arise from TLRs

3.1 The NF-κB pathway

NF-κB activation leads to the induction of pro-inflammatory cytokines which establish the initial stage of inflammation [2]. If inflammation persists, chronic inflammation ensues and

is linked to cancer and disease. NF-κB regulates the expression of proteins that promote cell proliferation and differentiation, and anti-apoptotic effects [3, 4]. The suppression of NF-κB is critical for the induction of apoptosis of tumor cells such as breast cancer cells [5], multiple myeloma cells [6, 7], T cell lymphoma [8], and prostate cancer cells [9].

3.2 The IRF-7 pathway

IRF-7 controls the other arm of TLR9 signaling and results in the induction of type I IFNs (IFN-α and IFN-β) and IFN-stimulated genes (ISGs) [2]. Recently, IRF-7 was shown to prevent the metastasis of breast cancer cells [10]. ISGs have been found to be downregulated in breast cancer patients, and type I IFN signaling was impaired in T cells and B cells of breast cancer, melanoma, and gastrointestinal cancer patients [11]. Type I IFNs were initially recognized for their antiviral activity. Over the past five decades, additional functions of type I IFNs have been discovered: type I IFNs enhance T cell, dendritic cell, and NK cell activation; promote cell differentiation; and induce apoptosis and cell cycle arrest [12, 13]. In particular, type I IFNs were recently discovered to be essential for the $CD8\alpha^+$ DC subset to activate antigen-specific $CD8^+$ T cells and prevent tumor growth [14, 15]. Type I IFNs are currently used as anticancer drugs for hairy-cell leukemia, malignant melanoma, and follicular lymphoma [16].

3.3 Potential role of controlled TLR activation in cancer

Given the pro-tumor and anti-tumor effects of NF-κB and IRF-7 activation, respectively, we hypothesize that the simultaneous inhibition of NF-κB and activation of IRF-7 would be a potent anticancer treatment. Currently, the systemic administration of type I IFNs poses disadvantages as a treatment. In order to minimize the inhibitory mechanisms of a negative feedback loop, intermittent dosing of type I IFN is necessary [17]. In addition, stabilized formulations of IFN-α that increase the cytokine half-life still require repeated dosing [17].

Inhibitors that suppress NF-κB signaling cascade events are effective at preventing tumor growth. However, instead of solely suppressing NF-κB activation, we propose to design biomaterials that prevent NF-κB activation while promoting IRF-7 activation through TLR signaling. In this work, we seek to control TLR activation and subsequent immune responses for applications in cancer therapy.

4. Specific Aims

Chapter 1 - Determine the effects of particle size on toll-like receptor 9-mediated cytokine profiles:

The size of biomaterials affects the level of retention in tissues [18, 19], the efficiency of cellular uptake [20-22], and their intracellular trafficking [23-25]. Given the critical role of the intracellular location of TLR9 ligands which dictates the subsequent induction of signaling pathways [26-28], we hypothesized that the size of biomaterials could affect the TLR9-mediated cytokine profiles. Model submicro- and micro- PS particles as TLR9-ligand (CpG ODN) carriers were used in this study. The cytokine production was correlated with the endosomal pH environment that particles of different sizes were exposed to. Our findings suggest that the size of biomaterials and the ability to regulate endosomal pH have a profound effect on the TLR9-mediated production of cytokines that regulate innate and adaptive immune responses.

Chapter 2 - Control toll-like receptor 9 signaling by using polymer-blend nanoparticles:

Given the distinct functions of the two arms of TLR9 signaling, we sought to use biomaterials to control the activation of TLR9 signaling pathways. We incorporated type A CpG ODN into polymer-blend nanoparticles of precise compositions and evaluated their effects on the cytokine profile of cells. Of the various copolymer compositions tested, the terpolymer was able

to present CpG to TLR9 without activating the NF-κB pathway, but only the IRF-7 pathway. Particle characterization at physiologically relevant conditions indicated that CpGs were retained inside particles. This suggests that polymer-blend particles mediated the selective activation of IRF-7 through TLR9.

Chapter 3 - Characterize breast cancer cell responsiveness to polymer blend nanoparticles:

The selective activation of IRF-7 is a unique property of polymer blend nanoparticles that we seek to exploit for breast cancer immunotherapy. We hypothesize that polymer-blend particles could selectively induce type I IFN secretion from human breast cancer cell lines or patient tissue, and lead to type I IFN-mediated apoptosis. In this study, we investigated the applicability of polymer blend particles for breast cancer immunotherapy.

5. References

[1] Latz E, Schoenemeyer A, Visintin A, Fitzgerald KA, Monks BG, Knetter CF, et al. TLR9 signals after translocating from the ER to CpG DNA in the lysosome. Nat Immunol. 2004;5:190-8.

[2] Akira S, Uematsu S, Takeuchi O. Pathogen recognition and innate immunity. Cell. 2006;124:783-801.

[3] Karin M, Greten FR. NF kappa B: Linking inflammation and immunity to cancer development and progression. Nat Rev Immunol. 2005;5:749-59.

[4] Dolcet X, Llobet D, Pallares J, Matias-Guiu X. NF-kB in development and progression of human cancer. Virchows Arch. 2005;446:475-82.

[5] Biswas DK, Shi Q, Baily S, Strickland I, Ghosh S, Pardee AB, et al. NF-KB activation in human breast cancer specimens and its role in cell proliferation and apoptosis. P Natl Acad Sci USA. 2004;101:10137-42.

[6] Bharti AC, Shishodia S, Reuben JM, Weber D, Alexanian R, Raj-Vadhan S, et al. Nuclear factor-kappa B and STAT3 are constitutively active in CD138(+) cells derived from multiple myeloma patients, and suppression of these transcription factors leads to apoptosis. Blood. 2004;103:3175-84.

[7] Hideshima T, Chauhan D, Richardson P, Mitsiades C, Mitsiades N, Hayashi T, et al. NF-kappa B as a therapeutic target in multiple myeloma. J Biol Chem. 2002;277:16639-47.

[8] Giri DK, Aggarwal BB. Constitutive activation of NF-kappa B causes resistance to apoptosis in human cutaneous T cell lymphoma HuT-78 cells - Autocrine role of tumor necrosis factor and reactive oxygen intermediates. J Biol Chem. 1998;273:14008-14.

[9] Rabi T, Shukla S, Gupta S. Betulinic Acid Suppresses Constitutive and TNF alpha-Induced NF-kappa B Activation and Induces Apoptosis in Human Prostate Carcinoma PC-3 Cells. Mol Carcinogen. 2008;47:964-73.

[10] Bidwell BN, Slaney CY, Withana NP, Forster S, Cao Y, Loi S, et al. Silencing of Irf7 pathways in breast cancer cells promotes bone metastasis through immune escape. Nat Med. 2012;18:1224-+.
[11] Critchley-Thorne RJ, Simons DL, Yan N, Miyahira AK, Dirbas FM, Johnson DL, et al. Impaired interferon signaling is a common immune defect in human cancer. P Natl Acad Sci USA. 2009;106:9010-5.
[12] Stetson DB, Medzhitov R. Type I interferons in host defense. Immunity. 2006;25:373-81.
[13] Chawla-Sarkar M, Lindner DJ, Liu YF, Williams B, Sen GC, Silverman RH, et al. Apoptosis and interferons: Role of interferon-stimulated genes as mediators of apoptosis. Apoptosis. 2003;8:237-49.
[14] Fuertes MB, Kacha AK, Kline J, Woo SR, Kranz DM, Murphy KM, et al. Host type I IFN signals are required for antitumor CD8(+) T cell responses through CD8 alpha(+) dendritic cells. J Exp Med. 2011;208:2005-16.
[15] Diamond MS, Kinder M, Matsushita H, Mashayekhi M, Dunn GP, Archambault JM, et al. Type I interferon is selectively required by dendritic cells for immune rejection of tumors. J Exp Med. 2011;208:1989-2003.
[16] Friedman RM. Clinical uses of interferons. Brit J Clin Pharmaco. 2008;65:158-62.
[17] Hervas-Stubbs S, Perez-Gracia JL, Rouzaut A, Sanmamed MF, Le Bon A, Melero I. Direct Effects of Type I Interferons on Cells of the Immune System. Clin Cancer Res. 2011;17:2619-27.
[18] De Jong WH, Hagens WI, Krystek P, Burger MC, Sips A, Geertsma RE. Particle size-dependent organ distribution of gold nanoparticles after intravenous administration. Biomaterials. 2008;29:1912-9.
[19] Tabata Y, Inoue Y, Ikada Y. Size effect on systemic and mucosal immune responses induced by oral administration of biodegradable microspheres. Vaccine. 1996;14:1677-85.
[20] Tabata Y, Ikada Y. Effect of the size and surface charge of polymer microspheres on their phagocytosis by macrophage. Biomaterials. 1988;9:356-62.
[21] Chono S, Tanino T, Seki T, Morimoto K. Influence of particle size on drug delivery to rat alveolar macrophages following pulmonary administration of ciprofloxacin incorporated into liposomes. J Drug Targeting. 2006;14:557-66.
[22] Champion JA, Walker A, Mitragotri S. Role of particle size in phagocytosis of polymeric microspheres. Pharm Res. 2008;25:1815-21.
[23] Tran KK, Shen H. The role of phagosomal pH on the size-dependent efficiency of cross-presentation by dendritic cells. Biomaterials. 2009;30:1356-62.
[24] Brewer JM, Pollock KGJ, Tetley L, Russell DG. Vesicle size influences the trafficking, processing, and presentation of antigens in lipid vesicles. J Immunol. 2004;173:6143-50.
[25] Rejman J, Oberle V, Zuhorn IS, Hoekstra D. Size-dependent internalization of particles via the pathways of clathrin-and caveolae-mediated endocytosis. Biochem J. 2004;377:159-69.
[26] Okuya K, Tamura Y, Saito K, Kutomi G, Torigoe T, Hirata K, et al. Spatiotemporal Regulation of Heat Shock Protein 90-Chaperoned Self-DNA and CpG-Oligodeoxynucleotide for Type I IFN Induction via Targeting to Static Early Endosome. J Immunol. 2010;184:7092-9.
[27] Honda K, Ohba Y, Yanai H, Negishi H, Mizutani T, Takaoka A, et al. Spatiotemporal regulation of MyD88-IRF-7 signalling for robust type-I interferon induction. Nature. 2005;434:1035-40.
[28] Sasai M, Linehan MM, Iwasaki A. Bifurcation of Toll-Like Receptor 9 Signaling by Adaptor Protein 3. Science. 2010;329:1530-4.

Chapter 1: Effects of particle size on toll-like receptor 9-mediated cytokine profiles

1.1 Abstract

Biomaterials interface with toll-like receptor (TLR) 9-mediated innate immunity in a wide range of medical applications, such as tissue implants and drug delivery systems. The stimulation of TLR9 can lead to two different signaling pathways, resulting in the generation of pro-inflammatory cytokines (i.e. IL-6) and/or type I interferons (IFNs, i.e. IFN-α). These two categories of cytokines differentially influence both innate and adaptive immunity. Although particle size is known to be a critical parameter of biomaterials, its role in TLR9-mediated cytokine profiles is not clear. Here, we examined how the size of biomaterials impacted cytokine profiles by using polystyrene particles of defined sizes as model carriers for TLR9 agonists (CpG oligonucleotides (CpG ODNs)). CpG ODNs bound to nano- to submicro- particles stimulated the production of both IL-6 and IFN-α, while those bound to micro particles resulted in IL-6 secretions only. The differential TLR9-mediated cytokine profiles were attributed to the pH of endosomes that particles trafficked to. The magnitude of IFN-α production was highly sensitive to the change in endosomal pH in comparison to that of IL-6. Our results define two critical design variables, size and the ability to modulate endosomal pH, for the engineering of biomaterials that potentially interface with TLR9-mediated innate immunity. The fine control of these two variables will allow us to fully exploit the beneficial facets of TLR9-mediated innate immunity while minimizing undesirable side effects.

1.2 Introduction

Toll-like receptors (TLRs) have been well recognized for their pivotal role in the detection of pathogen associated molecular patterns (PAMPs). Twelve TLRs, each detecting a distinct set of PAMPs, have been identified in mammals [1]. TLR9 was first identified as a

sensor for bacterial DNA [2], which contains unmethylated CpG motifs. Subsequently, a broad range of natural TLR9 ligands has been identified, including DNA derived from dead cells [3, 4], fungi [5, 6], viruses [7-9], and chromatin-IgG complexes [10, 11]. A recent study has suggested that TLR9 can detect any single stranded DNA [12]. Since its initial discovery, TLR9 has become one of the central targets for mediating immune responses. Many different types of synthetic TLR9 ligands, CpG motif-containing oligonucleotides (CpG ODNs), have been characterized and utilized as adjuvants for vaccines [13-16] and microbicides [17-20] against pathogen infections.

The role of TLR9 in the design of biomaterials for medical applications is implicated in three main areas: (1) particulate systems that deliver TLR9 ligands for vaccination or microbicidal activities [21-26]; (2) non-viral DNA delivery systems, which can control the interaction of DNA with TLR9 and thus minimize their immunogenicity for their application in gene therapy [27-31]; (3) tissue implants, which release degraded or eroded biomaterial fragments. These fragments are potentially deposited with DNA derived from bacteria or dead cells and endocytosed by phagocytic cells (such as macrophages). As a result, the endocytosed DNA can trigger the TLR9-based innate immune system and lead to the failure of tissue implants [32-34].

TLR9 is situated in the endoplasmic reticulum (ER) and recruited to endosomal/lysosomal compartments upon the endocytosis of pathogens or particulates [35]. The stimulation of TLR9 can lead to two distinct signaling pathways in which two transcription factors, NF-κB and IRF-7, are translocated into the nucleus, resulting in the generation of proinflammatory cytokines (such as IL-6 and IL-12) and/or type I interferons (IFNs) (such as IFN-α), respectively [1]. These two types of cytokines play independent roles in the induction

and maintenance of innate and adaptive immune responses. For example, IL-6 is a key mediator of the acute phase response [36]. IL-6 is critical in the proliferation, differentiation and survival of B cells, and $CD4^+$ T cell differentiation to Th2 cells [37]. Type I IFNs, such as IFN-α, inhibit viral replication and induce apoptosis to clear infected cells. IFN-α promotes the proliferation and function of $CD8^+$ T cells, and maintains $CD4^+$ Th1/Th2 cell populations. IFN-α plays a key role in the pathogenesis of the autoimmune disease, systemic lupus erythematosus (SLE), as well [38]. Additionally, proinflammatory cytokines and type I IFNs play differential roles in bone tissue engineering. IL-6 promotes osteoclast formation [39], whereas type I IFNs, such as IFN-α and IFN-β, inhibit osteoclast differentiation [40]. Due to the functional diversity of proinflammatory cytokines and type I IFNs, the ability to control the TLR9-mediated signaling pathways is essential for the design of biomaterials that interface with TLR9-based innate immunity.

The size of biomaterials is considered to be critical for the three aforementioned medical applications because it affects the level of retention in tissues [41, 42] and the efficiency of cellular uptake [43-45]. Others and we have demonstrated that the size of biomaterials also affects their intracellular trafficking [46-48]. Given the critical role of the intracellular location of TLR9 ligands which dictates the subsequent induction of signaling pathways [49-51], we hypothesized that the size of biomaterials could affect the TLR9-mediated cytokine profiles. The cytokine profiles in turn would impact the immunogenicity of biomaterials and lead to either beneficial or detrimental effects depending on the clinical applications of the designed biomaterials.

To test this hypothesis, in this study, we used polystyrene particles of defined sizes as model carriers for CpG ODNs to investigate the effect of particle size on the cytokine profiles mediated through the TLR9 signaling pathway and possible mechanisms involved.

1.3 Materials and Methods

1.3.1 Cell culture

A dendritic cell line, BC-1 (a gift from Dr. Yoshiki Yanagawa), was maintained in Iscove's Modified Dulbecco's Medium (IMDM) supplemented with 20% NIH-3T3 supernatant, 4 mM L-glutamine, 50 μM 2-mercaptoethanol, 5% granulocyte-macrophage colony-stimulating factor (GM-CSF)–containing supernatants, 100 units/ml penicillin and 100 μg/ml streptomycin. The fibroblast cell line, NIH-3T3, was maintained in IMDM supplemented with 10% fetal bovine serum (FBS), 100 units/ml penicillin and 100 μg/ml streptomycin. Cells were maintained at 37 °C under an atmosphere with 5% CO_2. 5% GM-CSF-containing supernatants were obtained from GM-CSF conditioned medium from the GM-CSF-secreting mouse cell line J558L.

1.3.2 Preparation and characterization of ODN-coated PS particles (ODN-PLL-PS)

Fluorescent polystyrene (PS) particles (Polysciences, Inc., Warrington, PA) of different sizes, 100 nm, 500 nm, and 3 μm in diameter, were used as model CpG ODN carriers. The particles were first coated with poly-L-lysine (PLL; Sigma-Aldrich, Inc., Saint Louis, MO; MW = 30,000-70,000 g/mol), a cationic polymer, to facilitate the adsorption of ODNs onto particles. PLL-coated particles are designated as PLL-PS. For 100 nm particles, 250 μl of PS (2.8×10^{12} particles per ml in 10 mM NaCl) was added drop-wise to an equal volume of PLL (0.8 mg/ml in 10 mM NaCl) under constant vortexing. For 500 nm and 3 μm particles, 1 ml of PS (2×10^{10} 500 nm particles per ml, 5×10^{8} 3 μm particles per ml) was added drop-wise to 1 ml of PLL (0.15 mg/ml (500 nm), 0.25 mg/ml (3 μm)). The final reaction volume was 500 μl for 100 nm

particles, and 2 ml for 500 nm and 3 μm particles. The adsorption was conducted for 1 h at room temperature (RT) and the reaction vessel was vortexed every 15 min. PLL-PS was washed three times in 10 mM NaCl by centrifugation at 4 °C, 8000 rcf for 2 h, 300 rcf for 1 h, and 25 rcf for 30 min for 100 nm, 500 nm, and 3 μm particles, respectively. 60% of 100 and 500 nm particles were recovered, and 100% of 3 μm particles were recovered. The duration and centrifuge speed were optimized to obtain mono-dispersed particles. CpG ODNs 1826 and 2216 (TriLink BioTechnologies, San Diego, CA) were attached onto PLL-PS by using the same procedures and reaction volumes as used for the coating of PLL onto particles. The final reaction mixtures contained 4×10^{11} particles per ml and 86 μg/ml ODN-1826, 4.5×10^{9} particles per ml and 40 μg/ml ODN-1826, and 1×10^{8} particles per ml and 33 μg/ml ODN-1826 for 100 nm, 500 nm, and 3 μm particles, respectively. The attachment of ODN 2216 onto PLL-PS was similar to that of ODN 1826. ODN-coated particles (ODN-PLL-PS are denoted as 1826-PLL-PS or 2216-PLL-PS, depending on the type of CpG ODN) were washed in the same manner as stated above. All of the washes were collected for further analysis of non-bound ODNs. The sequences of ODNs 1826 and 2216 were: 5'tcc atg acg ttc ctg acg tT3' and 5'ggG GGA CGA TCG TCg ggg gG3', respectively. Lowercase letters denote a phosphorothioate backone, and uppercase letters denote a phosphodiester backbone.

A Zetasizer Nano ZS (Malvern Instruments, Westborough, MA) was used to characterize the size distribution and zeta potential of the particles. 100 nm, 500 nm, and 3 μm particles were prepared at 3×10^{10}, 5×10^{7}, and 4×10^{6} particles per ml, respectively, in 10 mM NaCl with a pH of 5.9. Scanning electron microscopy (SEM) was used to confirm the particle size. SEM samples of particles were prepared in Milli-Q water, dried, sputter-coated with 12 nm of platinum using a

SPI Sputter Coater (Structure Probe, Inc., West Chester, PA), and analyzed using a JEOL 7000 SEM with a beam voltage of 10.0 kV (Electron Microscopy Center, University of Washington).

1.3.3 Quantification of the surface density of ODNs on ODN-PLL-PS particles

The surface density of ODNs was determined by quantifying both the total amount of ODNs adsorbed and the number of fluorescent particles. The OliGreen Assay Kit for ssDNA (Invitrogen, Frederick, MD) was used to measure non-bound ODNs in the adsorption reaction solutions and washes for the indirect determination of the amount of ODNs adsorbed onto particles. The number of 100 and 500 nm particles was quantified by fluorescence spectrometry. For 100 nm particles, the particles were suspended in 10 mM NaCl and the fluorescent intensity of the particle suspension was directly measured. For 500 nm particles, particles were dried under a stream of air, dried for an additional 4 h at RT, and then dissolved in chloroform overnight. The fluorescent intensity of dissolved particles in chloroform was subsequently determined. 500 nm articles were quantified by this method to minimize the effect of quenched fluorescence. For both sizes of particles, a series of standards with a known number of particles were used to construct standard curves. 3 μm particles were directly counted by a hemocytometer.

1.3.4 Regulation and measurement of endosomal pH

The pH of endosomes was controlled by exposing DCs to medium containing a weak acid, NH_4Cl [52]. The endosomal pH was measured by using a fluorescence ratiometric method that has been previously established [46]. Briefly, 100 nm amine-functionalized polystyrene particles (Polysciences, Inc., Warrington, PA) were reacted with pH-sensitive fluorescein isothiocyanate (FITC; Sigma-Aldrich, Inc., Saint Louis, MO), and pH-insensitive Alexa Fluor 647 carboxylic acid, succinimidyl ester (Invitrogen, Frederick, MD) for 4 h at RT in 0.1 M

sodium carbonate buffer (pH = 8.3). The conjugation reaction was quenched with the addition of NH_4Cl, and particles were washed three times in phosphate buffered saline (PBS, pH = 7.4). To ensure the equivalent uptake of particles, DCs were seeded in a 6-well plate at a density of 3×10^6 cells per well. DCs were pulsed with particles for 6 h. Afterwards, cells were harvested and aliquoted at 2×10^5 cells per aliquot. One set of aliquots was incubated in different concentrations of NH_4Cl in IMDM supplemented with 0.5% FBS for 1 h at 37 °C. The other set, used for constructing a standard curve, was fixed with 4% paraformaldehyde (PFA) for 20 min at RT, permeabilized with 0.1% Triton X-100 for 2 min at RT, and incubated in 0.1 M citrate buffer solutions of known pH values for 1 h at RT. Citrate buffer solutions were prepared in Dulbecco's phosphate buffered saline (DPBS). Cell suspensions were analyzed using a FACsCanto (Cell Analysis Facility, University of Washington). The geometric mean fluorescent intensity (gMFI) of cells was determined by FlowJo (Treestar, Inc., Ashland, OR). The ratio of gMFI of FITC to that of Alexa Fluor 647 was compared to the standard curve constructed in the citrate buffers with known pH values to obtain the endosomal pH of each sample.

1.3.5 Stimulation of DCs with ODN-PLL-PS

DCs were seeded at a density of 2.5×10^5 cells per well in a 24-well plate. Soluble ODNs (0.005 mg/ml), 1826- and 2216-PLL-PS (100 nm, 500 nm, 3 μm) were added to cells in 500 μl medium in the absence or presence of designated concentrations of NH_4Cl. After 24 h of incubation at 37 °C, cell supernatants were collected and stored at -20 °C until further analysis.

1.3.6 Measurement of cytokine concentrations

Cell supernatants were analyzed by enzyme-linked immunosorbent assay (ELISA) for the quantification of IL-6 and IFN-α. The procedures for the ELISA for IL-6 were adapted from the

manufacturer's protocol (eBiosciences, San Diego, CA). The procedures for IFN-α were described previously [8, 53].

1.3.7 Statistical analysis

All experiments were repeated two to three times. The one-tailed and unpaired Student's *t* test was used to analyze the differences between experimental groups as specified. A value of $p < 0.05$ was considered to be statistically significant.

1.4 Results and Discussion

1.4.1 Characterization of ODN-PLL-PS particles

To examine the effect of particle size on the TLR9-mediated cytokine production, it was critical that ODN-PLL-PS maintained mono-dispersity and a defined size. Commercially available PS particles of defined sizes (Polydispersity Index (PDI) = 0.037 ± 0.032, 0.242 ± 0.010, 0.234 ± 0.038, for 100 nm, 500 nm, and 3 μm particles, respectively) were chosen as model ODN carriers. Because PS particles bear a negative surface charge, a cationic polymer was first adsorbed onto the surface of the particles to enhance the electrostatic adsorption of ODN onto particles. Several cationic polymers, such as poly(ethylenimine), chitosan, poly(2-dimethyl-amino)ethyl methacrylate (pDMAEMA), or poly-L-lysine (PLL), have been used to facilitate the attachment of DNA onto the carrier [54, 55]. PLL was used in this study because PLL induced minimal escape of particles from endosomal compartments and did not affect the endosomal pH [56]. PLL concentrations were optimized in order to achieve mono-dispersed particles with the maximal coverage of PLL (Figure S1). The PLL coating shifted the surface charge of the particles from a negative to a positive zeta potential. At the maximal coverage of PLL, the zeta potential was 45, 65, and 43 mV for 100 nm, 500 nm, and 3μm particles, respectively.

Mono-dispersed PLL-PS was subsequently complexed with ODNs to yield ODN-PLL-PS. The negatively charged phosphate groups of the ODN backbone were expected to interact with the amine group side chain of lysine and result in ODN adsorption onto PS particles [57]. The size and zeta potential of 100 nm 1826-PLL-PS at different solution concentrations of CpG ODNs are shown in Figure 1. At the lowest ODN concentration examined, 0.005 mg/ml, particles tended to aggregate; the measured particle diameter and surface charge was approximately 300 nm and -10.6 mV. At the highest ODN concentration examined, 0.05 mg/ml, electrostatic stability was achieved and aggregation was minimal; the measured diameter and zeta potential was 129 nm and -19.2 mV. 500 nm and 3 μm 1826-PLL-PS exhibited a similar trend. At the optimized ODN concentrations, as stated in the Materials and Methods section, 500 nm and 3 μm ODN-PLL-PS had a surface charge of approximately -32 and -39 mV, respectively, and measured diameters of 433 nm and 3.5 μm. The measured diameter of 500 nm ODN-PLL-PS was less than 500 nm by DLS, and 500 nm PLL-PS was approximately 500 nm. Therefore, the polyelectrolyte coating may have affected the size measurement by DLS. The type of CpG ODN (1826 or 2216) did not have a significant effect on the size and zeta potential of ODN-PLL-PS (data not shown). Optimized conditions were used to prepare mono-disperse particles of uniform sizes for all experiments.

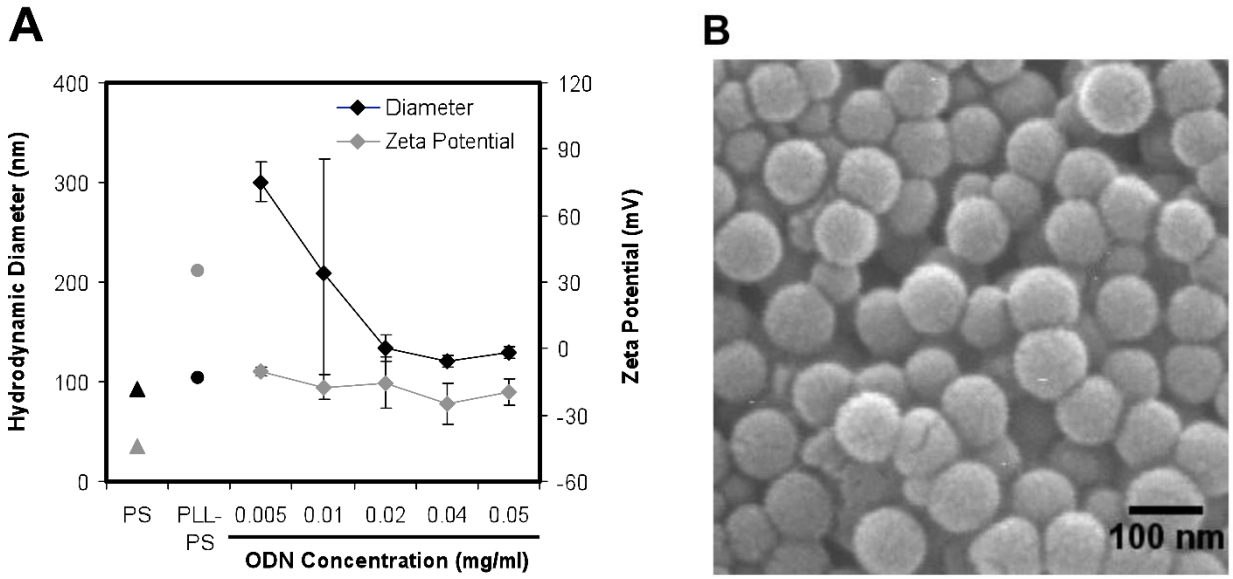

Figure 1. Characterization of ODN-PLL-PS. (A) Characterization of the size and zeta potential of 100 nm 1826-PLL-PS. (B) A SEM image of 100 nm CpG-PLL-PS.

1.4.2 Differential cytokine profiles induced by CpG ODNs

Two different classes of CpG ODNs, B (i.e. CpG ODN 1826) and A (i.e. CpG ODN 2216) were adsorbed onto particles of different sizes. While both ODN types induce cytokines through the stimulation of TLR9, type B is particularly effective at inducing proinflammatory cytokines, such as IL-6, but not type I IFNs [50, 58], and type A is known to induce both proinflammatory cytokines and type I IFNs, such as IFN-α [50, 59]. For CpG ODN 1826, regardless of the size of particles, only IL-6 but not IFN-α was induced (Figure 2 and Figure S2), which was consistent with what was observed with soluble CpG ODN 1826.

For CpG ODN 2216, both IL-6 and IFN-α were detected when ODNs were bound to 100 and 500 nm particles, which was again consistent with what was observed with soluble ODNs (Figure 2 D, E, G, H). Surprisingly, when CpG ODN 2216 was bound to 3 μm particles, IFN-α was completely diminished within the wide range of the concentrations of ODNs tested (Figure 2I), while IL-6 secretions remained at a significantly high level (Figure 2F). We note that we did

not attempt to compare the efficiencies of stimulation of TLR9 by the three different sizes of particles because it is challenging to deliver equivalent amounts of ODNs due to the large difference in the surface area among the three particle sizes. Regardless of this issue, we have clearly demonstrated that ODNs bound to sub-micro and micro particles yield distinct cytokine profiles.

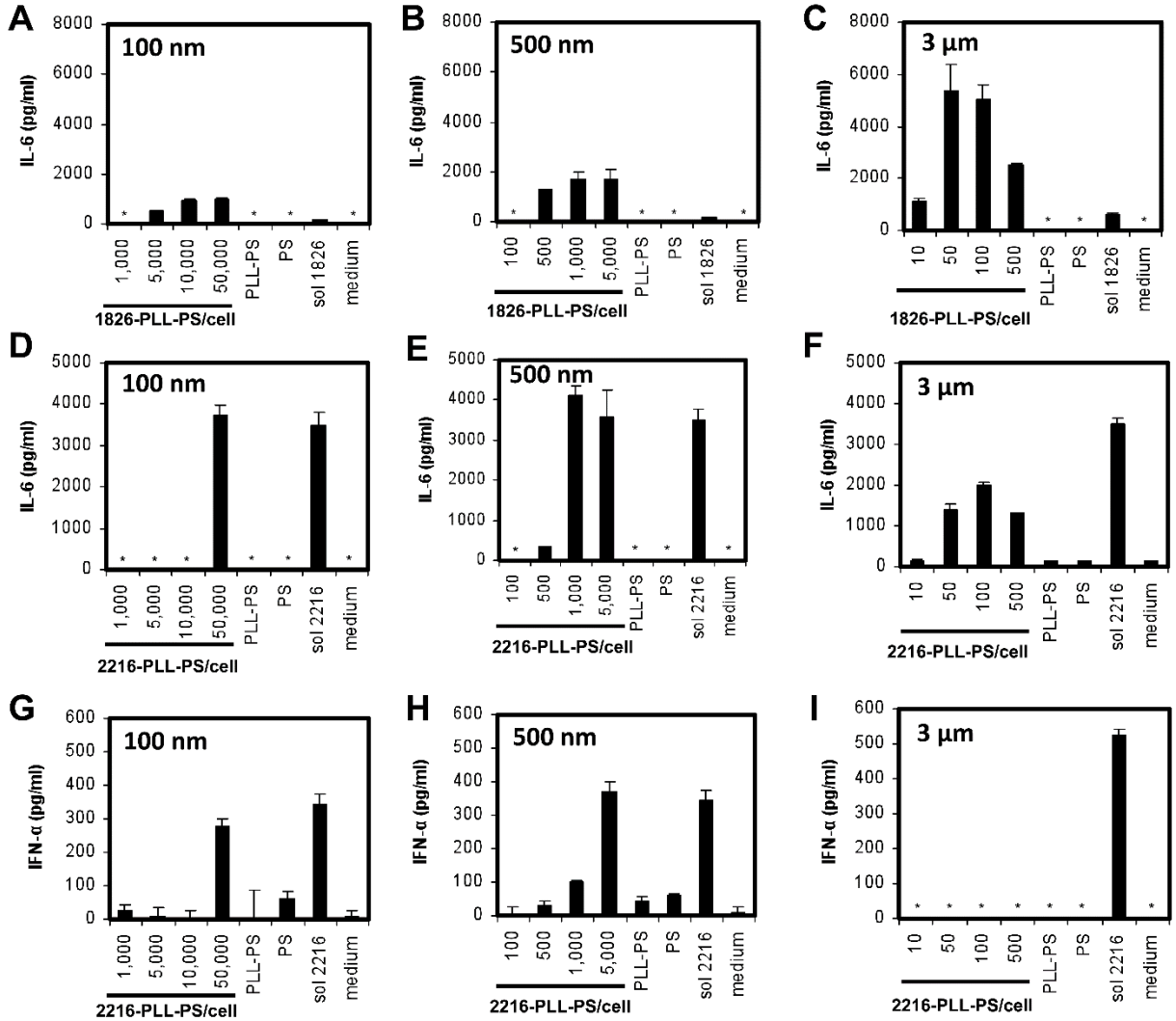

Figure 2. The effect of particle size on the production of IL-6 and IFN-α. BC-1 cells were stimulated by 100 nm, 500 nm, and 3 µm (A-C) 1826- and (D-I) 2216-PLL-PS. PLL-PS and PS served as negative controls and were used at the highest particle-to-cell ratio of the corresponding particle size. Soluble ODNs (sol 1826 or sol 2216) at 0.005 mg/ml served as a positive control. The supernatants of cells were collected after 24 h and analyzed by ELISA for the (A-F) IL-6 and (G-I) IFN-α concentrations. The symbol * indicates that no cytokine secretions were detected.

1.4.3 The effect of endosomal pH on cytokine profiles induced by CpG ODNs

Previous studies have suggested that pH plays a critical role in TLR9-mediated signaling. Both the recruitment of TLR9 into endosomal compartments and the interactions between TLR9 and its ligands require the acidification of the endosomes [35, 60]. Cells treated with inhibitors of acidification of endosomes, such as chloroquine or bafilomycin, exhibit impaired TLR9 stimulation [8, 60, 61]. We have demonstrated that the initial pH of endosomal compartments where 3 μm particles reside is 6.0. After 30 min, it increased to 7 and remained at 7. In contrast, submicron particles reside in endosomal compartments of pH 5.0 to 6.0 [46]. We hypothesized that the pH of endosomal compartments might affect the cytokine profiles induced by CpG ODN 2216. We tested this hypothesis by exposing both soluble CpG ODN 2216 and 100 nm 2216-PLL-PS to a broad range of endosomal pH environments.

The addition of NH_4Cl to the cell culture medium can inhibit endosomal acidification due to the rapid transport of NH_3 across the endosomal membranes and the low permeability of NH_4^+ [52, 62]. We first confirmed the change in pH of endosomal compartments while cells were exposed to different concentrations of NH_4Cl. As shown in Figure 3, the pH of endosomal compartments increased by 1.2 while the NH_4Cl concentration increased from 0 to 16 mM. The change in endosomal pH of DCs was consistent with a previous report on the change in endosomal pH of mouse peritoneal macrophages, although only 0.16 mM NH_4Cl was needed to increase the pH by 1.6 in macrophages [62]. This discrepancy may be because the regulation of pH by NH_4Cl is cell-type dependent. By varying the concentration of NH_4Cl, we were able to obtain a distribution of pH environments that spanned from 5.21 to 6.38 in DCs.

We then studied the effect of the endosomal pH environment on the production of cytokines. A gradual increase in endosomal pH (Figure 3) corresponded to a gradual decline in

IFN-α production by both soluble ODN 2216 and 2216-PLL-PS (Figure 4A). For 2216-PLL-PS, the production of IFN-α reduced by 80% when the pH increased from 5.21 to 5.82. The production of IL-6, however, remained constant (Figure 4B). At pH = 6.38, the levels of both IL-6 and IFN-α were diminished. Subsequently, we tested whether the cellular uptake of 2216-PLL-PS was affected by the presence of NH_4Cl. The addition of NH_4Cl slightly reduced the cellular uptake at concentrations up to 16 mM, which resulted in the endosomal pH of 6.38. However, there was not a significant difference in the level of cellular uptake at lower NH_4Cl concentrations, except at 16 mM (Figure S3). At pH = 6.38, the cellular uptake of 2216-PLL-PS decreased (Figure S3), which could contribute to the reduction in the level of both IL-6 and IFN-α. In addition, the recruitment of TLR9 to endosomes at pH = 6.38 may be impaired as suggested previously [35]. Our results demonstrate that the endosomal pH affected the TLR9-mediated cytokine profiles. Therefore, the distinct cytokine profiles exhibited by micro- and submicro-particles can be attributed to the endosomal pH they are exposed to.

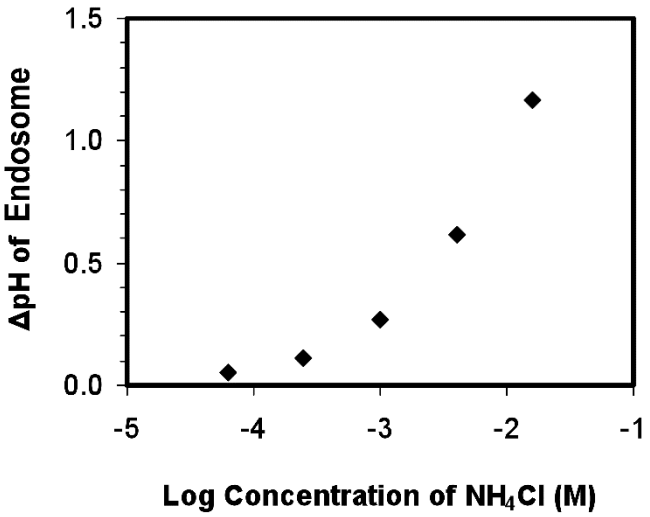

Figure 3. The change in the pH of endosomes by the addition of NH_4Cl. Concentrations of NH_4Cl (0.063, 0.25, 1, 4, 16 mM) are presented as Log_{10} of molar concentrations. The change in endosomal pH was calculated relative to the unmodified endosomal pH, which was 5.21.

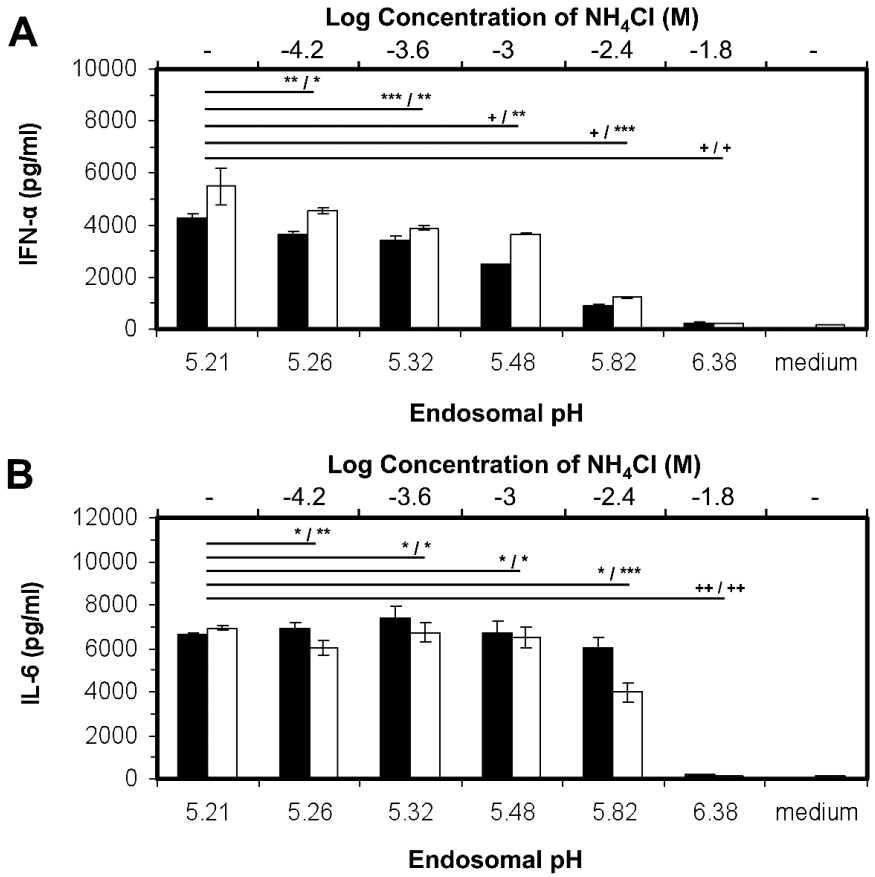

Figure 4. The effect of endosomal pH on the production of cytokines. (■) 100 nm 2216-PLL-PS at 100,000 particles per cell, and (□) soluble ODN 2216 at 0.005 mg/ml, were added to BC-1 cells in the presence or absence of NH_4Cl. The cell supernatants were collected after 24 h and analyzed by ELISA for the (A) IL-6 and (B) IFN-α concentrations. The top and bottom x axes represent the Log_{10} of the molar concentration of NH_4Cl and the corresponding endosomal pH values, respectively. The symbols *, **, ***, +, and ++ indicate the level of the statistical significance of cytokine production concentrations: $1.0 > p > 0.1$, $0.1 > p > 0.05$, $0.05 > p > 0.01$, $0.01 > p > 0.001$, and $p < 0.001$, respectively. The statistical calculations were performed by using a two-tailed, unpaired Student's *t* test. All *p* values are shown relative to the unmodified pH of endosomes, and are presented as: *p* value for ODN-PLL-PS / *p* value for soluble ODNs.

The intracellular location of TLR9 ligands has recently been shown to affect cytokine profiles. Honda et al. suggested that the retention of TLR9 agonists (CpG oligonucleotides) in early endosomal compartments led to a much higher level of type I IFNs than in late endosomal/lysosomal compartments [50]. Okuya et al. further confirmed this study and showed that the targeting of CpG ODNs to static early endosomes, which are a subpopulation of early

endosomes and exhibit slow maturation kinetics and low mobility along microtubules [63], enhanced the generation of type I IFNs, but diminished the generation of pro-inflammatory cytokines [49]. Our previous study has shown that micrometer particles do not co-localize with LysoTracker, which was used to distinguish late endosomes and lysosomes from early endosomes, while submicrometer particles do [46]. We also confirmed that 3 μm particles were localized in early endosomes by using an early endosome-specific marker, early endosomal antigen-1 (EEA-1) (Figure S4). The FITC-labeled 3 μm particles associated with EEA-1 (Figure S4A). In addition, a cross-sectional image showing EEA-1 only (S4B) revealed ring-like structures that surrounded the particles, suggesting that the particles were contained within early endosomes.

Our results appeared to be inconsistent with the studies by Honda et al. [50] and Okuya et al. [49]. The inconsistent observations may arise from differences in carrier-specific intracellular trafficking and ODN release mechanisms. In this study, ODN-decorated PS particles of defined sizes were used. Our previous study showed that particles of different sizes were transported to different intracellular compartments that exhibited distinct kinetics of pH change and steady state pH. The correlation of cytokine production with the endosomal pH environment that TLR9 ligands were exposed to suggested that the endosomal pH affected TLR9-mediated cytokine profiles. In the study by Honda et al., the cationic liposome, N-[1-(2,3-Dioleoyloxy)propyl]-N,N,N-trimethylammonium methylsuflate (DOTAP), had been used as a CpG ODN carrier. It has been documented that the lipid membrane charge density and size of lipid-based DNA delivery systems determines the intracellular fate of lipoplexes [47, 64, 65]. In addition, the release of ODNs from DOTAP/ODN complexes is dependent on size and charge ratio, and is mediated by the fusogenic interaction between DOTAP and the anionic lipid membrane of

intracellular compartments [66]. No detailed information in the study by Honda et al. was available to determine the size, charge ratio, and membrane charge density of the DOTAP/ODN complexes. In the study by Okuya et al., the heat-shock protein Hsp90 was used as the ODN carrier. However, the intracellular transport of heat-shock proteins remains elusive: endocytosed Hsps may transit through endosomes, into the cytoplasm, and/or into other intracellular vesicles [67, 68], which can potentially affect TLR9-mediated signaling. It is clear that endosomal markers, such as EEA-1 and LysoTracker, are not sufficient to distinguish the intracellular compartments that the three TLR9-ligand carriers, i.e. PS, DOTAP, and Hsp90, are transported to. More detailed studies are required to determine whether the carriers used in all three studies reside in the same intracellular compartment. A recent model of the bifurcation of TLR9 signaling proposed by Sasai et al. suggested that the adaptor protein 3 (AP-3), which finely controlled the trafficking of TLR9 within the endosomal system, was essential for the activation of type I IFN genes [51]. An understanding of how the carrier type and the dynamics of endosomal pH affect the recruitment of AP-3 to TLR9-residing compartments may reconcile the differences observed.

Previous studies have suggested that pH plays a critical role in TLR9-mediated signaling. In this study, the change in pH may have affected the trafficking of particles, but this was not examined. Our results suggest that the endosomal pH affects the profiles of cytokines mediated by TLR9 activation. Carriers which possess the ability to modulate endosomal pH could potentially be used to regulate TLR9-mediated innate immunity. Collectively, our findings indicate that cytokine profiles may be manipulated by controlling the size and/or the composition of biomaterials containing TLR9 ligands.

1.5 Conclusion

In this study, we demonstrated that the size of particles affected the cytokine profiles mediated by TLR9 signaling pathways. By examining the pH of endosomes at which particles of different sizes trafficked to, we showed that type I IFNs, such as IFN-α, were much more sensitive to the change in endosomal pH compared to proinflammatory cytokines, such as IL-6. The role of TLR9 in the applications of biomaterials in medicine lies in delivery systems for vaccines, microbicides, and plasmid DNA and tissue implants. Our findings provide significant implications for two major design parameters: size and composition of biomaterials. The fine control of either or both parameters allows the exploitation of the beneficial aspects of TLR9-mediated innate immunity while minimizing unwanted side effects.

1.6 References

[1] Akira S, Uematsu S, Takeuchi O. Pathogen recognition and innate immunity. Cell. 2006;124:783-801.
[2] Hemmi H, Takeuchi O, Kawai T, Kaisho T, Sato S, Sanjo H, et al. A Toll-like receptor recognizes bacterial DNA. Nature. 2000;408:740-5.
[3] Means TK, Latz E, Hayashi F, Murali MR, Golenbock DT, Luster AD. Human lupus autoantibody-DNA complexes activate DCs through cooperation of CD32 and TLR9. J Clin Invest. 2005;115:407-17.
[4] Barrat FJ, Meeker T, Gregorio J, Chan JH, Uematsu S, Akira S, et al. Nucleic acids of mammalian origin can act as endogenous ligands for toll-like receptors and may promote systemic lupus erythematosus. J Exp Med. 2005;202:1131-9.
[5] Ramirez-Ortiz ZG, Specht CA, Wang JP, Lee CK, Bartholomeu DC, Gazzinelli RT, et al. Toll-like receptor 9-dependent immune activation by unmethylated CpG motifs in Aspergillus fumigatus DNA. Infect Immun. 2008;76:2123-9.
[6] Nakamura K, Miyazato A, Xiao G, Hatta M, Inden K, Aoyagi T, et al. Deoxynucleic acids from Cryptococcus neoformans activate myeloid dendritic cells via a TLR9-dependent pathway. J Immunol. 2008;180:4067-74.
[7] Krug A, Luker GD, Barchet W, Leib DA, Akira S, Colonna M. Herpes simplex virus type 1 activates murine natural interferon-producing cells through toll-like receptor 9. Blood. 2004;103:1433-7.
[8] Lund J, Sato A, Akira S, Medzhitov R, Iwasaki A. Toll-like receptor 9-mediated recognition of herpes simplex virus-2 by plasmacytoid dendritic cells. J Exp Med. 2003;198:513-20.
[9] Krug A, French AR, Barchet W, Fischer JAA, Dzionek A, Pingel JT, et al. TL-139-dependent recognition of MCMV by IPC and DC generates coordinated cytokine responses that activate antiviral NK cell function. Immunity. 2004;21:107-19.

[10] Leadbetter EA, Rifkin IR, Hohlbaum AM, Beaudette BC, Shlomchik MJ, Marshak-Rothstein A. Chromatin-IgG complexes activate B cells by dual engagement of IgM and Toll-like receptors. Nature. 2002;416:603-7.
[11] Boule MW, Broughton C, Mackay F, Akira S, Marshak-Rothstein A, Rifkin IR. Toll-like receptor 9-dependent and -independent dendritic cell activation by chromatin-immunoglobulin G complexes. J Exp Med. 2004;199:1631-40.
[12] Haas T, Metzger J, Schmitz F, Heit A, Muller T, Latz E, et al. The DNA sugar backbone 2 ' deoxyribose determines toll-like receptor 9 activation. Immunity. 2008;28:315-23.
[13] Rhee EG, Mendez S, Shah JA, Wu CY, Kirman JR, Turon TN, et al. Vaccination with heat-killed Leishmania antigen or recombinant leishmanial protein and CpG oligodeoxynucleotides induces long-term memory CD4(+) and CD8(+) T cell responses and protection against Leishmania major infection. J Exp Med. 2002;195:1565-73.
[14] Weeratna RD, Makinen SR, McCluskie MJ, Davis HL. TLR agonists as vaccine adjuvants: comparison of CpG ODN and Resiquimod (R-848). Vaccine. 2005;23:5263-70.
[15] Stacey KJ, Blackwell JM. Immunostimulatory DNA as an adjuvant in vaccination against Leishmania major. Infect Immun. 1999;67:3719-26.
[16] Chu RS, Targoni OS, Krieg AM, Lehmann PV, Harding CV. CpG oligodeoxynucleotides act as adjuvants that switch on T helper 1 (Th1) immunity. J Exp Med. 1997;186:1623-31.
[17] Shen H, Iwasaki A. A crucial role for plasmacytoid dendritic cells in antiviral protection by CpG ODN-based vaginal microbicide. J Clin Invest. 2006;116:2237-43.
[18] Wang YC, Abel K, Lantz K, Krieg AM, McChesney MB, Miller CJ. The toll-like receptor 7 (TLR7) agonist, imiquimod, and the TLR9 agonist, CpG ODN, induce antiviral cytokines and chemokines but do not prevent vaginal transmission of simian immunodeficiency virus when applied intravaginally to rhesus macaques. J Virol. 2005;79:14355-70.
[19] Pyles RB, Higgins D, Chalk C, Zalar A, Eiden J, Brown C, et al. Use of immunostimulatory sequence-containing oligonucleotides as topical therapy for genital herpes simplex virus type 2 infection. J Virol. 2002;76:11387-96.
[20] Ashkar AA, Bauer S, Mitchell WJ, Vieira J, Rosenthal KL. Local delivery of CpG oligodeoxynucleotides induces rapid changes in the genital mucosa and inhibits replication, but not entry, of herpes simplex virus type 2. J Virol. 2003;77:8948-56.
[21] Bourquin C, Anz D, Zwiorek K, Lanz AL, Fuchs S, Weigel S, et al. Targeting CpG oligonucleotides to the lymph node by nanoparticles elicits efficient antitumoral immunity. J Immunol. 2008;181:2990-8.
[22] de Jong S, Chikh G, Sekirov L, Raney S, Semple S, Klimuk S, et al. Encapsulation in liposomal nanoparticles enhances the immunostimulatory, adjuvant and anti-tumor activity of subcutaneously administered CpG ODN. Cancer Immunol Immunother. 2007;56:1251-64.
[23] Diwan M, Elamanchili P, Lane H, Gainer A, Samuel J. Biodegradable nanoparticle mediated antigen delivery to human cord blood derived dendritic cells for induction of primary T cell responses. J Drug Targeting. 2004;11:495-507.
[24] Kwon YJ, Standley SM, Goh SL, Frechet JMJ. Enhanced antigen presentation and immunostimulation of dendritic cells using acid-degradable cationic nanoparticles. J Controlled Release. 2005;105:199-212.
[25] Sokolova V, Knuschke T, Kovtun A, Buer J, Epple M, Westendorf AM. The use of calcium phosphate nanoparticles encapsulating Toll-like receptor ligands and the antigen hemagglutinin to induce dendritic cell maturation and T cell activation. Biomaterials. 2010;31:5627-33.

[26] Wilsonl KD, de Jong SD, Kazem M, Lall R, Hope MJ, Cullis PR, et al. The combination of stabilized plasmid lipid particles and lipid nanoparticle encapsulated CpG containing oligodeoxynucleotides as a systemic genetic vaccine. J Gene Med. 2009;11:14-25.
[27] Saito Y, Higuchi Y, Kawakami S, Yamashita F, Hashida M. Immunostimulatory Characteristics Induced by Linear Polyethyleneimine-Plasmid DNA Complexes in Cultured Macrophages. Hum Gene Ther. 2009;20:137-45.
[28] Tan YD, Li S, Pitt BR, Huang L. The inhibitory role of CpG immunostimulatory motifs in cationic lipid vector-mediated transgene expression in vivo. Hum Gene Ther. 1999;10:2153-61.
[29] Yasuda K, Ogawa Y, Yamane I, Nishikawa M, Takakura Y. Macrophage activation by a DNA/cationic liposome complex requires endosomal acidification and TLR9-dependent and -independent pathways. J Leukocyte Biol. 2005;77:71-9.
[30] Zhang JS, Liu F, Conwell CC, Tan Y, Huang L. Mechanistic studies of sequential injection of cationic liposome and plasmid DNA. Mol Ther. 2006;13:429-37.
[31] Walker WE, Booth CJ, Goldstein DR. TLR9 and IRF3 Cooperate to Induce a Systemic Inflammatory Response in Mice Injected With Liposome:DNA. Mol Ther. 2010;18:775-84.
[32] Lahdeoja T, Pajarinen J, Kouri VP, Sillat T, Salo J, Konttinen YT. Toll-Like Receptors and Aseptic Loosening of Hip Endoprosthesis-A Potential to Respond against Danger Signals? J Orth Res. 2010;28:184-90.
[33] Tamaki Y, Takakubo Y, Goto K, Hirayama T, Sasaki K, Konttinen YT, et al. Increased Expression of Toll-like Receptors in Aseptic Loose Periprosthetic Tissues and Septic Synovial Membranes Around Total Hip Implants. J Rheumatol. 2009;36:598-608.
[34] Pajarinen J, Mackiewicz Z, Pollanen R, Takagi M, Epstein NJ, Ma T, et al. Titanium particles modulate expression of Toll-like receptor proteins. J Biomed Mater Res A. 2010;92A:1528-37.
[35] Latz E, Schoenemeyer A, Visintin A, Fitzgerald KA, Monks BG, Knetter CF, et al. TLR9 signals after translocating from the ER to CpG DNA in the lysosome. Nat Immunol. 2004;5:190-8.
[36] Heinrich PC, Castell JV, Andus T. Interleukin-6 and the acute phase response. Biochem J. 1990;265:621-36.
[37] Vansnick J. Interleukin-6: an overview. Annu Rev Immunol. 1990;8:253-78.
[38] Stetson DB, Medzhitov R. Type I interferons in host defense. Immunity. 2006;25:373-81.
[39] Jilka RL, Hangoc G, Girasole G, Passeri G, Williams DC, Abrams JS, et al. Increased osteoclast development after estrogen loss - mediation by interleukin-6. Science. 1992;257:88-91.
[40] Coelho LFL, Almeida GMD, Mennechet FJD, Blangy A, Uze G. Interferon-alpha and -beta differentially regulate osteoclastogenesis: Role of differential induction of chemokine CXCL11 expression. Proc Natl Acad Sci USA. 2005;102:11917-22.
[41] De Jong WH, Hagens WI, Krystek P, Burger MC, Sips A, Geertsma RE. Particle size-dependent organ distribution of gold nanoparticles after intravenous administration. Biomaterials. 2008;29:1912-9.
[42] Tabata Y, Inoue Y, Ikada Y. Size effect on systemic and mucosal immune responses induced by oral administration of biodegradable microspheres. Vaccine. 1996;14:1677-85.
[43] Tabata Y, Ikada Y. Effect of the size and surface charge of polymer microspheres on their phagocytosis by macrophage. Biomaterials. 1988;9:356-62.

[44] Chono S, Tanino T, Seki T, Morimoto K. Influence of particle size on drug delivery to rat alveolar macrophages following pulmonary administration of ciprofloxacin incorporated into liposomes. J Drug Targeting. 2006;14:557-66.
[45] Champion JA, Walker A, Mitragotri S. Role of particle size in phagocytosis of polymeric microspheres. Pharm Res. 2008;25:1815-21.
[46] Tran KK, Shen H. The role of phagosomal pH on the size-dependent efficiency of cross-presentation by dendritic cells. Biomaterials. 2009;30:1356-62.
[47] Brewer JM, Pollock KGJ, Tetley L, Russell DG. Vesicle size influences the trafficking, processing, and presentation of antigens in lipid vesicles. J Immunol. 2004;173:6143-50.
[48] Rejman J, Oberle V, Zuhorn IS, Hoekstra D. Size-dependent internalization of particles via the pathways of clathrin-and caveolae-mediated endocytosis. Biochem J. 2004;377:159-69.
[49] Okuya K, Tamura Y, Saito K, Kutomi G, Torigoe T, Hirata K, et al. Spatiotemporal Regulation of Heat Shock Protein 90-Chaperoned Self-DNA and CpG-Oligodeoxynucleotide for Type I IFN Induction via Targeting to Static Early Endosome. J Immunol. 2010;184:7092-9.
[50] Honda K, Ohba Y, Yanai H, Negishi H, Mizutani T, Takaoka A, et al. Spatiotemporal regulation of MyD88-IRF-7 signalling for robust type-I interferon induction. Nature. 2005;434:1035-40.
[51] Sasai M, Linehan MM, Iwasaki A. Bifurcation of Toll-Like Receptor 9 Signaling by Adaptor Protein 3. Science. 2010;329:1530-4.
[52] Ohkuma S, Poole B. Fluorescence probe measurement of intralysosomal pH in living cells and perturbation of pH by various agents. Proc Natl Acad Sci USA. 1978;75:3327-31.
[53] Dalod M, Salazar-Mather TP, Malmgaard L, Lewis C, Asselin-Paturel C, Briere F, et al. Interferon alpha/beta and interleukin 12 responses to viral infections: Pathways regulating dendritic cell cytokine expression in vivo. J Exp Med. 2002;195:517-28.
[54] Trubetskoy VS, Loomis A, Hagstrom JE, Budker VG, Wolff JA. Layer-by-layer deposition of oppositely charged polyelectrolytes on the surface of condensed DNA particles. Nucleic Acids Res. 1999;27:3090-5.
[55] Munier S, Messai I, Delair T, Verrier B, Ataman-Onal Y. Cationic PLA nanoparticles for DNA delivery: Comparison of three surface polycations for DNA binding, protection and transfection properties. Colloids Surf B. 2005;43:163-73.
[56] Akinc A, Langer R. Measuring the pH environment of DNA delivered using nonviral vectors: Implications for lysosomal trafficking. Biotechnol Bioeng. 2002;78:503-8.
[57] Rouzina I, Bloomfield VA. DNA bending by small, mobile multivalent cations. Biophys J. 1998;74:3152-64.
[58] Lipford GB, Sparwasser T, Bauer M, Zimmermann S, Koch ES, Heeg K, et al. Immunostimulatory DNA: sequence-dependent production of potentially harmful or useful cytokines. Eur J Immunol. 1997;27:3420-6.
[59] Krug A, Rothenfusser S, Hornung V, Jahrsdorfer B, Blackwell S, Ballas ZK, et al. Identification of CpG oligonucleotide sequences with high induction of IFN-alpha/beta in plasmacytoid dendritic cells. Eur J Immunol. 2001;31:2154-63.
[60] Ahmad-Nejad P, Hacker H, Rutz M, Bauer S, Vabulas RM, Wagner H. Bacterial CpG-DNA and lipopolysaccharides activate Toll-like receptors at distinct cellular compartments. Eur J Immunol. 2002;32:1958-68.
[61] Manzel L, Strekowski L, Ismail FMD, Smith JC, Macfarlane DE. Antagonism of immunostimulatory CpG-oligodeoxynucleotides by 4-aminoquinolines and other weak bases: Mechanistic studies. J Pharmacol Exp Ther. 1999;291:1337-47.

[62] Poole B, Ohkuma S. Effect of weak bases on the intralysosomal pH in mouse peritoneal macrophages. J Cell Biol. 1981;90:665-9.
[63] Lakadamyali M, Rust MJ, Zhuang XW. Ligands for clathrin-mediated endocytosis are differentially sorted into distinct populations of early endosomes. Cell. 2006;124:997-1009.
[64] Ahmad A, Evans HM, Ewert K, George CX, Samuel CE, Safinya CR. New multivalent cationic lipids reveal bell curve for transfection efficiency versus membrane charge density: lipid-DNA complexes for gene delivery. J Gene Med. 2005;7:739-48.
[65] Lin AJ, Slack NL, Ahmad A, George CX, Samuel CE, Safinya CR. Three-dimensional imaging of lipid gene-carriers: Membrane charge density controls universal transfection behavior in lamellar cationic liposome-DNA complexes. Biophys J. 2003;84:3307-16.
[66] Zelphati O, Szoka FC. Mechanism of oligonucleotide release from cationic liposomes. Proc Natl Acad Sci USA. 1996;93:11493-8.
[67] Kutomi G, Tamura Y, Okuya K, Yamamoto T, Hirohashi Y, Kamiguchi K, et al. Targeting to Static Endosome Is Required for Efficient Cross-Presentation of Endoplasmic Reticulum-Resident Oxygen-Regulated Protein 150-Peptide Complexes. J Immunol. 2009;183:5861-9.
[68] Fujihara SM, Nadler SG. Intranuclear targeted delivery of functional NF-kappa B by 70 kDa heat shock protein. EMBO J. 1999;18:411-9.

Chapter 2: Selectively targeting the toll-like receptor 9 (TLR9) – IRF 7 signaling pathway by polymer blend particles

2.1 Abstract

Signaling through toll-like receptor 9 (TLR9) has been exploited for cancer therapy. The stimulation of TLR9 leads to two bifurcating signaling pathways – NF-κB-dependent pro-inflammatory cytokines and IRF-7-dependent type I interferons (IFNs) pathway. In this study, we employ polymer blend particles to present the synthetic ligand, CpG oligonucleotides (CpG ODNs) to TLR9. The polymer blend particles are made from the blend of pH-insensitive and pH-sensitive copolymer. By tailoring the composition of the pH-sensitive polymer, CpG ODNs are presented to TLR9 in a way that only activates the IRF-7 signaling pathway. CpG ODNs have been used for cancer therapy in both preclinical and clinical studies. The selective activation of IRF-7 could potentially enhance the apoptosis of tumor cells and immunological control of tumor progression without inadvertently activating NF-κB-dependent oncogenesis.

2.2 Introduction

Signaling through Toll-like receptor 9 (TLR9) has been exploited for stimulating the innate and adaptive immunity or intrinsic factors of infected and cancer cells for treating infectious diseases and cancers [1]. TLR9 was first identified as the receptor for bacterial DNA [2], which contains unmethylated cytosine-phosphate-guanine (CpG) motifs. Subsequently, several natural and synthetic TLR9 ligands have been identified, including DNA of viruses [3-5], fungi [6, 7], and dead cells [8, 9], as well as chromatin-IgG complexes [10, 11], dinucleotides [12] and CpG oligodeoxynucleotides (ODNs) [13]. In particular, CpG ODNs have demonstrated potential as vaccine adjuvants, microbicides, and anti-cancer drugs [14].

TLR9 resides in the endoplasmic reticulum. In order to signal, TLR9 has to be transported to and cleaved in endolysosomal compartments [15, 16]. Upon the ligation with its cognate ligands, TLR9 recruits the MyD88 adapter protein. Subsequently, two distinct pathways are initiated. One is nuclear factor κB (NF-κB)–dependent pro-inflammatory cytokines, and the other is interferon regulatory factor 7 (IRF7)–dependent type I interferons (IFNs) pathway [17, 18]. NF-κB is a family of transcription factors that control many biological responses. It is well established that the activation of NF-κB regulates immune responses and inflammation. Increasing evidence have shown that the unregulated activation of NF-κB is linked to oncogenesis [19]. NF-κB regulates the expression of proteins that promote cell proliferation and differentiation, migration and anti-apoptotic effects [20, 21]. The suppression of NF-κB has been shown to be critical for the induction of apoptosis of a number of tumor cells such as multiple myeloma cells [22, 23], T cell lymphoma [24], prostate cancer cells [25] and breast cancer cells [26].

The activation of IRF-7 results in the production of type I IFNs (IFN-α and IFN-β) [17]. Type I IFNs play multiple roles in cancer therapy. They directly act on cancer cells and induce their apoptosis [27]. They also promote immunological control of cancer cells by increasing the number of tumor-antigen specific cytotoxic T cells [28, 29], programming dendritic cells (DCs) (i.e. enhancing the ability of cross presentation and priming of $CD8^+$ T cells by CD8α DCs [30], and regulating functions of NK cells [31]. Recently, it has been shown that IRF-7 controls the metastasis of breast cancer cells. The down-regulation of IRF-7 leads to the dissemination of breast cancer cells to distal sites [32].

Clearly, the activation of the two arms of TLR9 signaling by CpG ODNs or other ligands of TLR9 would have distinct consequences in cancer therapy. It is known that type B CpG

ODNs activate the NF-κB pathway only whereas type A CpG ODNs activate both NF-κB and IRF-7 pathways [13]. It would be beneficial to selectively activate the IRF-7 pathway while minimizing the activation of NF-κB by CpG ODNs. In this study, we demonstrate we are able to present type A CpG ODNs, i.e. CpG 2216, to TLR9 in a way that does not activate the NF-κB pathway, but only the IRF-7 pathway, by using polymer blend particles made from a pH-insensitive polymer, PLGA and a pH-sensitive copolymer.

2.3 Materials and Methods

2.3.1 Cell culture

A dendritic cell line, BC-1 (a gift from Dr. Yoshiki Yanagawa), was maintained as described previously [33]. The single cell suspension of splenocytes was obtained from C57BL/6 mice (Jackson Laboratory). Spleens were collected and re-suspended in 0.5 ml of RPMI 1640 supplemented with 10% fetal bovine serum (FBS), 1% penicillin/streptomycin, 2 mM L-glutamine, and 1 mM sodium pyruvate (complete media). Spleens were minced into small pieces. Tissues were incubated with 1.8 mg/ml collagenase D and 30 μg/ml of DNAse at 37 °C for 30 min. Tissues were centrifuged, the solutions discarded, and then re-suspended in Hank's Balance Salt Solution (HBSS) containing 5 mM EDTA and 1% FBS for 5 min at 37 °C. A single cell suspension was obtained by grinding the tissues through a 70 μm cell strainer. The cells were incubated with ACK lysis buffer (0.15 M NH_4Cl, 1 M $KHCO_3$, and 0.1 mM Na2.EDTA, pH 7.4) to lyse red blood cells. Cells were washed, re-suspended in complete media and counted.

2.3.2 Reagents

ODNs, CpG 2216 and FITC-CpG 2216, were purchased from TriLink BioTechnologies (San Diego, CA). The sequence of CpG 2216 is 5′ggG GGA CGA TCG TCg ggg gG3'. Lowercase letters denote a phosphorothioate backbone, and uppercase letters denote a

phosphodiester backbone. FITC-CpG 2216 was synthesized by labeling the ODN with FITC at the 5' end. Antibodies used for immunocytochemistry were purchased from Abcam and Invitrogen. Antibodies used for ELISA were purchased from eBioscience, PBL InterferonSource, Cell Sciences, and Jackson ImmunoResearch. All cell culture reagents were from Life Technologies, NY. Tetrahydrofuran (THF) and dichloromethane (DCM) were supplied by EMD Chemicals Inc., NJ. Diethyl propylmalonate, butyl methacrylate, 2-(dimethylamino)ethyl methacrylate, 2,2'-azobis(2-methylpropionitrile) (AIBN) and poly(vinyl alcohol) (PVA) were purchased from Sigma-Aldrich. Poly(lactic-co-glycolic acid) (PLGA, 50:50, IV=0.65dL/g) was from LACTEL (DURECT Corporation, AL).

2.3.3 Synthesis of pH-sensitive polymers

The synthesis and characterization of polymers were performed by Xi Zhan. The free radical polymerization of 2-propylacrylic acid (PAA), butyl methacrylate (BMA) and 2-(dimethylamino)ethyl methacrylate (DMAEMA) was followed by a procedure reported previously [34]. The PAA monomer was synthesized by following a protocol adapted from a method reported previously [35]. PAA, BMA and DMAEMA were vacuum distilled before use. Monomers (PAA:DMAEMA:BMA=1:1:2, DMAEMA:BMA=1:1 or DMAEMA:BMA=1:4 (mole ratio)) and AIBN (2 mM) were mixed in THF (monomer:THF = 10 wt%). The polymerization was carried out at 60 °C for 15 h (terpolymer) or 80 °C for 20 h (dipolymer) under nitrogen. The polymer was precipitated in an excess amount of diethyl ether and pentane and dried under vacuum. These three polymers (BMA-PAA-DMAEMA (terpolymer), BMA-DMAEMA (1:1) (1:1 dipolymer) and BMA-DMAEMA (3:1) (3:1 dipolymer)) were characterized by proton nuclear magnetic resonance (H^1NMR) spectroscopy.

2.3.4 Fabrication of polymer blend particles

The fabrication of blend polymer particles was performed by Xi Zhan. The blend particles were fabricated by using the double emulsion method. The mixture of PLGA and pH-sensitive polymer (terpolymer, 1:1 dipolymer or 1:3 dipolymer) mixture was dissolved in 1 ml of DCM with a weight ratio of 4:1 (PLGA: pH-sensitive polymer) overnight. HiLyte647-labeled PLGA (10 wt% in total polymer) was also doped into the mixture of the polymers in order to label particles. FITC-CpG 2216 or CpG 2216 was dissolved in 100 µl of Dulbecco's Phosphate-Buffered Saline (DPBS) to different concentrations (10 or 5 mg/ml, respectively), and the CpG 2216 solution was added to the polymer solution drop-wise. 2 ml of 5% PVA was then added drop-wise into the polymer solution while vortexing, and the solution was sonicated and paused for 10 seconds alternately. The emulsion was then added to 4 ml of 5% PVA under stirring and followed by the sonication as described before. Then the emulsion was poured into 4 ml of 0.06% PVA solution under stirring, and the final emulsion was stirred for 3 to 4 h at room temperature to completely evaporate DCM and allow blend particles to harden. The particles were washed 3 times with Milli-Q water and stored in DPBS at 4^{o}C. The particles were named as Terpolymer, 1:1 Dipolymer and 3:1 Dipolymer depending on the pH-sensitive polymer used, and Terpolymer – CpG, Dipolymer 1:1 – CpG or Dipolymer 3:1 – CpG if CpG ODNs were incorporated.

2.3.5 Characterization of blend particles

A Zetasizer Nano ZS (Malvern Instruments, Westborough, MA) was used to characterize the size distribution by dynamic light scattering (DLS) and the zeta potential of the particles. Particles were prepared at 0.05 mg particle/ml for DLS measurements. Size and zeta potential measurements were performed at room temperature in 10 mM of KNO_3 at different pHs from 4

to 9. To determine the surface charge of the particles at physiological temperature and pH, zeta potential measurements were also performed at 37 °C in a buffer composed of 10 mM citric acid and 20 mM disodium hydrogen phosphate at the pH ranging from 4.57 to 7.30. SEM and TEM were used to determine the particle size and examine the morphology of the particles. Xi Zhan prepared SEM and TEM samples and acquired the micrographs. The analysis of the micrographs was performed by myself. SEM samples of particles were spin-coated onto silica, sputter-coated with 12 nm of platinum using a SPI Sputter Coater (Structure Probe, Inc., West Chester, PA), and analyzed using a Siron SEM with a beam voltage of 5.0 kV (NTUF, University of Washington). For TEM samples, 6 μl of particle solution was added onto 400 mesh copper TEM grids coated with continuous carbon film. After 2 minutes, the TEM grid was blotted with Whatman filter paper from the side and dried in air. TEM samples were examined by a Tecnai TF20 transmission electron microscope (FEI) at 200 kV. Electron images were recorded on a 4k × 4k CCD camera (Gatan, Inc., CA) at 50,000 magnification (effective pixel size of 0.4 nm) and approximately -1 mm defocus. The electron dose for each exposure was approximately 20 e/Å^2.

2.3.6 Quantification of the polymer composition and the loading of CpG 2216 in blend particles

For NMR spectroscopy, which was performed by Xi Zhan, blend particles were dissolved in deuterated methylene chloride and samples were analyzed using a ^{1}H Bruker AV500 spectrometer. Using the hydrogens on the ester groups of PLGA (5.2 ppm) and the side chain of BMA (3.9 ppm), and the known ratios of the monomers of the polymers, the fraction of terpolymer in blend particles was calculated.

CpG 2216-containing particles were diluted in 0.05 ml DPBS and centrifuged at 13,200 rpm for 10 min. The supernatant was collected. The pellet was dissolved in 0.5 ml of 1% (w/w) sodium dodecyl sulfate (SDS)/0.1 M NaOH, and subsequently incubated in a water bath at 90 °C for 5 min to ensure the complete dissolution of particles. In parallel, a known concentration of soluble FITC-CpG 2216 prepared in 1% (w/w) SDS/0.1 M NaOH and subjected to heating as samples was used for preparing standard curve. It was confirmed that incubation at 90 °C did not affect the fluorescent properties of FITC-CpG. SpectraMax (Molecular Devices) was used to quantify the fluorescence of FITC-CpG 2216 at excitation and emission wavelengths of 494 and 520 nm, respectively. The amount of CpG 2216 in the supernatant and pellet was quantified by using the standard curve.

2.3.7 Quantification of FITC-CpG 2216 released from particles at 37 °C at different pHs

To determine the release of CpG 2216 from particles, particles were incubated in buffer solutions that mimicked the pH and temperature that endocytosed particles were exposed to. The buffer solutions were composed of 10 mM citric acid and 20 mM disodium hydrogen phosphate at pH 4.57 to 7.30. Particles were diluted in the buffer solutions at room temperature, and aliquoted at 0.1 ml (50 μg particles) per micro-centrifuge tube. Next, the aliquots were immersed in a water bath at 37 °C. At the given time point, an aliquot was centrifuged at 13,200 rpm for 10 min at room temperature. The supernatant was collected and the pellet was dissolved as described above to completely release FITC-CpG 2216. The FITC-CpG 2216 in the supernatant and pellet was quantified according to the procedure stated above.

2.3.8 Preparation and characterization of CpG 2216-adsorbed particles

Fluorescent polystyrene (PS) particles (Polysciences, Inc., Warrington, PA) of 100 nm in diameter were coated with CpG 2216 in our previous work [33]. Briefly, 100 nm PS particles

were coated with poly-L-lysine (PLL; Sigma–Aldrich, Inc., Saint Louis, MO; MW = 30,000–70,000 g/mol). Next, CpG 2216 (TriLink BioTechnologies, San Diego, CA) was adsorbed onto PLL-coated particles, since PLL is a cationic polymer and able to facilitate the adsorption of CpG 2216. CpG 2216-adsorbed particles are denoted as 2216-PLL-PS. We have previously characterized the cytokine profile of BC-1 cells stimulated with 2216-PLL-PS [33]. 2216-PLL-PS was used as a positive control in this study.

Terpolymer-coated CpG 2216 particles were fabricated by preparing blank terpolymer particles in 10 mM KNO_3 at pH 2.5, and CpG 2216 in 10 mM KNO_3 at pH 2.5. Next, 0.25 ml of particles was added drop-wise to 0.25 ml of CpG while vortexing after adding each drop. The final concentrations in the mixture were 0.66 mg terpolymer particle/ml and 0.15 mg CpG/ml. The adsorption reaction proceeded for 2 h at room temperature. Particles were washed three times in 10 mM KNO_3 at pH 6 by centrifugation at 2000 rpm for 30 min.

2.3.9 Stimulation of cells by CpG 2216

BC-1 cells were seeded at a density of 2.5×10^5 cells per well in a 24-well plate. Cells were incubated at 37 °C overnight to allow cells to adhere to the plate surface. CpG 2216-loaded blend particles, 2216-PLL-PS, and soluble FITC-CpG 2216 and CpG 2216 (0.005 mg/ml) were added to cells in 0.5 ml of medium. After 24 h of incubation at 37 °C, cell supernatants were collected and stored at −20 °C for the measurement of cytokines.

1×10^6 splenocytes in 0.1 ml medium were added to a well of a 96-well round-bottom plate. Next, 0.1 ml of CpG 2216-containing samples were added to the cells so that the final volume was 0.2 ml per well. After 24 h of incubation at 37 °C, cell supernatants were collected and stored at −20 °C for the measurement of cytokines.

2.3.10 Measurement of endosomal pH

The endosomal pH was measured by using a fluorescent ratiometric method that was adapted from a previously established method [36]. For cells used for standard curves, BC-1 cells were seeded at a density of 3×10^6 cells per well in a 6-well plate, and incubated overnight at 37 °C. Cells were subsequently incubated with particles for 3 h (pulse), washed and further incubated for an additional 4 h (chase). Particles contained pH-sensitive FITC-labeled CpG 2216 and pH-insensitive HiLyte 647-labeled PLGA. Afterwards, cells were harvested and processed to construct a standard curve. The cells were fixed with 4% paraformaldehyde (PFA) for 20 min at room temperature, permeabilized with 0.1% Triton X-100 for 2 min at room temperature, and resuspended in 0.1 M citrate buffer solutions of known pH values. Citrate buffer solutions were prepared in Dulbecco's phosphate buffered saline (DPBS). For samples in which endosomal pH was measured, cells were seeded at 2.5×10^5 cells per well, and incubated overnight at 37 °C. The pulse and chase condition was the same as above. Cells were harvested and re-suspended in different concentrations of NH_4Cl in Isocove's Modified Dulbecco's Medium (IMDM) supplemented with 0.5% FBS and incubated for 1 h at 37 °C. NH_4Cl was used to adjust endosomal pH as in our previous study [33]. Cell suspensions were analyzed using a FACSCanto (Cell Analysis Facility, University of Washington). The geometric mean fluorescent intensity (gMFI) of cells was determined by FlowJo (Treestar, Inc., Ashland, OR). The ratio of gMFI of FITC to that of HiLyte 647 was compared to the standard curve constructed in citrate buffers with known pH values to obtain the endosomal pH of each sample.

2.3.11 Measurement of cytokine concentrations

Cytokine concentrations in cell supernatants were analyzed by enzyme-linked immunosorbent assay (ELISA). The procedures for assaying IL-6 were adapted from the

manufacturer's protocol (eBioscience, San Diego, CA). The procedures for IFN-α were described previously [4, 37].

2.3.12 Immunocytochemistry

BC-1 cells were plated at a density of 2.5×10^5 cells per well in 500 µl medium onto 24 well plates. Cells were allowed to adhere to the surface overnight at 37 °C. Cells were pulsed with particles or control samples at 100 µg/ml in 500 µl medium for 3.5 h at 37 °C. Then, particles were removed and cells were washed with DPBS. Cells were detached from the tissue-culture surface by trypsinization and then plated onto 12 mm circular glass coverslips (Erie Scientific Co., Portsmouth, NH). To enhance the adherence of cells to coverslips, coverslips were first pre-treated with poly-D-lysine (PDL, Sigma-Aldrich, Inc., Saint Louis, MO) by incubating them with 400 µl PDL at 0.025 mg/ml for 30 min at room temperature. Coverslips were washed three times with 500 µl Milli-Q water and allowed to dry before the seeding of cells. Cells were allowed to adhere for 20 min. Afterward, cells were fixed and permeabilized with 250 µl of BD Cytofix/Cytoperm™ (Invitrogen, Frederick, MD) for 20 min at 4 °C. Cells were washed twice with 250 µl of blocking buffer. Blocking buffer contained 1 wt% bovine serum albumin (Sigma-Aldrich, Inc., Saint Louis, MO) in BD Perm/Wash Buffer™ (Invitrogen, Frederick, MD). Next, cells were blocked with the blocking buffer for 1.5 h at room temperature. To examine p65 and IRF7, cells were labeled with 250 µl blocking buffer containing either 2 µg/ml rabbit polyclonal anti-p65 (Abcam, Cambridge, MA) or 2 µg/ml rabbit polyclonal anti-IRF7 (Abcam, Cambridge, MA) for 1 h at room temperature. Cells were washed twice with the blocking buffer. To detect primary antibodies, cells were incubated with 250 µl of blocking buffer containing 2 µg/ml Cy3-anti rabbit IgG (Abcam, Cambridge, MA). Lastly, cells were washed twice with the blocking buffer. Coverslips were rinsed with Milli-Q water and then

mounted onto glass slides using DAPI-containing HardSet Vectashield Mounting Medium (Vector Laboratories, Inc., Burlingame, CA) for confocal microscopic analysis.

2.3.13 Confocal microscopy and image analysis

Images were acquired with a Zeiss LSM 510 META confocal microscope equipped with a 63 × 1.40 numerical aperture (N.A.) PLAN APO oil immersion differential interference contrast objective lens (Keck Imaging Center, University of Washington). All images were acquired by using the line sequential scanning mode (one channel is scanned at a time). Images were acquired for single-stained samples to confirm that crosstalk between channels did not exist. The cross-reactivity of the secondary antibody was examined and determined to be undetectable.

Nuclei were approximately 1 μm thick in the z direction. The middle optical section of the nucleus was used to determine whether a significant amount of p65 or IRF-7 was present in the nuclei. Each optical section was 0.9 μm thick, so the middle optical section of nuclei represented a significant portion of a nucleus.

2.3.14 Statistical analysis

All experiments were repeated two to three times. The one-tailed and unpaired Student's *t* test was used to analyze the differences between experimental groups as specified. $p < 0.05$ is considered as statistically different between two experimental groups.

2.4 Results and Discussion

2.4.1 Characterization of pH-sensitive copolymers

The pH-sensitive copolymers used for particle fabrication were composed of all three or two of the following monomers, 2-propylacrylic acid (PAA), 2-(dimethylamino)ethyl methacrylate (DMAEMA) and butyl methacrylate (BMA) (Fig. 1). They were synthesized by radical polymerization with a number-averaged MW of 20 kDa. BMA facilitates the mixing of

pH-sensitive copolymers with PLGA to form the particles. The PAA and DMAEMA monomers have pK_a of 6.7 and 7.5, respectively [38, 39]. Both monomers are protonated, and undergo conformational changes at the endosomal/lysosomal pH [40]. The copolymer that consisted of all three monomers is termed as terpolymer, and of two monomers (DMAEMA and BMA) as dipolymer throughout the text. Based on proton nuclear magnetic resonance (^{1}H NMR) analysis (Fig. S5), the molar ratio of monomers in the terpolymer was 3:2:5 (PAA:DMAEMA:BMA). The dipolymers were composed of either 1:1 (dipolymer 1:1) or 3:1 (dipolymer 3:1) of BMA to DMAEMA.

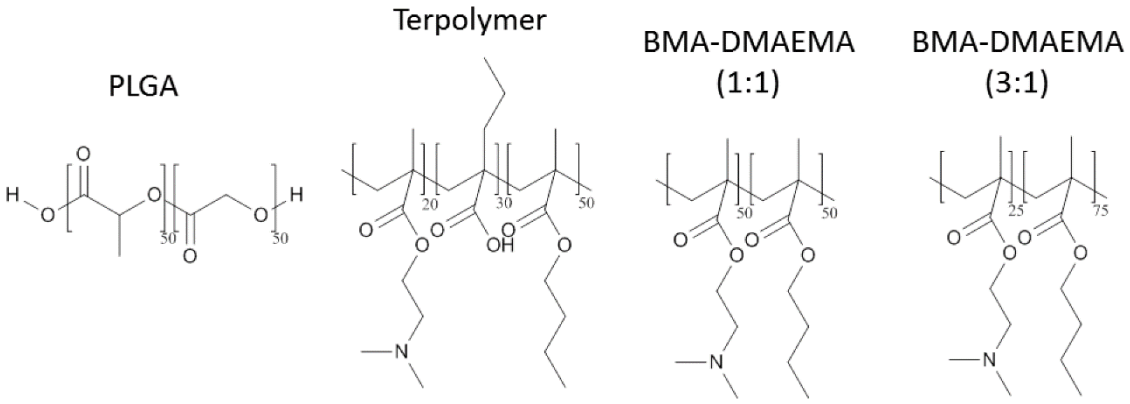

Fig. 1. Chemical structure of PLGA, Terpolymer, Dipolymer 1:1 and Dipolymer 3:1.

2.4.2 Composition, size, morphology, and surface charge of polymer blend particles

Blend particles were made from the mixture of pH-sensitive copolymers and PLGA by the double-emulsion method [41]. The Type A CpG ODN, CpG 2216, was incorporated into the particles. These particles are denoted as Terpolymer, Dipolymer 1:1 or Dipolymer 3:1 depending on which pH-sensitive copolymer was used. Terpolymer blend particles onto which CpG 2216 was adsorbed are called Terpolymer-adsorb CpG. The composition of polymers in the blend particles was determined by ^{1}HNMR. The BMA peak (3.9 ppm) and PLGA peak (5.3 ppm)

were used to calculate the actual polymer ratio in the blend particles (Fig. S5 and Table 1). All three pH-sensitive polymers and CpG 2216 were successfully incorporated into blend particles. The amount of CpG 2216 in each type of blend particle was nearly the same.

Table 1. The polymer compositions and CpG 2216 in blend particles.

Particle name	Copolymer used in fabrication (wt. fraction)	Actual copolymer in particle (wt. fraction)	mg CpG 2216 per mg particle
Terpolymer-CpG	0.2	0.15	0.041
Terpolymer	0.2	0.24	0
Dipolymer 1:1-CpG	0.2	0.11	0.037
Dipolymer 1:1	0.2	0.11	0
Dipolymer 3:1-CpG	0.2	0.21	0.031
Dipolymer 3:1	0.2	0.32	0

The hydrodynamic diameters of polymer blend particles were between 150 to 250 nm at pH 7.0 ± 0.1 (Fig. 2A). They were nearly spherical as examined by scanning electron microscopy (SEM) (Fig. 2C) and transmission electron microscopy (TEM) (Fig. 2D). The micrographs of TEM also revealed that blend particles appeared as core/shell structures. pH-sensitive copolymers contained hydrophilic side chains. They likely remained at the interface of aqueous and organic phases during the particle fabrication process, resulting in two distinct phases in blend particles. The negatively charged CpG ODNs were expected to interact with the positively charged DMAEMA and increased the tendency of phase separation of the two polymers in the blend particles.

The zeta potential of polymer blend particles was measured at different pHs (Fig. 2B). The control particles (Terpolymer-adsorb CpG), onto which negatively charged CpG ODNs are adsorbed, had a strong negative charge (-35 mV) as expected. Blend particles with (Terpolymer-CpG) and without CpG 2216 (Terpolymer) had a strong positive surface charge at an acidic pH (23 and 32 mV, respectively), which can be attributed to the tertiary amine in the DMAEMA monomer. The zeta potential of both types of particles decreased as the pH reached neutral and basic conditions due to the deprotonation of PAA and DMAEMA. Terpolymer-CpG exhibited a

lower zeta potential than Terpolymer within the range of pHs examined, indicating a fraction of the negatively-charged CpG ODNs were present on the surface of particles. The zeta potential of particles made from the dipolymer exhibited different trends. Dipolymer 1:1 (particles without CpG 2216) exhibited positive surface charge between pH 4 and 9, indicating the dipolymer 1:1 was present on the surface of particles. In contrast, the zeta potential of Dipolymer 1:1-CpG displayed a higher positive charge below pH 7 and a lower positive charge above pH 7. This indicates that CpG 2216 was still present on the surface, but the positive charge from the protonated DMAEMA dominated over the negatively charged CpG 2216 when pH was below 7. The zeta potential of Dipolymer 3:1-CpG was approximately -30 mV between pH 5 and 9 and approached to neutral at pH 4 while that of Dipolymer 3:1 (particles without CpG) were nearly neutral between pH 5 and 9 and increased up to 5 mV at pH 4. This result suggests that CpG 2216 was present on the surface of Dipolymer 3:1 and dominated over the positive charge from DMAEMA between pH 5 and 9. In comparison with particles made from the dipolymer 1:1, it indicates that the increasing ratio of BMA resulted in less DMAEMA in dipolymers to be present on the surface of particles. In summary, CpG 2216 was present on the surface of all the types of blend particles. By comparing the zeta potential of particles with and without CpG 2216 at pH 9.0, it can be estimated that the amount of CpG 2216 was on the surface of particles in the order of Terpolymer ~ Dipolymer 3:1 > Dipolymer 1:1.

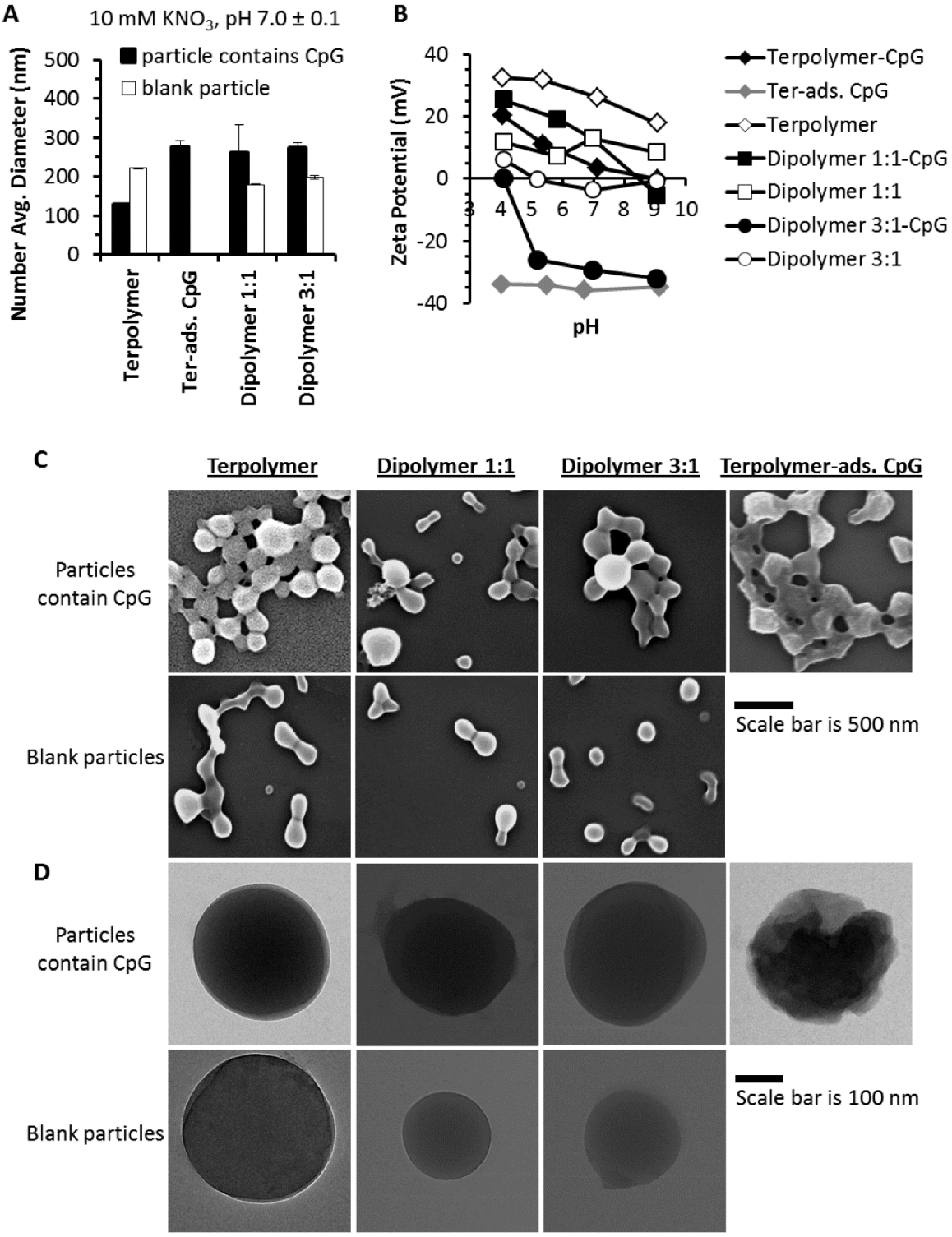

Fig. 2. Size, zeta potential, and morphology of polymer blend particles. (A) The number average of hydrodynamic diameter and (B) zeta potential of polymer blend particles suspended in 10 mM KNO_3 at designated pHs. (C) SEM and (D) TEM images of polymer blend particles.

2.4.3 Cytokine profiles induced by CpG2216-containing polymer blend particles

CpG 2216 is a Type A CpG motif-containing ODN, which is known to induce both pro-inflammatory cytokines (i.e. IL-6, IL-12, TNF-α) through the activation of NF-κB and type I IFNs, such as IFN-α, through the activation of IRF-7 [13]. The cytokine secretions induced by different CpG 2216-containing or -coated particles were assessed by using splenocytes isolated from mice. CpG 2216 was labeled with fluorescein (FITC) for the ease of quantification of CpG 2216 in particles. When CpG 2216 was incorporated into the dipolymer 1:1 (Dipolymer 1:1-CpG), negligible amounts of IL-6 and IFN-α were secreted. When the amount of DMAEMA in the dipolymer was reduced to a molar ratio of BMA to DMAEMA of 3:1 (Dipolymer 3:1-CpG), both IL-6 and IFN-α were secreted. When CpG 2216 was incorporated into the terpolymer particles (Terpolymer-CpG), only IFN-α secretions could be detected – the pro-inflammatory cytokines, such as IL-6, nearly diminished over the wide range of concentrations of CpG 2216 (Fig. 3A). Interestingly, both IL-6 and IFN-α were secreted upon the stimulation by terpolymer particles onto which CpG 2216 were directly adsorbed (Terpolymer-adsorb CpG), suggesting the incorporation of CpG 2216 into particles – which may result in a unique interaction between CpG 2216 with TLR9 – was critical for selectively targeting the IRF-7 pathway. Terpolymer particles loaded with non-fluorescent CpG 2216 exhibited similar results, indicating that the modification of CpG 2216 by FITC did not contribute to the observed trend (Fig. S6).

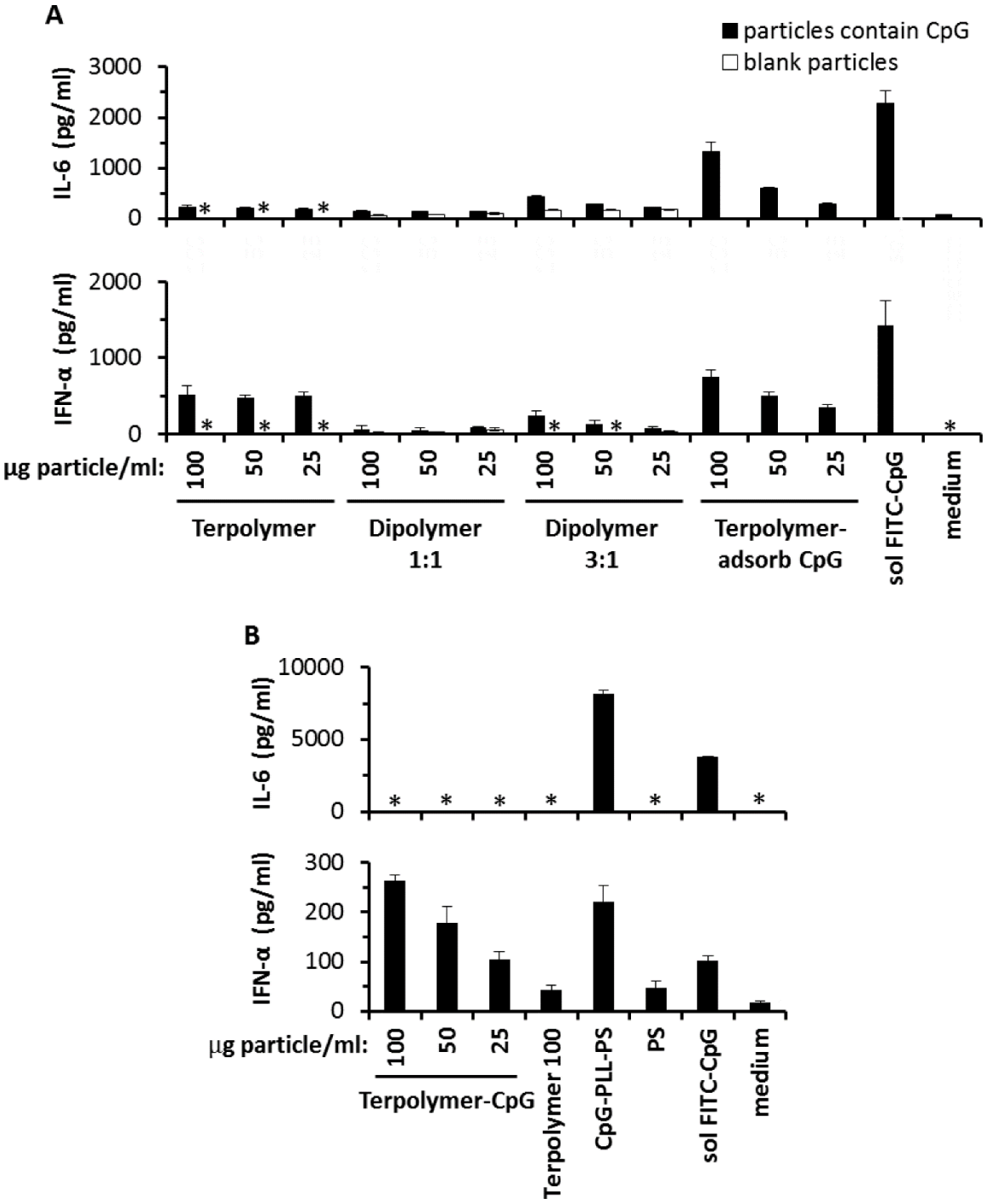

Fig. 3. Effect of the composition of the pH-sensitive polymer on the cytokine secretions of cells. The levels of IL-6 and IFN-α from (A) splenocytes and (B) BC-1 cells after 24 h incubation with the indicated stimulants. 5 μg/ml of soluble CpG 2216 was used. The * indicates that the cytokine level was undetectable.

These results indicate that cytokine profiles can be tuned through the presentation of CpG ODNs by polymer blend particles. Encouraged by these results, we subsequently focused on the Terpolymer-CpG particle only. For convenience and the humane use of mice, the dendritic cell line, BC-1 cells [42], was used for all the subsequent studies. We confirmed the cytokine profiles in BC-1 cells stimulated with Terpolymer-CpG. Terpolymer-CpG induced the secretions of IFN-α, but not IL-6 as observed in splenocytes from mice (Fig. 3B). Cytokine secretions from controls, such as soluble CpG 2216, and CpG 2216-adsorbed polystyrene (CpG-PLL-PS), were expected and consistent with previous reports [33].

2.4.4 Impaired translocation of NF-κB by Terpolymer-CpG

IL-6 is one of the pro-inflammatory cytokines whose induction is regulated by the transcription factor, NF-κB, while IFN-α, is regulated by the transcription factor, IRF-7, upon the ligation of TLR9 by CpG ODNs. In resting cells, NF-κB complexes are sequestered in the cytoplasm. Upon the activation, they enter nuclei and bind to the target gene. To confirm Terpolymer-CpG was not able to activate the NF-κB complexes, we then investigated the translocation of p65, one of the subunits of the NF-κB complex, as well as IRF-7 from the cytoplasm to the nucleus through immunofluorescence (Fig. 4). The amount of p65 that was present in the nuclei of cells treated with Terpolymer-CpG was similar to those treated with Terpolymer or no particles, but significantly lower than those treated with Terpolymer-adsorb CpG particles. IRF-7 was present at significantly higher amounts in the nuclei of cells treated with Terpolymer-CpG and Terpolymer-adsorbed CpG particles than in the nuclei of cells treated with Terpolymer or no particles. We did notice that the overall level of IRF-7 was reduced in cells treated with Terpolymer-CpG in comparison to cells treated with Terpolymer-adsorb CpG particles. We speculate that the level of IRF-7 is regulated by NF-κb as suggested by previous

studies [43-45]. Our results so far suggest that Terpolymer-CpG is able to regulate TLR9 signaling by selectively activating the IRF-7 pathway, but not the NF-κB pathway.

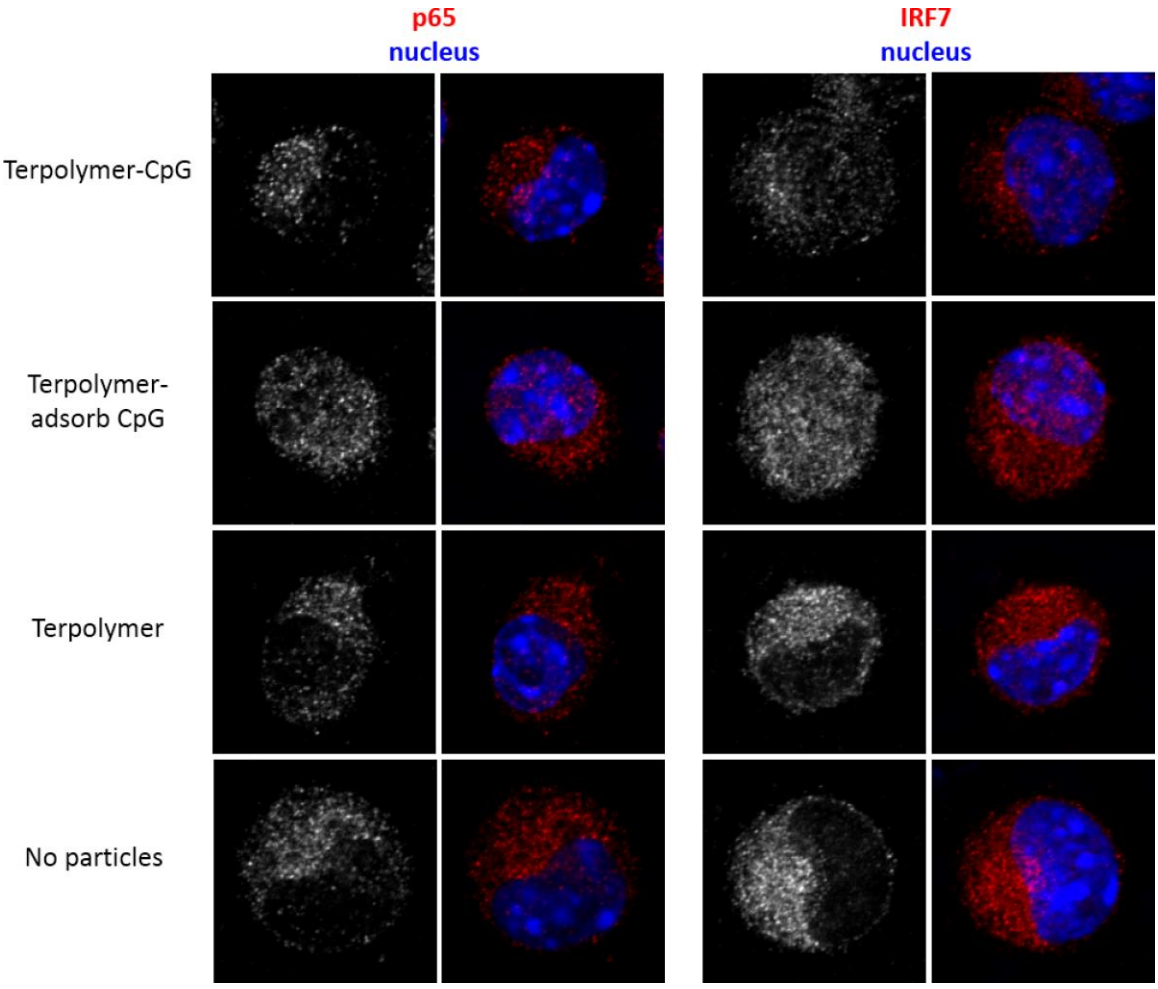

Fig. 4. Effect of Terpolymer-CpG particles on the nuclear translocation of transcription factors. Particles were incubated with BC-1 cells for 4 h at 37 °C followed by a 3 h chase. Next, cells were stained with either rabbit anti-p65 or rabbit anti-IRF7, followed by the detection antibody, Cy3-goat anti-rabbit IgG (red). Nuclei were stained with DAPI (blue). 11 ~ 35 cells in total were examined for each sample.

2.4.5 Mechanisms of selectively targeting the IRF-7 pathway by Terpolymer-CpG

Next we attempted to understand the mechanisms by which Terpolymer-CpG selectively targeted the IRF-7 pathway. Endosomal pH is known to affect TLR9 signaling. The recruitment of TLR9 to endocytic compartments is pH-dependent, and the interaction between TLR9 and

CpG ODNs requires the acidification of endosomes [15, 46]. Our previous studies have also shown that pro-inflammatory cytokines are induced when TLR9 signaling occurred in a more basic environment (pH > 6.0) as well as a more acidic environment. The induction of type I IFNs required the acidification of endosomal compartments. First we measured the pH of endosomal compartments containing Terpolymer-CpG. After a 3 h pulse and 4 h chase, the endosomal pH was 5.08 and 4.82 for 50 and 100 μg/ml of Terpolymer-CpG particles, respectively (Fig. 5A). We hypothesized that it was possible that Terpolymer-CpG was quickly routed to an acidic environment and did not permit the sufficient interaction between TLR9 and CpG ODNs in a more basic environment for the activation of NF-κB. We were not able to measure endosomal pH at short durations. Instead, we used NH_4Cl to buffer the acidification of endosomes as we did previously [33]. We tested a range of concentrations of NH_4Cl (Fig. 5B). At higher than 1 mM NH_4Cl, CpG 2216 adsorbed on PS beads (CpG-PLL-PS) did not induce any IL-6, indicating that the recruitment of TLR9 or the interaction of TLR9 with CpG ODNs at a more basic environment was compromised. We decided to use 1 mM of NH_4Cl to test whether raising the pH could rescue the signaling of TLR9 for the generation of IL-6. The presence of 1 mM of NH_4Cl raised the endosomal pH by 0.20 and 0.24 pH units for 100 and 50 μg of Terpolymer-CpG particle/ml, respectively (Fig. 5A), and the IFN-α response induced by Terpolymer-CpG significantly reduced (Fig. 5B) as expected. Still, no IL-6 was detected. In contrast, in the presence of NH_4Cl at 1 mM, CpG 2216-coated PS beads (2216-PLL-PS) induced less IFN-α, but IL-6 production was unaffected (Fig. 5B), consistent with our previous observations [33]. These results demonstrate that the retention of Terpolymer-CpG in a less acidic environment did not promote the interaction of CpG 2216 with TLR9 for the induction of pro-inflammatory cytokines.

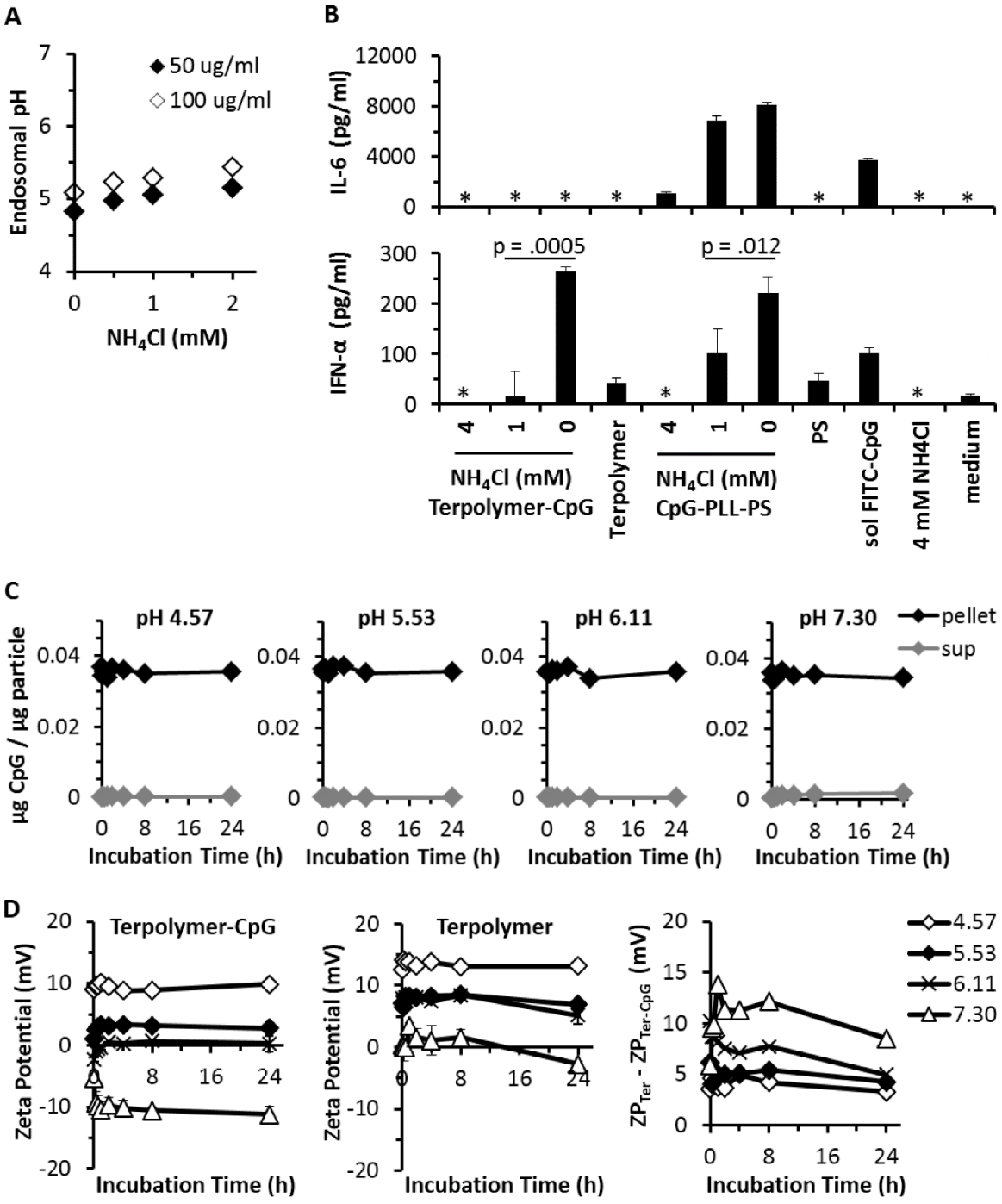

Fig. 5. Mechanisms of selectively targeting IRF-7 pathway by Terpolymer-CpG particles. (A) The pH of particle-containing endosomes 6 h after cells were exposed to Terpolymer-CpG at 50 and 100 µg particle/ml. (B) The level of IL-6 and IFN-α secreted by BC-1 cells after 24 h-incubation with Terpolymer-CpG and CpG-PLL-PS. 5 µg/ml of soluble CpG 2216 was used. The * symbol indicates that the cytokine level was undetectable. (C) Effect of pH on the release profile of CpG 2216 from Terpolymer-CpG. Particles were incubated in 10 mM citric acid and 20 mM disodium hydrogen phosphate at 37 °C. "Pellet" indicates the amount of CpG 2216 in particles, and "sup" indicates the CpG 2216 released from particles. (D) Effect of pH on the zeta

potential (surface charge) of Terpolymer-CpG. Particles were incubated in 10 mM citric acid and 20 mM disodium hydrogen phosphate at 37 °C. The surface charge of Terpolymer-CpG and Terpolymer were measured at 37 °C. "$ZP_{Terpolymer}$-$ZP_{Ter\text{-}CpG}$" is the difference between the surface charge of Terpolymer and Terpolymer-CpG.

We then measured the quantity of CpG 2216 that was released from Terpolymer-CpG under conditions that mimicked the pH and temperature that endocytosed particles were exposed to. Surprisingly, throughout the period of 24 h, the amount of CpG 2216 that was released from particles was negligible at pH 4.57 to 6.11 (Fig. 5C), which is the pH range of endocytic compartments. At pH 7.30, the pH of the extracellular environment, approximately 5% of the incorporated CpG was released from the particles. This indicated that most of the CpG was retained in the particles prior to and after particle internalization. The release of CpG 2216 at different pH environments was unlikely the factor for selectively targeting the IRF-7 pathway.

CpG 2216 was retained in particles within a range of pH 4.57 to 6.11 (Fig. 5C). Then we tested whether CpG 2216 was present on the surface of Terpolymer-CpG within the pH range of endocytic compartments. We measured the surface charge of Terpolymer-CpG and Terpolymer (particles without CpG ODNs) and compared them to determine whether CpG 2216 was exposed at the particle surface at pHs between 5 and 7 (Fig. 5D). In the terpolymer, the two functional units in PAA and DMAEMA have a pK_a of 6.7 and 7.5, respectively [38, 39]. The pK_a of both monomers was expected to increase within a polymer matrix. Nearly all of the DMAEMA was expected to be ionized within the pH range of endosomal compartments suggested by the zeta potential change of Dipolymer 1:1 (Fig. 2B), and 50% of PAA to be ionized at pH 6.5 suggested by the zeta potential change of blend particles containing a dipolymer of BMA and PAA (1:1) (Data not shown). Ionized DMAEMA endowed the terpolymer particles with a positively charged surface (and positive zeta potential) while ionized PAA yielded a negative charge. The

zeta potential of Terpolymer particles (without CpG 2216) between pH 4.57 and 6.11 decreased from 13 to 7 mV, indicating more and more PAA was de-ionized and counteracted the positive charge of DMAEMA. The CpG 2216 was negatively charged and expected to counteract the positive charge of the terpolymer as well. Between pH 7.30 and 4.57, the surface charge of Terpolymer-CpG was less than that of Terpolymer particles, which suggested that a portion of CpG 2216 was displayed on the surface of particles at the pH of all the endocytic compartments.

Then we asked whether the terpolymer would affect the interaction of binding between TLR9 and CpG 2216 at different pHs. The TLR9 structure has not been resolved yet. But the structure of TLR3, which binds to double stranded RNA (dsRNA), has been resolved recently [47, 48]. It has been suggested that the phosphodiester backbone contributes to critical interactions but not the base sequence of the RNA. Histidines are the key residues of TLR3 that interact with dsRNA [49, 50]. The binding of TLR9 to ssDNA is suggested to be similar to that of TLR3 to dsRNA [51]. At a more basic pH, more PAA was ionized and negatively charged, which might compete with the interaction between CpG 2216 and TLR9. This is also consistent with our observation that Dipolymer 3:1, which only consisted of DMAEMA, was able to stimulate IL-6. At pH 5.53 and 4.57, the majority of PAA was de-ionized, which left more opportunities for CpG 2216 to interact with TLR9 for the activation of the IRF-7 pathway. So far we do not have the direct evidence to prove the above speculation. Detailed structural studies, surface analysis and the survey of a library of different compositions of Terpolymer (such as varying ratios of PAA and DMAEMA) will elucidate mechanisms of selectively targeting TLR9 signaling pathways by Terpolymer-CpG blend particles.

2.5 Conclusion

Our results have demonstrated the use of polymer blend particles for the controlled activation of TLR9 signaling pathways. Terpolymer blend particles exhibit the unique ability to present Type A CpG ODNs to TLR9 and induce IRF-7 activation only. To our knowledge, the selective activation of the IRF-7 pathway has not yet been shown. In the context of cancer immunotherapy, the selective activation of IRF-7 pathway could potentially enhance the apoptosis of tumor cells and immunological control of tumor progression without inadvertently activating NF-κB-dependent oncogenesis. Broadly, blend particles offer an excellent biomaterial tool for finely tailoring both innate and adaptive immunity instigated through TLR9 signaling, and for understanding molecular and cellular mechanisms underlying the bifurcation of TLR9 signaling.

2.6 References

[1] Krieg AM. Therapeutic potential of Toll-like receptor 9 activation. Nat Rev Drug Discov. 2006;5:471-84.
[2] Hemmi H, Takeuchi O, Kawai T, Kaisho T, Sato S, Sanjo H, et al. A Toll-like receptor recognizes bacterial DNA. Nature. 2000;408:740-5.
[3] Krug A, Luker GD, Barchet W, Leib DA, Akira S, Colonna M. Herpes simplex virus type 1 activates murine natural interferon-producing cells through toll-like receptor 9. Blood. 2004;103:1433-7.
[4] Lund J, Sato A, Akira S, Medzhitov R, Iwasaki A. Toll-like receptor 9-mediated recognition of herpes simplex virus-2 by plasmacytoid dendritic cells. J Exp Med. 2003;198:513-20.
[5] Krug A, French AR, Barchet W, Fischer JAA, Dzionek A, Pingel JT, et al. TLR9-dependent recognition of MCMV by IPC and DC generates coordinated cytokine responses that activate antiviral NK cell function. Immunity. 2004;21:107-19.
[6] Ramirez-Ortiz ZG, Specht CA, Wang JP, Lee CK, Bartholomeu DC, Gazzinelli RT, et al. Toll-like receptor 9-dependent immune activation by unmethylated CpG motifs in Aspergillus fumigatus DNA. Infect Immun. 2008;76:2123-9.
[7] Nakamura K, Miyazato A, Xiao G, Hatta M, Inden K, Aoyagi T, et al. Deoxynucleic acids from Cryptococcus neoformans activate myeloid dendritic cells via a TLR9-dependent pathway. J Immunol. 2008;180:4067-74.
[8] Means TK, Latz E, Hayashi F, Murali MR, Golenbock DT, Luster AD. Human lupus autoantibody-DNA complexes activate DCs through cooperation of CD32 and TLR9. J Clin Invest. 2005;115:407-17.

[9] Barrat FJ, Meeker T, Gregorio J, Chan JH, Uematsu S, Akira S, et al. Nucleic acids of mammalian origin can act as endogenous ligands for toll-like receptors and may promote systemic lupus erythematosus. J Exp Med. 2005;202:1131-9.
[10] Leadbetter EA, Rifkin IR, Hohlbaum AM, Beaudette BC, Shlomchik MJ, Marshak-Rothstein A. Chromatin-IgG complexes activate B cells by dual engagement of IgM and Toll-like receptors. Nature. 2002;416:603-7.
[11] Boule MW, Broughton C, Mackay F, Akira S, Marshak-Rothstein A, Rifkin IR. Toll-like receptor 9-dependent and -independent dendritic cell activation by chromatin-immunoglobulin G complexes. J Exp Med. 2004;199:1631-40.
[12] Kandimalla ER, Bhagat L, Li YK, Yu D, Wang D, Cong YP, et al. Immunomodulatory oligonucleotides containing a cytosine-phosphate-2'-deoxy-7-deazaguanosine motif as potent toll-like receptor 9 agonists. P Natl Acad Sci USA. 2005;102:6925-30.
[13] Krieg AM. CpG motifs in bacterial DNA and their immune effects. Annu Rev Immunol. 2002;20:709-60.
[14] Krieg AM. CpG Still Rocks! Update on an Accidental Drug. Nucleic Acid Ther. 2012;22:77-89.
[15] Latz E, Schoenemeyer A, Visintin A, Fitzgerald KA, Monks BG, Knetter CF, et al. TLR9 signals after translocating from the ER to CpG DNA in the lysosome. Nat Immunol. 2004;5:190-8.
[16] Ewald SE, Lee BL, Lau L, Wickliffe KE, Shi GP, Chapman HA, et al. The ectodomain of Toll-like receptor 9 is cleaved to generate a functional receptor. Nature. 2008;456:658-U88.
[17] Akira S, Uematsu S, Takeuchi O. Pathogen recognition and innate immunity. Cell. 2006;124:783-801.
[18] Honda K, Yanai H, Takaoka A, Taniguchi T. Regulation of the type IIFN induction: a current view. Int Immunol. 2005;17:1367-78.
[19] Aggarwal BB. Nuclear factor-kappa-B: The enemy within. Cancer Cell. 2004;6:203-8.
[20] Karin M, Greten FR. NF kappa B: Linking inflammation and immunity to cancer development and progression. Nat Rev Immunol. 2005;5:749-59.
[21] Dolcet X, Llobet D, Pallares J, Matias-Guiu X. NF-kB in development and progression of human cancer. Virchows Arch. 2005;446:475-82.
[22] Bharti AC, Shishodia S, Reuben JM, Weber D, Alexanian R, Raj-Vadhan S, et al. Nuclear factor-kappa B and STAT3 are constitutively active in CD138(+) cells derived from multiple myeloma patients, and suppression of these transcription factors leads to apoptosis. Blood. 2004;103:3175-84.
[23] Hideshima T, Chauhan D, Richardson P, Mitsiades C, Mitsiades N, Hayashi T, et al. NF-kappa B as a therapeutic target in multiple myeloma. J Biol Chem. 2002;277:16639-47.
[24] Giri DK, Aggarwal BB. Constitutive activation of NF-kappa B causes resistance to apoptosis in human cutaneous T cell lymphoma HuT-78 cells - Autocrine role of tumor necrosis factor and reactive oxygen intermediates. J Biol Chem. 1998;273:14008-14.
[25] Rabi T, Shukla S, Gupta S. Betulinic Acid Suppresses Constitutive and TNF alpha-Induced NF-kappa B Activation and Induces Apoptosis in Human Prostate Carcinoma PC-3 Cells. Mol Carcinogen. 2008;47:964-73.
[26] Biswas DK, Shi Q, Baily S, Strickland I, Ghosh S, Pardee AB, et al. NF-KB activation in human breast cancer specimens and its role in cell proliferation and apoptosis. P Natl Acad Sci USA. 2004;101:10137-42.

[27] Chiron D, Pellat-Deceunynck C, Amiot M, Bataille R, Jego G. TLR3 Ligand Induces NF-kappa B Activation and Various Fates of Multiple Myeloma Cells Depending on IFN-alpha Production. J Immunol. 2009;182:4471-8.
[28] Fuertes MB, Kacha AK, Kline J, Woo SR, Kranz DM, Murphy KM, et al. Host type I IFN signals are required for antitumor CD8(+) T cell responses through CD8 alpha(+) dendritic cells. J Exp Med. 2011;208:2005-16.
[29] Diamond MS, Kinder M, Matsushita H, Mashayekhi M, Dunn GP, Archambault JM, et al. Type I interferon is selectively required by dendritic cells for immune rejection of tumors. J Exp Med. 2011;208:1989-2003.
[30] Lorenzi S, Mattei F, Sistigu A, Bracci L, Spadaro F, Sanchez M, et al. Type I IFNs Control Antigen Retention and Survival of CD8 alpha(+) Dendritic Cells after Uptake of Tumor Apoptotic Cells Leading to Cross-Priming. J Immunol. 2011;186:5142-50.
[31] Swann JB, Hayakawa Y, Zerafa N, Sheehan KCF, Scott B, Schreiber RD, et al. Type I IFN contributes to NK cell homeostasis, activation, and antitumor function. J Immunol. 2007;178:7540-9.
[32] Bidwell BN, Slaney CY, Withana NP, Forster S, Cao Y, Loi S, et al. Silencing of Irf7 pathways in breast cancer cells promotes bone metastasis through immune escape. Nat Med. 2012;18:1224-+.
[33] Chen HC, Sun BB, Tran KK, Shen H. Effects of particle size on toll-like receptor 9-mediated cytokine profiles. Biomaterials. 2011;32:1731-7.
[34] Takeda N, Nakamura E, Yokoyama M, Okano T. Temperature-responsive polymeric carriers incorporating hydrophobic monomers for effective transfection in small doses. J Control Release. 2004;95:343-55.
[35] Ferrito MT, D.A. Poly(2-ethylacrylic acid). Macromolecular Syntheses. 1992;11:59-62.
[36] Tran KK, Shen H. The role of phagosomal pH on the size-dependent efficiency of cross-presentation by dendritic cells. Biomaterials. 2009;30:1356-62.
[37] Dalod M, Salazar-Mather TP, Malmgaard L, Lewis C, Asselin-Paturel C, Briere F, et al. Interferon alpha/beta and interleukin 12 responses to viral infections: Pathways regulating dendritic cell cytokine expression in vivo. J Exp Med. 2002;195:517-28.
[38] Grainger SJE-S, M.E.H. Stimuli-Sensitive Particles for Drug Delivery. Biologically-Responsive Hybrid Biomaterials. Singapore: World Scientific Publishing 2010. p. 171-90.
[39] van de Wetering P, Moret EE, Schuurmans-Nieuwenbroek NME, van Steenbergen MJ, Hennink WE. Structure-activity relationships of water-soluble cationic methacrylate/methacrylamide polymers for nonviral gene delivery. Bioconjugate Chem. 1999;10:589-97.
[40] Convertine AJ, Benoit DSW, Duvall CL, Hoffman AS, Stayton PS. Development of a novel endosomolytic diblock copolymer for siRNA delivery. J Control Release. 2009;133:221-9.
[41] Shen H, Ackerman AL, Cody V, Giodini A, Hinson ER, Cresswell P, et al. Enhanced and prolonged cross-presentation following endosomal escape of exogenous antigens encapsulated in biodegradable nanoparticles. Immunology. 2006;117:78-88.
[42] Yanagawa Y, Iijima N, Iwabuchi K, Onoe K. Activation of extracellular signal-related kinase by TNF-alpha controls the maturation and function of murine dendritic cells. J Leukocyte Biol. 2002;71:125-32.
[43] Sharma S, tenOever BR, Grandvaux N, Zhou GP, Lin RT, Hiscott J. Triggering the interferon antiviral response through an IKK-related pathway. Science. 2003;300:1148-51.

[44] Fitzgerald KA, McWhirter SM, Faia KL, Rowe DC, Latz E, Golenbock DT, et al. IKK epsilon and TBK1 are essential components of the IRF3 signaling pathway. Nat Immunol. 2003;4:491-6.
[45] Sato M, Suemori H, Hata N, Asagiri M, Ogasawara K, Nakao K, et al. Distinct and essential roles of transcription factors IRF-3 and IRF-7 in response to viruses for IFN-alpha/beta gene induction. Immunity. 2000;13:539-48.
[46] Ahmad-Nejad P, Hacker H, Rutz M, Bauer S, Vabulas RM, Wagner H. Bacterial CpG-DNA and lipopolysaccharides activate Toll-like receptors at distinct cellular compartments. Eur J Immunol. 2002;32:1958-68.
[47] Bell JK, Botos I, Hall PR, Askins J, Shiloach J, Segal DM, et al. The molecular structure of the Toll-like receptor 3 ligand-binding domain. P Natl Acad Sci USA. 2005;102:10976-80.
[48] Choe J, Kelker MS, Wilson IA. Crystal structure of human Toll-like receptor 3 (TLR3) ectodomain. Science. 2005;309:581-5.
[49] Bell JK, Askins J, Hall PR, Davies DR, Segal DM. The dsRNA binding site of human toll-like receptor 3. Faseb J. 2006;20:A96-A.
[50] Liu L, Botos I, Wang Y, Leonard JN, Shiloach J, Segal DM, et al. Structural basis of toll-like receptor 3 signaling with double-stranded RNA. Science. 2008;320:379-81.
[51] Peter ME, Kubarenko AV, Weber ANR, Dalpke AH. Identification of an N-Terminal Recognition Site in TLR9 That Contributes to CpG-DNA-Mediated Receptor Activation. J Immunol. 2009;182:7690-7.

Chapter 3: Characterization of breast cancer cell responsiveness to Terpolymer particles

3.1 Abstract

TLR3 and TLR9 ligands encapsulated in terpolymer particles were used to treat triple negative breast cancer (TNBC) cell lines. The effect of terpolymer particles on cells was characterized by quantifying the cell proliferation, cell death, and cell migration, and by evaluating the cytokine secretion profile. All types of particle treatments were ineffective at inhibiting MDA-MB-231 cell proliferation and inducing cell death after 3 and 6 days of treatment. Ter-polyIC induced type I IFN secretion from BT-20 cells and was the most effective at inhibiting BT-20 cell proliferation and inducing cell death. However, residual BT-20 cells remained after Ter-polyIC treatment. The live and dead BT-20 cells were characterized by their expression level of CD44, a marker associated with the metastasis of breast cancer cells. Three CD44 cell subpopulations were identified: CD44 low, medium, and high. Ter-polyIC treatment induced dose-dependent cell death of CD44 medium cells only, while having no effect on the viability of the CD44 high subpopulation.

3.2 Introduction

Type I IFNs were initially recognized for their antiviral activity because they were effective treatments for common colds [1], herpes virus infections [2], chicken pox [3], and hepatitis B virus [4]. Over the past five decades, additional functions of type I IFNs have been discovered: type I IFNs enhance T cell, dendritic cell, and NK cell activation; promote cell differentiation; and induce apoptosis and cell cycle arrest [5, 6]. In the context of cancer therapy, type I IFNs are used as anticancer drugs for hairy-cell leukemia, malignant melanoma, and follicular lymphoma [7]. Although type I IFNs have been widely studied in cancer therapy (Table 1), efficacy is dependent on the sensitivity of cancer cells to type I IFN – certain cancer

cell lines are partially or completely resistant to type I IFN [8]. Type I IFN treatment of IFN-sensitive cells enhances apoptosis through various mechanisms, such as caspase activation, reduction in mitochondria membrane potential, mitochondrial release of cytochrome c [9], activation of apoptotic Bcl-2 proteins Bak and Bax in multiple myeloma cells [10]; and p53 upregulation in hepatocellular carcinoma [11].

Table 1. Type I IFN in anticancer treatment

Cancer type	Cancer cell type	Evidence of type I IFN efficacy	Ref.
MCA-induced sarcoma	H31m1	~20 days after tumor cell inoculation, tumor size diminished in WT. Administration of IFNAR1 Ab at early time points prevented tumor rejection.	[12]
	d38m2	~30 days after tumor cell inoculation, tumor size increased in Ifnar1$^{-/-}$ mice	[12]
	1969	CD8α^{+} DCs require endogenous type I IFN for tumor rejection	[12]
	Transplanted MCA-induced sarcoma	Endogenous type I IFN from host hematopoietic cells are required for tumor rejection	[13]
	Primary carcinogen (MCA)-induced tumor	Endogenous type I IFN from host hematopoietic cells are required to inhibit formation of chemical induced primary tumors	[13, 14]
Melanoma	B16.F10.SIY	Endogenous type I IFN signaling is required for CD8α^{+} DC to prime CD8^{+} T cells and reduce tumor size	[15]
	B16.F10	Endogenous type I IFN signaling is required for tumor rejection; IL-2 cytokine therapy is compromised in IFNAR-deficient mice	[14]

Thymoma	RMA-S (mouse)	Endogenous type I IFN signaling is required for tumor rejection; it is suggested that endogenous type I IFN act on host NK cells	[14]
Lewis lung carcinoma	3LL	Endogenous type I IFN signaling is required for tumor rejection; IL-2 cytokine therapy is compromised in IFNAR-deficient mice	[14]
Friend erythroleukemia growth in mouse liver	FLC	Endogenous type I IFN signaling is required to prevent tumor growth in liver (i.v. injection of FLC into C57Bl/6 and C3H mice)	[16]
Breast	4T1.2-Irf7 (mouse)	tumor growth insensitive to IFNα1 i.p. injection; however, bone metastasis was reduced after IFNα1 i.p. injection	[17]
	MDA-MB-231	*In vitro* IFNα2 treatment → reduced cell proliferation, enhanced 2'5' oligoadenylate synthetase activity	[18]
	MCF-7	*In vitro* IFNα2 treatment → reduced cell proliferation, enhanced 2'5' oligoadenylate synthetase activity	[18]
	BT20	*In vitro* IFNα treatment → reduced cell proliferation	[19]
	Hs578T	*In vitro* IFNα treatment → reduced cell proliferation	[19]
	T1068	*In vivo* IFNα treatment → primary tumor mass reduced	[19, 20]
	ZR-75-1	*In vitro* IFNα treatment → reduced cell proliferation	[21]

Currently, tumors are treated with the systemic administration of type I IFNs. A few dosing regimens for type I IFNs are used. For example, the intermittent dosing of type I IFN is a strategy used to minimize inhibitory mechanisms due to SOCS1 induction. Intermittent type I

IFN doses at an optimized pace may prevent a negative feedback loop. In contrast, stabilized formulations of IFN-α that increase the cytokine half-life consist of PEG-conjugated IFN-α or fusion proteins with albumin [22]. Recent clinical trials for type I IFN therapy for breast cancer have included PEG-IFN-2α in combination with capecitabine; the overexpression of IFN-β; thermal therapy combined with 5-fluorouracil, Doxil, and IFN-α; and IFN-α in combination with granulocyte-macrophage colony-stimulating factor (GM-CSF).

Triple-negative breast cancer (TNBC) represents 10 to 15% of all breast cancers. TNBC cells lack the expression of estrogen receptor, progesterone receptor, and human epidermal growth factor receptor 2 (HER2). It is the most difficult type of breast cancer to treat because most chemotherapies target one of the three receptors. Patients with TNBC have a poor outcome compared to other subtypes of cancer. Treatments include a combination of surgery, radiation therapy, and chemotherapy. TNBC therapies that are currently being evaluated include poly ADP-ribose polymerase (PARP) inhibitors [23], cisplatin [24], carboplatin, and paclitaxel.

It was shown in Chapter 2 that the stimulation of TLR9 with Ter-CpG particles can be controlled to induce type I IFN induction only. Ter-CpG particles failed to activate NF-κB. We hypothesize that the controlled activation of TLR9 through Ter-CpG particles would be an effective treatment for cancer cells. TLR9 is constitutively expressed in numerous cancer cell lines and cancer tissues (Table 2). Given the challenges in TNBC treatment, we chose to test our system on TNBC cell lines which have endogenous TLR9 expression and are sensitive to type I IFN.

Table 2. Constitutive TLR9 expression in various tumor cells and tumor tissues

Cancer type	Cancer cell type	Cancer tissue	Method(s) to assess constitutive TLR9 expression	Note	Ref.
Breast	MDA-MB-231		DNA array Flow cytometry IHC Western blot RT-PCR [25] RT-PCR; flow [26]	Stimulants: -Type A, B, C CpG ODN -non-CpG ODN	[25-27]
	4T1 (mouse)		RT-PCR	Low TLR9 expression No TLR9 expression[28]	[29, 30]
	T47-D		RT-PCR [25, 31] Western blot [27]	Low TLR9 expression	[25, 27, 31]
	MCF-7		RT-PCR [31] Western blot [27]	Low TLR9 expression	[27, 31]

	BT-20		RT-PCR	High TLR9 expression	[25]
	Hs578T		RT-PCR		[25]
	HBL-100		RT-PCR	Low TLR9 expression	[25]
		Breast cancer specimens	RT-PCR	10 of 12 specimens	[31]
		Breast cancer specimens	Western blot	73 of 74 patients	[32]
Brain	U373 astrocytoma		Western blot		[27]
	D54MG glioblastoma		Western blot		[27]
	GL261 glioma (mouse)		RT-PCR flow cytometry	CpG 1826 induced GL261 apoptosis in vitro	[33]
	U251 glioma		RT-PCR flow cytometry[33] ICC		[33, 34]
	U87 glioma		RT-PCR flow cytometry[33] ICC		[33, 34]
Gastric cancer		Intestinal gastric carcinoma	IHC	Focal and weak TLR9 expression in 6 of 22 gastric carcinomas	[35]
Non-small cell lung carcinoma		Squamous cell	IHC RT-PCR	No expression: 1 Weak: 14	[36]

		carcinoma of the lung		Strong: 8	
	A549		IHC	Stimulant: CpG M362 (type C)	[36]
	NCI-H727		IHC		[36]
	NCI-H23		IHC		[36]
	NCI-H125		IHC		[36]
Small cell lung carcinoma	CPC-N		IHC		[36]
Large cell lung carcinoma	NCI-H157		IHC		[36]
		Large cell carcinoma of the lung	IHC RT-PCR	No expression: 0 Weak: 2 Strong: 1	[36]
Lung adenocarcinoma	DV-90		IHC		[36]
		Adenocarcinoma of the lung	IHC RT-PCR	No expression:1 Weak: 7 Strong: 13	[36]
Cervical	HeLa (epithelial)		IHC [36] RT-PCR [37]	Stimulant: CpG M362 (type C)	[36, 37]
		Cervical intraepithelial neoplasia	IHC	Low grade CIN < high grade CIN < ISCC	[38]
		invasive squamous cell carcinoma	IHC RT-PCR		[38]
T cell leukemia	Jurkat (T cell)		IHC		[36]

Hodgkin lymphoma	L-428		IHC		[36]
Burkitt's lymphoma	Raji		IHC		[36]
Histiocytic lymphoma	U937 (macrophage)		IHC		[36]
Liver cancer	HepG2		RT-PCR		[37]
Prostate cancer	RM1 (mouse)		RT-PCR		[29]
	PC-3		Western blot	Intermediate TLR9 expression	[39]
	LnCaP		Western blot	High TLR9 expression	[39]
	C4-2B		Western blot	High TLR9 expression	[39]
	Du-145		Western blot	Intermediate TLR9 expression	[39]
		Prostate cancer tissue	IHC		[39]
Melanoma	B16 (mouse)		RT-PCR	Low TLR9 expression	[29]

3.3 Materials and Methods

3.3.1 Cell culture

BT-20 cells were a generous gift from Dr. David M. Hockenbery (Fred Hutchinson Cancer Research Center) and were maintained in RPMI 1640 supplemented with 10% fetal bovine serum (FBS), 1% penicillin/streptomycin, 2 mM L-glutamine, 25 mM 4-(2-hydroxyethyl)-1-piperazineethanesulfonic acid (HEPES buffer), and 1 mM sodium pyruvate. MDA-MB-231 cells were a generous gift from Yitong J. Zhang (Professor Tomikazu Sasaki's

lab, Department of Chemistry, UW). BHK-21 cells were a generous gift from Dr. Michael G. Katze. MDA-MB-231 cells and BHK-21 cells were maintained in DMEM supplemented with 4.5 g/L glucose, 10% FBS, 1% penicillin/streptomycin, and 4 mM L-glutamine. Vero cells were purchased from ATCC and were maintained in DMEM/low glucose, 10% FBS, and 1% penicillin/streptomycin. The single cell suspension of splenocytes was obtained from C57BL/6 mice (Jackson Laboratory) and prepared as described in Chapter 2.

3.3.2 Preparation and characterization of polymer blend particles

Blend particles containing a pH-sensitive terpolymer and HiLyte 647-labeled PLGA were fabricated by Xi Zhan by using the double emulsion method as described in Chapter 2. 1 mg polyIC (Sigma), a synthetic dsRNA that activates TLR3, was incorporated into particles and named Ter-polyIC. 1 mg CpG ODN 2216 or 1 mg GpC ODN 2216 (TriLink Biotechnologies) was incorporated into particles and named Ter-CpG or Ter-GpC ctrl, respectively.

PolyIC-coated terpolymer particles were fabricated by controlling the amount of polyIC adsorbed onto the surface. The fabrication method was described in Chapter 2. A high concentration (0.3 mg/ml polyIC in 10 mM KNO_3) or a low concentration (0.008 mg/ml in 10 mM KNO_3) of polyIC was used to control the amount of polyIC loaded onto Ter-adsorb polyIC high and Ter-adsorb polyIC low particles.

3.3.3 Quantification of polyIC loading in blend particles

Blank terpolymer particles were prepared in 50 µl of 1% (w/w) sodium dodecyl sulfate (SDS)/0.1 M NaOH, and subsequently incubated in a water bath at 90 °C for 5 min to dissolve the particles. In parallel, a known concentration of soluble polyIC was prepared in 1% (w/w) SDS/0.1 M NaOH and subjected to heating. The blank terpolymer particles were added at 2 mg particle/ml to known concentrations of soluble polyIC and the mixture was used as a standard

curve. Samples of Ter-polyIC and Ter-adsorb polyIC were prepared at 2 mg particle/ml in 50 µl of 1% (w/w) SDS/0.1 M NaOH and subjected to heating. A Nanodrop instrument in Professor Wenqing Xu's lab (Department of Structural Biology, UW) was used to measure the absorbance at 260 nm. To quantify polyIC, the absorbance of blank terpolymer particles in solvent was subtracted from the absorbance of samples.

3.3.4 Quantification of polyIC released from particles at 37 °C at different pHs

To determine the release of polyIC from particles, particles were incubated in buffer solutions that mimicked the pH and temperature that endocytosed particles were exposed to. The buffer solutions were composed of 10 mM citric acid and 20 mM disodium hydrogen phosphate at pH 4.57 to 7.30. Particles were diluted in the buffer solutions at room temperature, and aliquoted at 0.1 ml (3.2 mg particles) per micro-centrifuge tube. Next, the aliquots were immersed in a water bath at 37 °C. At the given time point, an aliquot was centrifuged at 13,200 rpm for 10 min at room temperature. The supernatant was collected and the pellet was dissolved in 0.1 ml 1% (w/w) SDS/0.1 M NaOH. The polyIC in the supernatant and pellet were quantified according to the procedure stated above.

3.3.5 MTT assay

BT-20 cells and MDA-MB-231 cells were plated at 1×10^5 cell/well and 3×10^4 cell/well, respectively, in 24-well plates and incubated overnight. Cells were pulsed with 0.5 ml stimulants for 4 h unless specified. A pulsed exposure was used to more closely mimic the temporary exposure of particles to cancer cells *in vivo*. After 1, 3, or 6 days, 0.2 ml of media was removed from the well. Next, 0.2 ml of MTT reagent (Sigma) was added to each well so that the final MTT reagent concentration in the well was 2 mg/ml. The cells were incubated with MTT

reagent for 1 h 15 min at 37 °C. Next, 1.5 ml DMSO was added to each well and cells were incubated at 37 °C for 30 min. The sample absorbance was measured at 570 nm.

3.3.6 Flow cytometry

To examine the effect of stimulants on MDA-MB-231 cell death, cells were plated at 3×10^4 cell/well in 24-well plates and incubated overnight. To examine the effect of stimulants on cell proliferation, MDA-MB-231 cells were stained in a separate set of experiments with 0.5 µM carboxyfluorescein diacetate, succinimidyl ester (CFSE, Invitrogen) prior to plating cells in 24-well plates. Stimulants were added to cells in 0.5 ml media and incubated for the indicated duration. As positive controls, cells were incubated with human leukocyte type I IFN (Sigma) at 10,000 units/ml, or camptothecin (Sigma) at 5 µM for 3 days. For cell death experiments, cells were stained for Annexin-V-Alexa Fluor 488 and 7-AAD (PerCP-Cy5.5) by following the manufacturer's protocol.

To examine the effects of stimulants on BT-20 cell death, BT-20 cells were plated at 1×10^5 cell/well in 24-well plates and incubated overnight. Cells were pulsed with 0.5 ml stimulants for 4 h. Next, cells were washed twice with DPBS and 0.5 ml media was added to the well. After 1, 3, or 6 days, cells were prepared for flow cytometry. Briefly, cells were incubated in human IgG at 10 µg/ml for 15 min at RT. Cells were incubated with anti-CD44-PE-Cy7 at 0.25 µg/ml for 20 min at 4 °C. Next, cells were stained for Annexin-V-Alexa Fluor 488 and 7-AAD (PerCP-Cy5.5) by following the manufacturer's protocol. Cells were analyzed using a FACSCanto (University of Washington). The geometric mean fluorescence intensity (gMFI) of cells and particles was determined by FlowJo (Treestar, Inc., Ashland, OR).

3.3.7 Measurement of cytokine concentrations

The mouse and human IL-6 cytokine concentrations in cell supernatants were determined by enzyme-linked immunosorbent assay (ELISA). The procedures for assaying IL-6 were adapted from the manufacturer's protocol (eBioscience, San Diego, CA). The procedures for measuring mouse IFN-α were described previously [40, 41].

The human type I IFN concentrations in breast cancer cell supernatants were determined by measuring the inhibition of the cytopathic effect of supernatants on VSV-GFP-infected Vero cells. VSV-GFP was a generous gift from Dr. John Rose. For the generation of VSV-GFP stocks, BHK-21 cells were plated in a T75 flask at 90% confluence and infected with VSV-GFP in DMEM/5% FBS. After 24 h, cell debris and nuclei were removed by centrifugation at 1250 rcf × 5 min. Virus stocks were frozen in media at -80 °C. The multiplicity of infection was determined by quantifying the number of GFP-expression cells by fluorescence microscopy, as described previously [42]. Briefly, Vero cells were plated at 2.5×10^3 cell/well in 96-well plates and incubated overnight. Vero cells were infected with serial tenfold virus dilutions in 50 µl DMEM/low glucose/5% FBS for 1 h at 37 °C. Next, 50 µl DMEM/low glucose/5% FBS was added. 20 h post-infection, the GFP-expressing cells were counted under a fluorescence microscope and the multiplicity of infection was determined. For the assay of type I IFN in cell supernatants, Vero cells were incubated for 24 h with 50 µl BT-20 cell supernatants or with 50 µl type I IFN standard prepared at serial tenfold dilutions. The cell supernatants and type I IFN standard were removed and Vero cells were infected with 50 µl VSV-GFP diluted 1000:1 for 1 h at 37 °C. Next, 50 µl DMEM/low glucose/5% FBS was added. 36 h post-infection, the viable cells protected from infection were quantified by MTT assay. Briefly, cells were incubated with MTT reagent at 0.8 mg/ml for 1 h at 37 °C. Plates were centrifuged at 1400 rpm × 5 min and

MTT reagent was removed. 100 µl DMSO was added and the plate was incubated at RT until crystals dissolved. The sample absorbance was measured at 570 nm.

3.3.8 *In vitro* scratch assay

The procedure for the scratch assay was adapted from a previously described method [43]. Melanie Coyne helped to establish the method. Etches were made on the bottom of wells of 6-well plates. BT-20 cells were plated at 8×10^5 cell/well in 6-well plates and incubated for 24 h. Cells were pulsed with stimulants for 4 h, and afterward, stimulants were removed. A 200 µl pipette tip was used to make a scratch across the cell monolayer, and cell debris was washed away with PBS. Images were acquired on the first day of the scratch. Cells were incubated at 37 °C, and images were acquired every 24 h for 4 consecutive days. A Nikon microscope and 4× objective were used to acquire images. The images were analyzed by Melanie Coyne and Siri Machiraju. ImageJ was used to measure the distance between the two edges of the scratch at each etch. The average distance was determined for 18 etches for each sample.

3.3.9 Statistical analysis

A one-tailed and unpaired student t-test was used to analyze the differences between experimental groups. $p < 0.05$ is considered as a statistically significant difference between experimental groups. The * symbol indicates $p < 0.05$, and the ** symbol indicates $p > 0.05$.

3.4 Results and Discussion

3.4.1 Characterization of Ter-polyIC particles

The morphology, size and surface charge of Ter-polyIC and Ter-adsorb polyIC are shown in Figures 1 to 3. The surface charge of Ter-polyIC is similar to the surface charge of Ter-CpG. Ter-adsorb polyIC high and Ter-adsorb polyIC low were fabricated by incubating Ter particles with polyIC at 300 µg/ml and 8 µg/ml polyIC, respectively. The surface charge of Ter-

adsorb polyIC high at acidic, neutral and basic pH is less than particles containing encapsulated TLR ligands, indicating that polyIC is present on the particle surface. Ter-adsorb polyIC contain nearly ten times more polyIC than Ter-polyIC (Table 3). The surface charge of Ter-adsorb polyIC low is similar to the surface charge of blank Ter particles, and its polyIC loading is similar to that of Ter-polyIC. By TEM, the morphology of Ter-adsorb polyIC high is distinct from Ter-adsorb polyIC low and other ligand-encapsulated particles. The polyIC adsorbed on the surface of Ter-adsorb polyIC low is too low to detect a change in the morphology of particles by TEM (Figure 2).

We also fabricated Ter-GpC ctrl particles because they had a similar pH-dependent change in surface charge (Figure 1) and uptake as Ter-polyIC (Figure 4A). Therefore, Ter-GpC served as a better negative control than blank Ter particles, which are positively charged (Figure 1C) and less efficiently internalized by BT-20 cells (Figure 4A). The number of particles per cell was estimated by dividing the gMFI (APC) of cells by the gMFI (APC) of particles. The number of particles per cell was less than unity because the particles had a higher gMFI than cells containing particles. This was because the APC fluorescent intensity distribution of cells containing particles was broader than that of pure particles and had a tail that overlapped with intensity distribution of cells treated with cell culture media (Figure 4B). This suggested that some cells internalized very few particles relative to the majority of the cells. In addition, the particles themselves exhibited a high side scatter that was comparable to that of cells and cells containing particles (Figure 4C-E). This suggested that the particle events were aggregates of high fluorescence intensity instead of individual particles of lower fluorescence intensity. This was observed for each type of particle. Altogether, the relative uptake of particles was roughly Ter-polyIC ~ Ter-CpG ~ Ter-GpC ctrl << Ter.

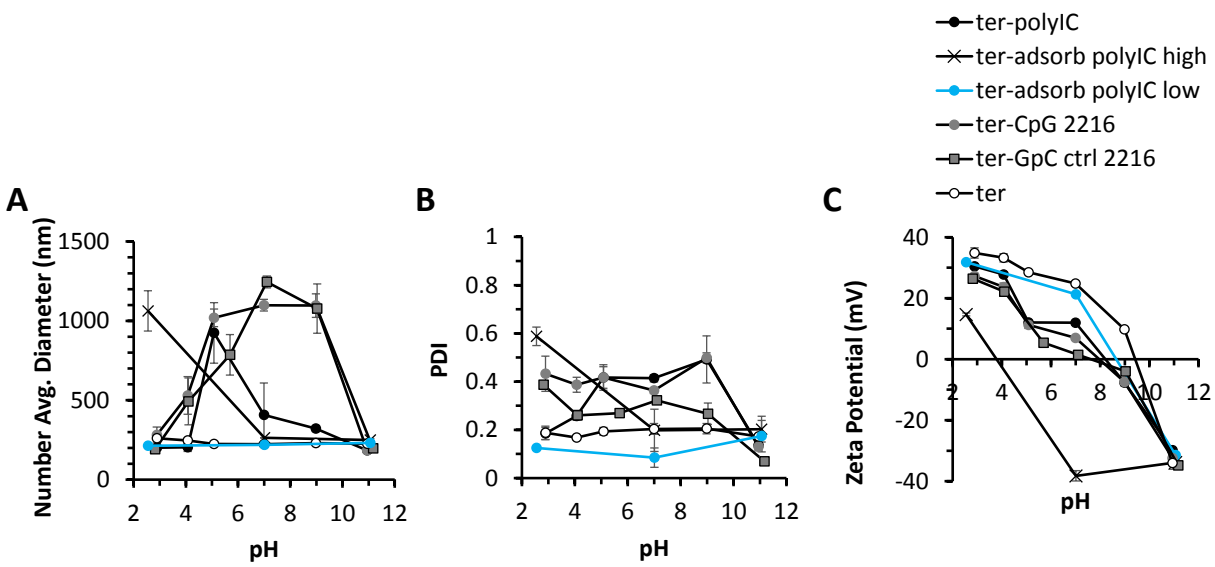

Figure 1. Characterization of Ter-polyIC, Ter-adsorb polyIC high, Ter-adsorb polyIC low and Ter-GpC particles. The (A) number average hydrodynamic diameter, (B) polydispersity index, and (C) zeta potential of polymer blend particles suspended in 10 mM KNO_3 at designated pHs at room temperature. Ter-adsorb polyIC high was fabricated by using 300 µg/ml polyIC, and Ter-adsorb polyIC low was fabricated by using 8 µg/ml polyIC for the adsorption reaction.

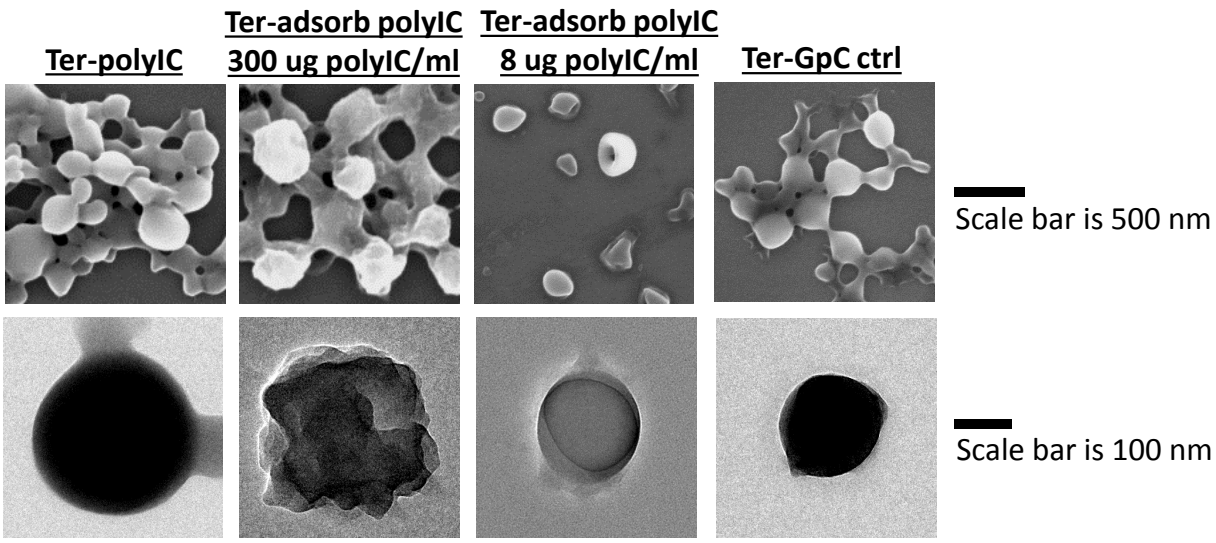

Figure 2. SEM and TEM images of Ter-polyIC, Ter-adsorb polyIC and Ter-GpC particles. SEM images and the scale bar are in the top row. TEM images and the scale bar are in the bottom row.

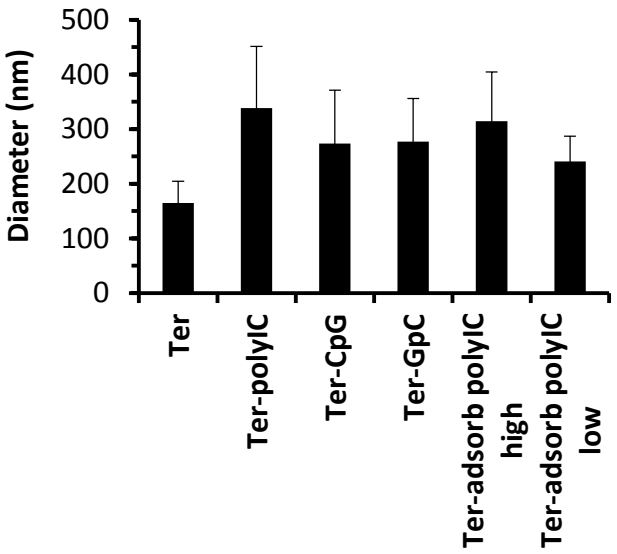

Figure 3. Size measurements of Ter-polyIC, Ter-adsorb polyIC, and Ter-GpC particles by SEM images. At least 50 particles were analyzed per particle type. The polyIC loading was quantified and is shown in Table 3.

Table 3. The polyIC loading in Ter-polyIC and Ter-adsorb polyIC. The polyIC loading was determined by quantifying the polyIC mass by absorbance measurements, and the particle mass.

Particle type	mg polyIC/mg particle
Ter-polyIC	0.015
Ter-adsorb polyIC low	0.024
Ter-adsorb polyIC high	0.12

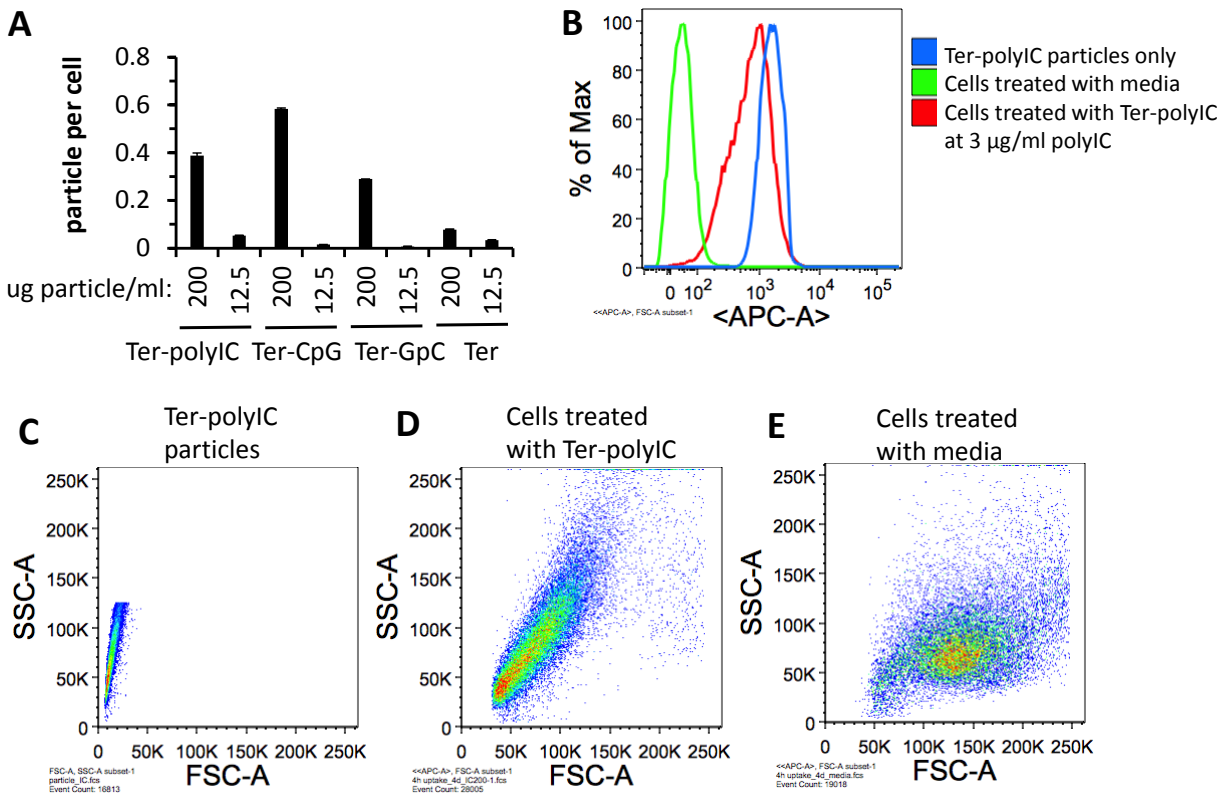

Figure 4. Relative uptake levels of polymer blend particles by BT-20 cells. Cells were incubated with particles for 4 h, then removed, and incubated for an additional 4 days and subsequently analyzed by flow cytometry. Another set of samples contained particles that were incubated in cell culture media. Particles were labeled with HiLyte647 (Chapter 2 methods section) and was detected in the APC fluorescence channel. (A) Particles per cell were quantified by dividing the gMFI of cells by the gMFI of particles. The Ter-polyIC particle concentrations (200 and 12.5 µg particle/ml) correspond to ligand concentrations of 3 and 0.2 µg polyIC/ml, respectively. The Ter-CpG and Ter-GpC particle concentrations (200 and 12.5 µg particle/ml) correspond to ligand concentrations of 8 and 0.5 µg CpG ODN 2216/ml, respectively. (B) The APC histogram of Ter-polyIC particles, cells treated with media, and cells treated with Ter-polyIC at 3 µg polyIC/ml. (C-E) The forward scatter vs. side scatter flow cytometry plots of Ter-polyIC particles, cells treated with Ter-polyIC at 3 µg polyIC/ml, and cells treated with media.

3.4.2 Cytokine secretion profile induced by Ter-polyIC from mouse splenocytes

The incorporation of polyIC into polymer blend particles resulted in an identical cytokine secretion profile as was previously obtained with Ter-CpG (Figure 5). As expected, Ter-GpC ctrl was non-immunostimulatory. Ter-polyIC was a much more potent inducer of IFN-α: 0.4

μg/ml polyIC induced a significantly higher level of IFN-α than soluble polyIC at 5 μg/ml. Soluble polyIC was less immunostimulatory than soluble CpG. The molecular weight of CpG ODN and polyIC is ~7 kDa, and 132 to 660 kDa (low molecular weight polyIC at Invivogen), respectively. The molar concentration of soluble CpG at 5 μg/ml is 1- to 4.6-fold the molar concentration of soluble polyIC at 100 μg/ml, yet soluble CpG induced 5-fold higher levels of IL-6 and IFN-α. This discrepancy may be attributed to a difference in uptake between soluble polyIC and CpG due to differences in molecular weight. Alternatively, the difference in cytokine secretion could arise from low expression levels of TLR3 relative to TLR9.

3.4.3 The cytotoxicity of Ter-polyIC is dependent on the type of triple negative breast cancer cell line

Ter-polyIC particles affected the viability of BT-20 cells, but not MDA-MB-231 cells (Figure 6). Ter-GpC was used as a negative control because they were of similar charge to Ter-polyIC (Figure 1C) and contained a non-immunostimulatory ligand (Figure 5). Compared to Ter-polyIC, the Ter-CpG and Ter-GpC ctrl were significantly less cytotoxic to BT-20 cells and MDA-MB-231 cells. It is important to note that compared to media-treated cells, the effect of Ter-GpC ctrl on BT-20 and MDA-MB-231 cell viability was significant.

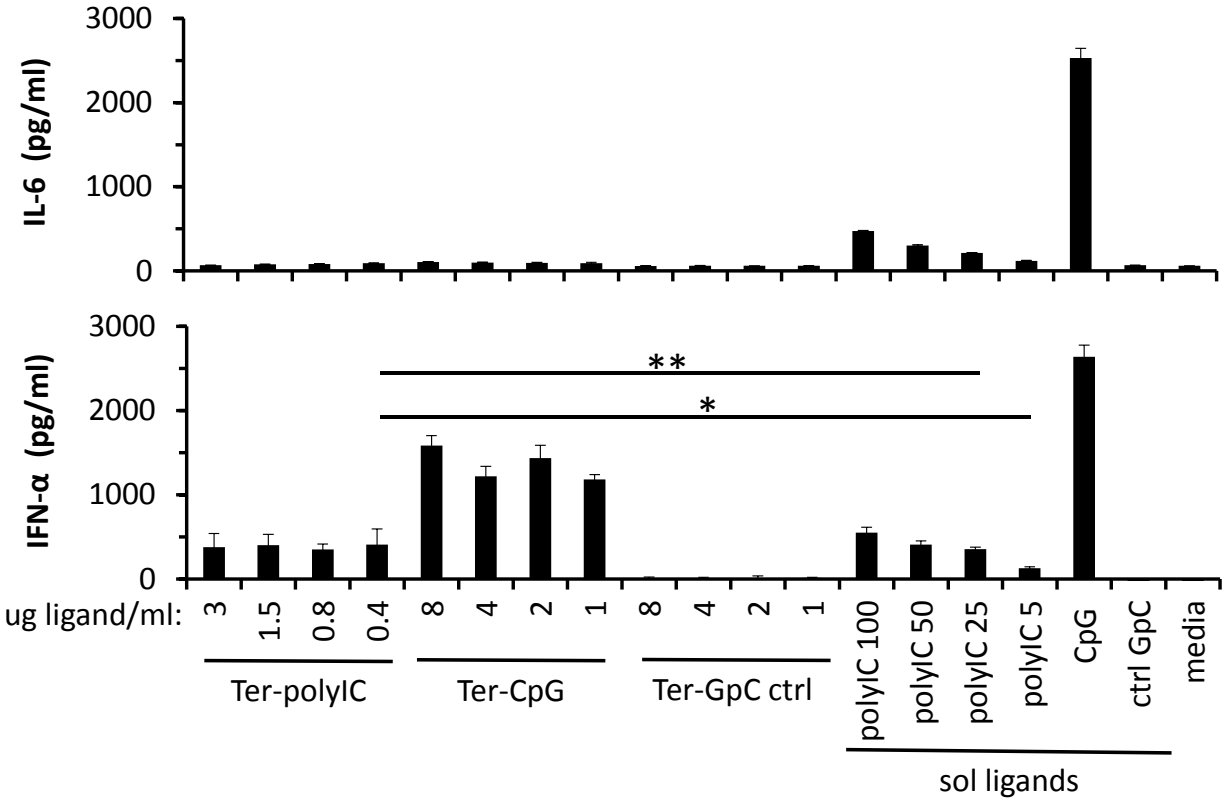

Figure 5. Cytokine secretion profile from mouse splenocytes induced by Ter-polyIC. Splenocytes were incubated with TLR3 and TLR9 ligands for 24 h. Soluble polyIC was used at 5 to 100 µg/ml, and soluble CpG and GpC ctrl were used at 5 µg/ml. A one-tailed and unpaired student t-test was used to analyze the differences between experimental groups. $p < 0.05$ is considered as a statistically significant difference between experimental groups. The * symbol indicates $p < 0.05$, and the ** symbol indicates $p > 0.05$.

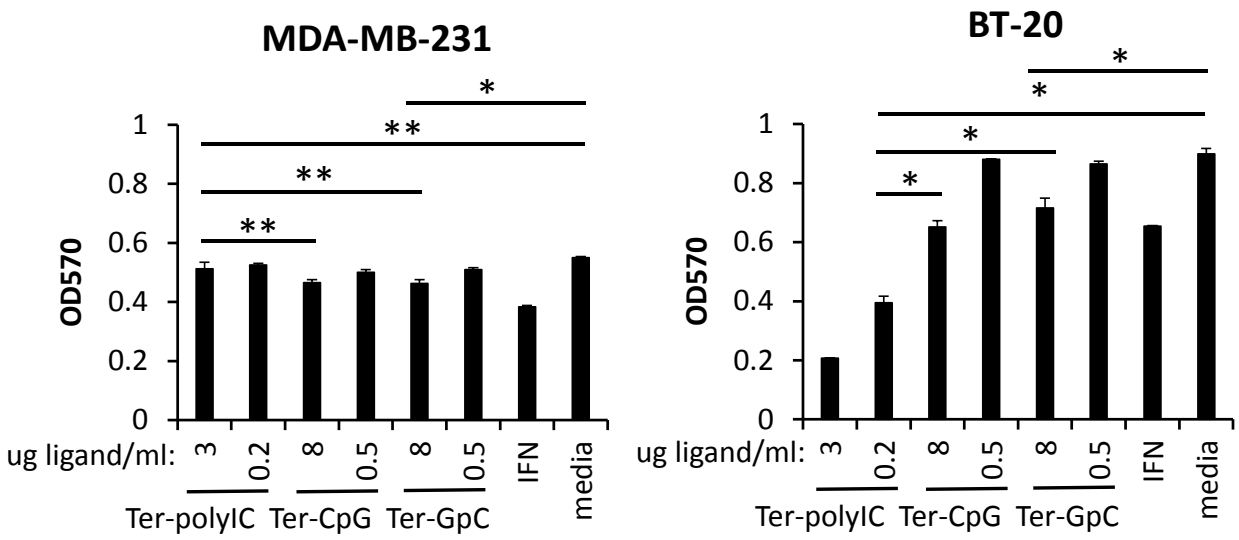

Figure 6. Effect of Ter-polyIC on MDA-MB-231 and BT-20 cell proliferation. Cells were pulsed with particles for 4 h, and MTT analysis was performed 3 days later. Type I IFN was not removed from cells. Type I IFN was prepared at 10,000 units/ml for MDA-MB-231 cells, and 1,000 units/ml for BT-20 cells. $p < 0.05$ is considered as a statistically significant difference between experimental groups. The * symbol indicates $p < 0.05$, and the ** symbol indicates $p > 0.05$.

MDA-MB-231 cells express TLR9 [25-27] and are sensitive to type I IFN treatment [18]. TLR3 expression in MDA-MB-231 cells is not yet confirmed in the current literature. We initially hypothesized that Ter-CpG would selectively induce type I IFN secretion which would cause apoptosis. Ter-CpG failed to induce cell death and failed to inhibit proliferation of MDA-MB-231 cells (Figures 6, S15 and S16). BT-20 is another triple negative breast cancer cell line that is sensitive to type I IFN treatment [19]. BT-20 cells express TLR9 [25], and our preliminary results suggest that BT-20 cells also express TLR3 (data not shown). We next focused on the characterization of BT-20 cell responsiveness to Ter-polyIC.

First, we compared the cytotoxic effects of polyIC in particulate (Ter-polyIC) versus soluble form. BT-20 cells are highly sensitive to Ter-polyIC compared to soluble polyIC (Figure 7). Within 1 day of treatment with Ter-polyIC at 0.4 µg/ml polyIC, two times less cells

remained viable compared to 6 days of treatment with 100 µg/ml soluble polyIC. The disparity in dose-responsiveness between Ter-polyIC and soluble polyIC may be attributed to a difference in the level of uptake of the ligand. This aspect can be examined in future work by comparing the amount of fluorescently-labeled polyIC internalized by BT-20 cells in particle-encapsulated and soluble forms.

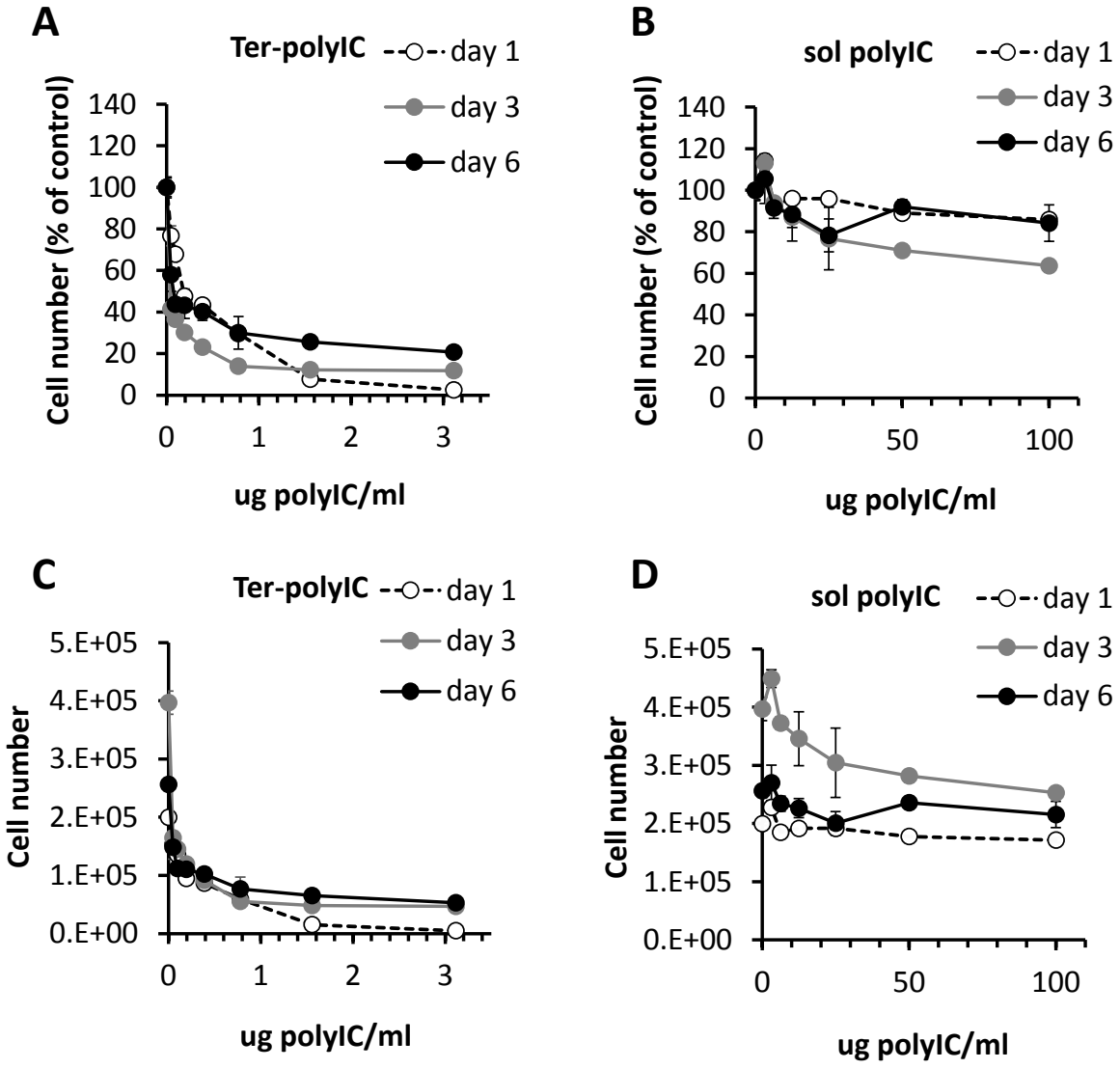

Figure 7. Dose-responsiveness of BT-20 cells to (A,C) Ter-polyIC and (B,D) soluble polyIC. Cells were pulsed with stimulants for 4 h. Cell number was assessed by MTT assay on the indicated days for a wide range of polyIC concentrations in particulate and soluble form. A standard curve of cells was used to calculate the cell number.

In Chapter 2, we determined that CpG ODN is retained in Ter-CpG particles upon the activation of TLR9. Preliminary results indicate that polyIC is not released from particles (Figure S22). Because Ter-polyIC appeared to retain polyIC, we hypothesized that the manner of presentation of polyIC to TLR3 would affect the efficacy of the treatment. We used Ter-polyIC, Ter-adsorb polyIC high and Ter-adsorb polyIC low to assess whether the manner of presentation of polyIC affected BT-20 cell viability. Ter-polyIC at 0.2 μg/ml polyIC was significantly more cytotoxic to BT-20 cells than Ter-adsorb polyIC high and Ter-adsorb polyIC low at 3 μg/ml (Figure 8).

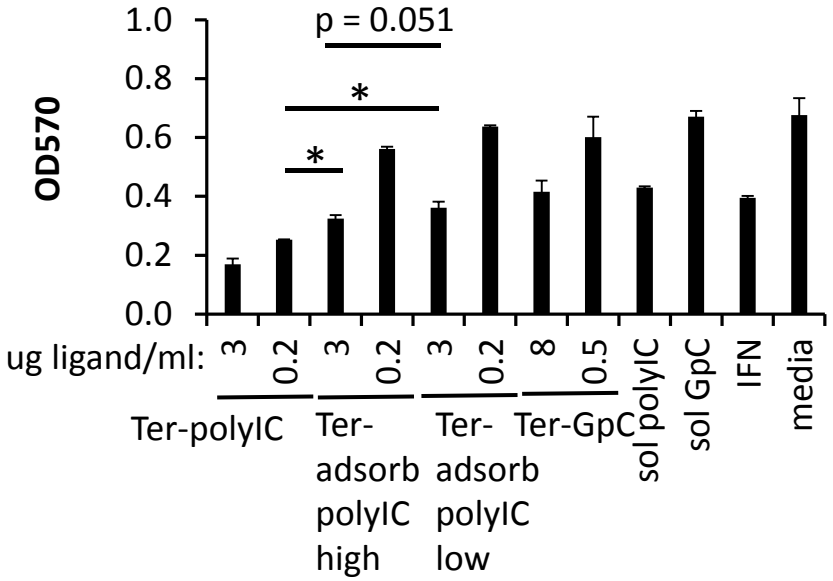

Figure 8. Effect of adsorbed polyIC amount on BT-20 cell viability. Cells were exposed to stimulants for 3 days, and cell viability was assessed by using the MTT assay. Ter-adsorb polyIC high and Ter-adsorb polyIC low contain different amounts of polyIC adsorbed to the particle surface. Soluble controls were prepared at 5 μg/ml. Type I IFN was prepared at 1,000 units/ml. A one-tailed, unpaired student t-test was used for statistical analysis. The * symbol represents a statistically significant difference between samples ($p < 0.05$).

3.4.4 Ter-polyIC induces cell death of a subpopulation of BT-20 cells

BT-20 cells express CD44 [44], which is a cell adhesion molecule that mediates cell-cell and cell-extracellular matrix interactions. CD44 plays a dual role in breast cancer progression. CD44-positive cells that interact with low molecular weight hyaluronan ($<10^6$ Da) are invasive [45], whereas CD44-positive cells that interact with high molecular weight hyaluronan ($>10^6$ Da) are not invasive [46]. Because complete killing could not be achieved with Ter-polyIC, we next characterized the dead cells and remaining viable cells by examining their CD44 expression levels. Ter-polyIC treatment induced cell death by days 1 and 3 (Figure 9). By day 6, the percentage of live cells reached that of non-treated cells. Ter-polyIC, Ter-adsorb polyIC, soluble polyIC, and type I IFN treatment were cytotoxic to the CD44 medium cell subpopulation (Figures 10-12), and Ter-polyIC was the most potent. CD44 low cells were not viable (Figures 10 and 11). Figures 10 and 13 show that the CD44 high subpopulation remained viable and was resistant to all of the treatments that were tested. CD44 high cell resistance to treatment was not likely attributed to a lack of particle uptake. The uptake of particles was relatively uniform among the CD44 subpopulations and among the entire cell population (Figure 17).

CD44-positive cells can be further classified by their CD24 expression level, as determined through personal communication with Prof. Hong Shen and Dr. Hai Nguyen. $CD44^+/CD24^-$ breast cancer cells have been identified as cells that are highly invasive. In breast cancer cell lines, such as BT-20, the $CD44^+/CD24^-$ subpopulation has been identified as cancer stem cells that are resistant to γ irradiation [44]. The CD44 high cells that were resistant to the tested treatments may indeed be cancer stem cells, but further work is needed to confirm this.

3.4.5 The effect of polymer blend particles on the cytokine profiles of triple negative breast cancer cell lines

It has been shown that CpG ODN 2006 treatment of primary multiple myeloma cells from patients and multiple myeloma cell lines promoted their growth, which was partly mediated through IL-6 autocrine signaling [47]. In addition, multiple myeloma cell lines treated with polyIC underwent apoptosis through type I IFN autocrine signaling, but not through IL-6 autocrine signaling [48]. We speculate that the survival of CD44 high cells was IL-6 dependent, and further work will be done to confirm this. The high percentage of viable CD44 high cells (Figure 10) after Ter-polyIC treatment correlated with high levels of IL-6 in the BT-20 cell supernatants (Figure 14A). By day 6, the IL-6 level was highest at the highest concentration of Ter-polyIC. Ter-adsorb polyIC, Ter-CpG and Ter-GpC ctrl did not induce type I IFN secretion from BT-20 cells (Figure 14B). Ter-polyIC at lower concentrations (0.8, 0.2, and 0.05 μg polyIC/ml) induced high levels of type I IFNs between 6 hours and 6 days, and the secretion peaked at 1 day. Similarly, the type I IFN level peaked at 1 day for type I IFN-treated cells. Because most CD44 medium cells remained viable at day 1 (Figure 12), while more died by days 3 and 6, we suspect that CD44 medium cells are the source for type I IFNs. Preliminary results suggest that CD44 medium cells secrete type I IFNs (data not shown).

MDA-MB-231 cells did not secrete type I IFNs but only IL-6 (Figure 16). The lack of type I IFN secretion could be the reason for MDA-MB-231 cell survival after incubation with Ter-polyIC. Further work is needed to confirm this. In addition, the effect of Ter-polyIC on IL-6 secretion may be investigated further because it is uncertain from preliminary results whether or not MDA-MB-231 cells secrete IL-6 endogenously (media controls in Figure 16 and Figure S17).

3.4.6 The effect of polymer blend particles on the *in vitro* migration of BT-20 cells

We determined that Ter-polyIC was effective at killing the CD44 medium BT-20 cell subpopulation. We continued to evaluate their effect on BT-20 cells by studying their migration. An *in vitro* scratch assay was used to assess the effects of TLR-ligand encapsulated polymer blend particles on the migration of BT-20 cells. Compared to soluble polyIC, the Ter-polyIC was more effective at inhibiting cell migration (Figure 18). Ter-CpG and Ter-polyIC were similarly effective at preventing cell migration. Interestingly, the overexpression of TLR9 in BT-20 cells promoted the migration of cells in response to CpG ODN 2006 lipoplexes [25]. It is important to note that the effect of cell proliferation could not be accounted for in migration studies. The serum concentration in cell culture media could be reduced to minimize the effect of cell proliferation (data not shown), however, we speculated that this condition would affect the migration of the cells.

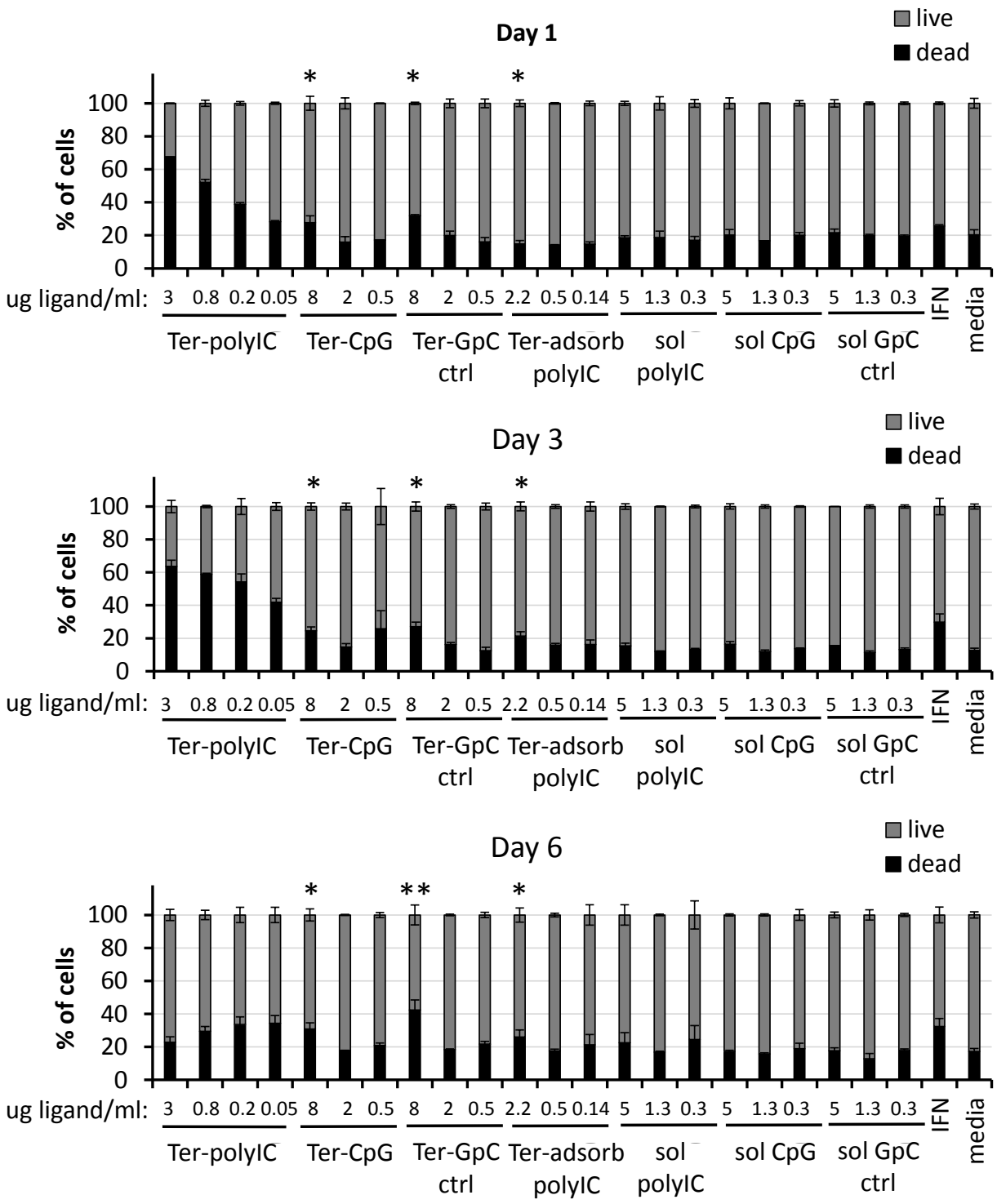

Figure 9. Effect of polymer blend particles on the percentage of total cells that are live and dead. Cells were exposed to stimulants for 4 hours, and then were removed. Type I IFN was prepared at 1,000 units/ml, but was not removed. A one-tailed and unpaired student t-test was used to analyze the differences between Ter-polyIC at 3 μg/ml polyIC and designated experimental groups. The * symbol indicates $p < 0.05$, and the ** symbol indicates $p > 0.05$.

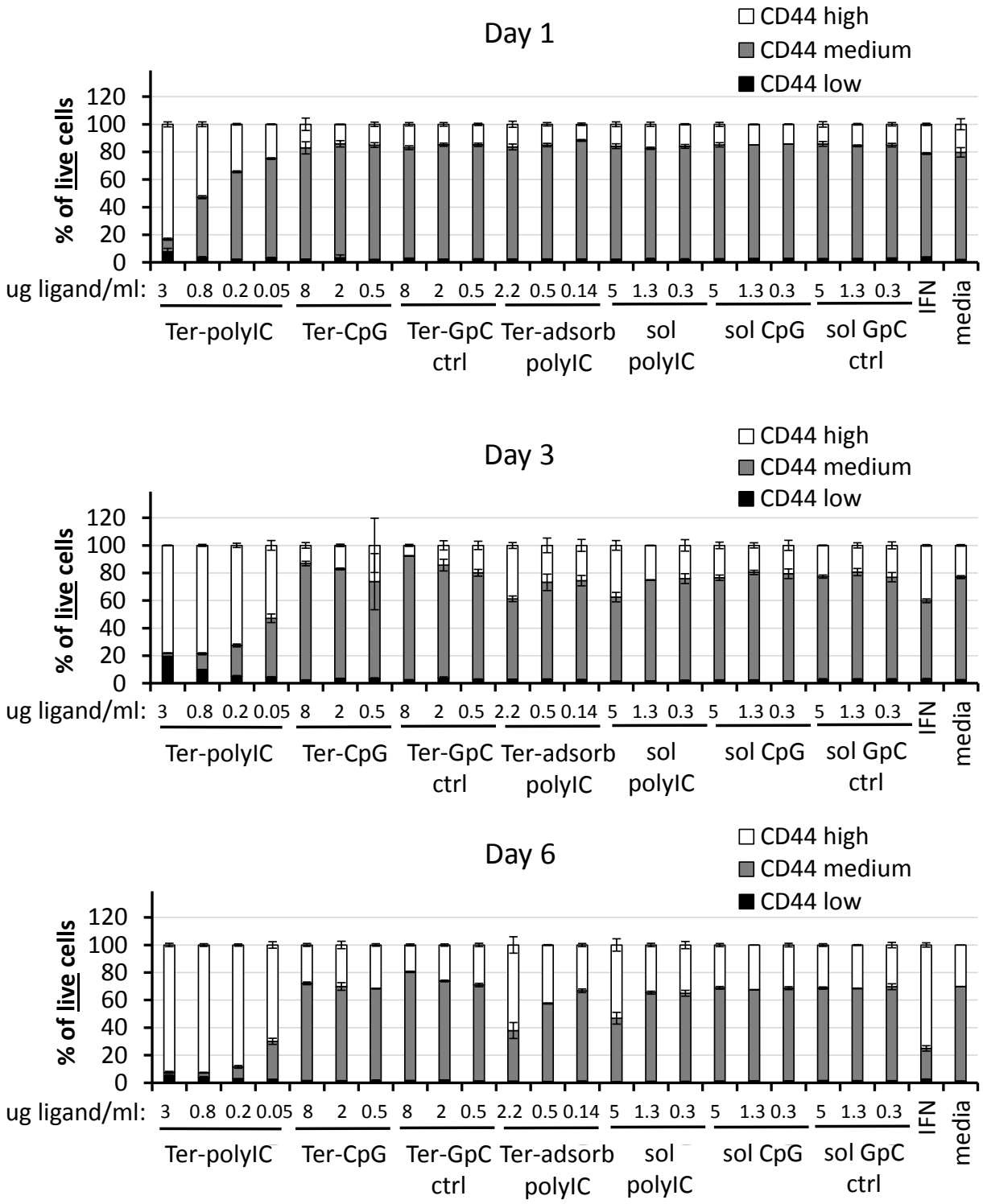

Figure 10. CD44 subpopulation analysis of live cells after treatment with polymer blend particles. Cells were exposed to stimulants for 4 hours, and then were removed. Type I IFN was prepared at 1,000 units/ml, and was not removed.

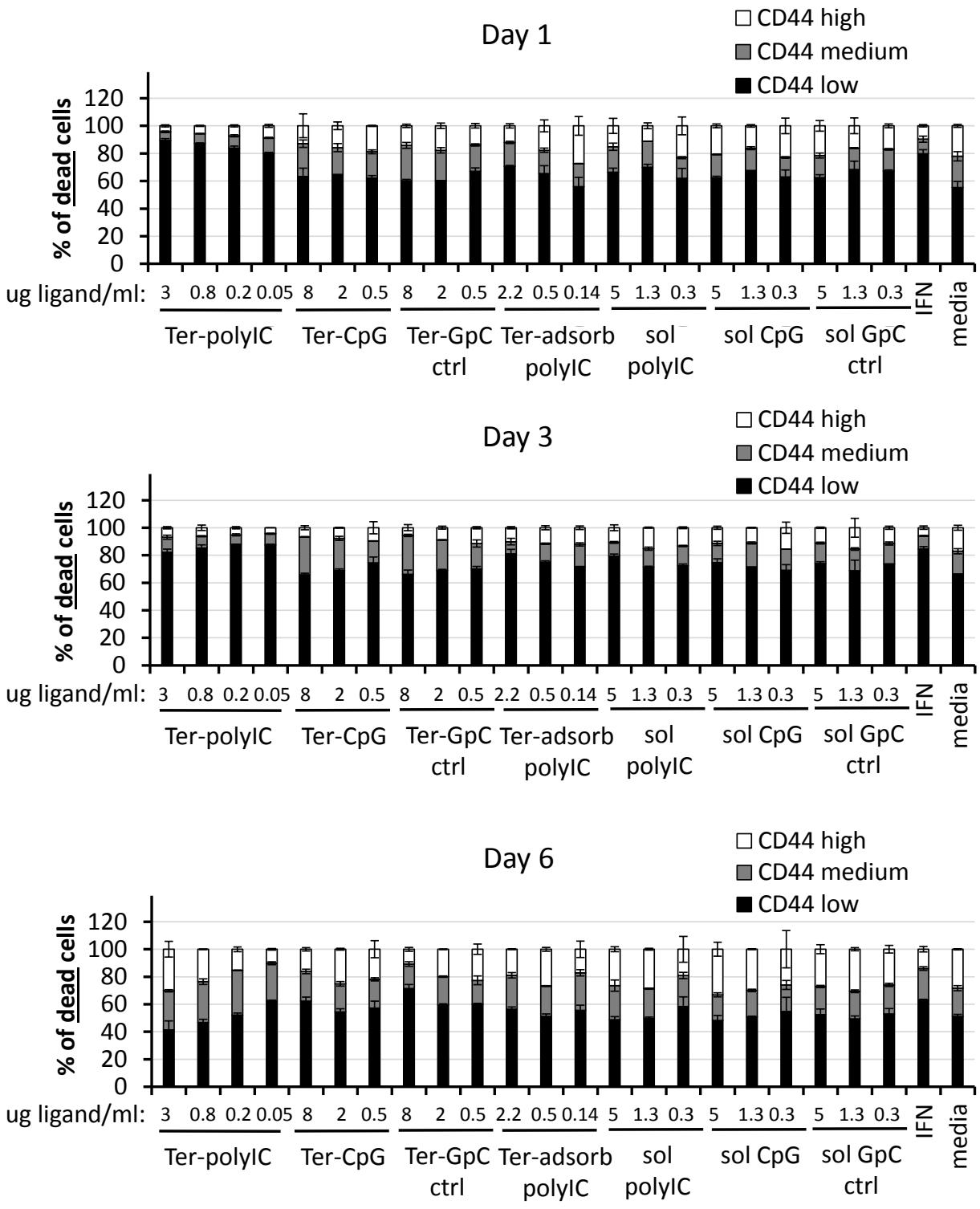

Figure 11. CD44 subpopulation analysis of dead cells after treatment with polymer blend particles. Cells were exposed to stimulants for 4 hours, and then were removed. Type I IFN was prepared at 1,000 units/ml, and was not removed.

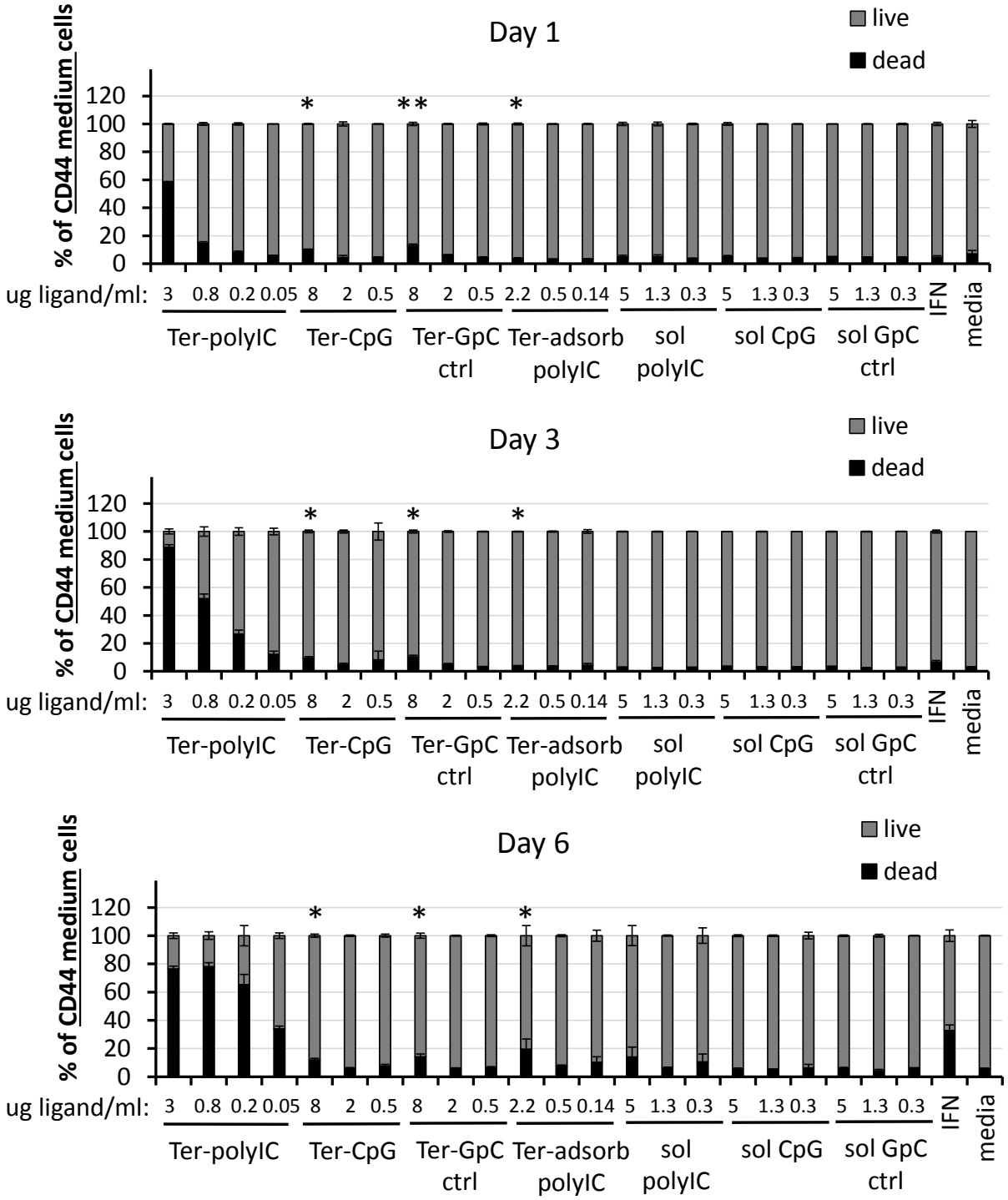

Figure 12. Analysis of CD44 medium cell subpopulation viability after treatment with polymer blend particles. Cells were exposed to stimulants for 4 hours, and then were removed. Type I IFN was prepared at 1,000 units/ml, and was not removed. A one-tailed and unpaired student t-test was used to analyze the differences between Ter-polyIC at 0.8 μg/ml polyIC and designated experimental groups. The * symbol indicates $p < 0.05$, and the ** symbol indicates $p > 0.05$.

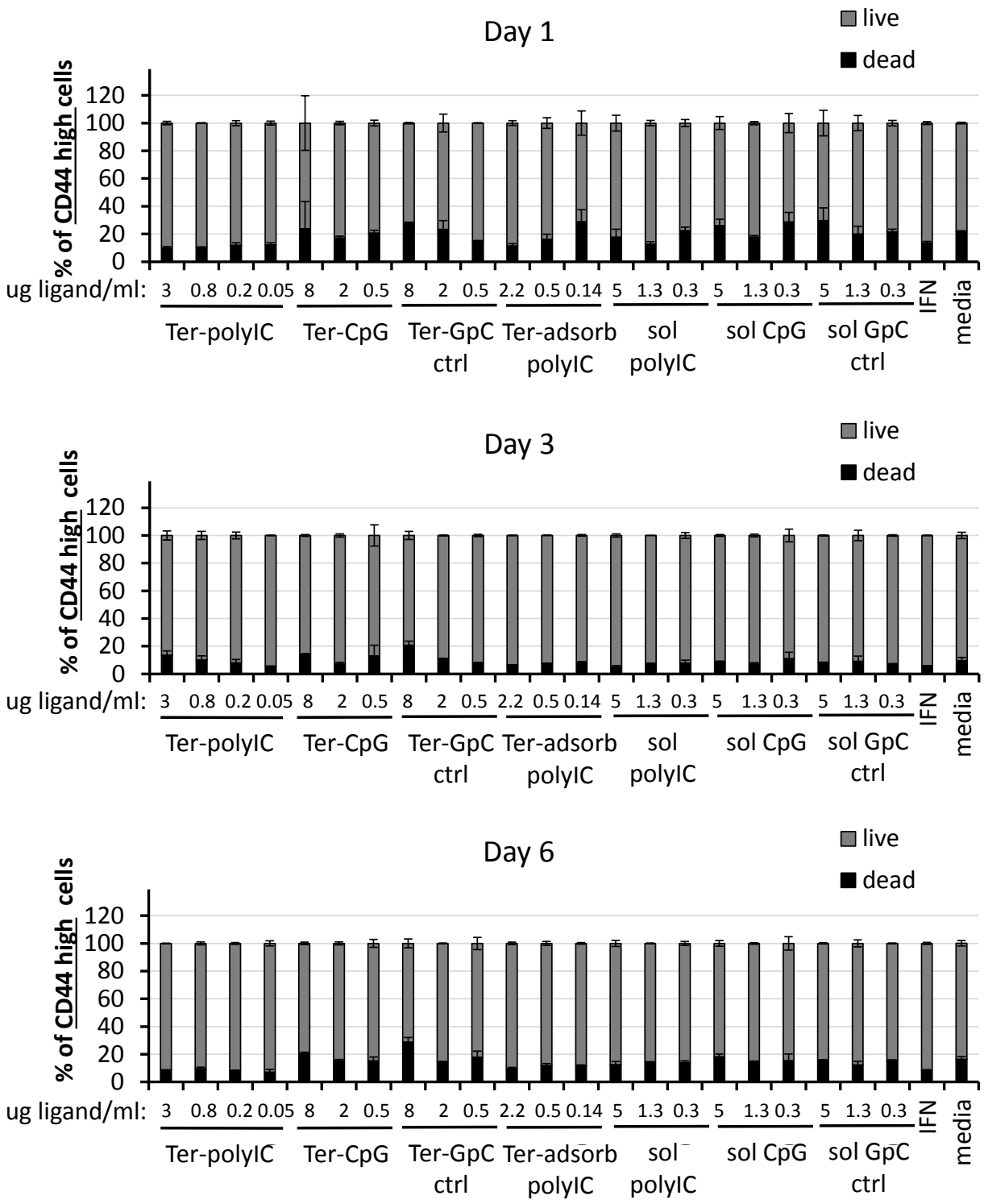

Figure 13. Analysis of CD44 high cell subpopulation viability after treatment with polymer blend particles. Cells were exposed to stimulants for 4 hours, and then were removed. Type I IFN was prepared at 1,000 units/ml, and was not removed.

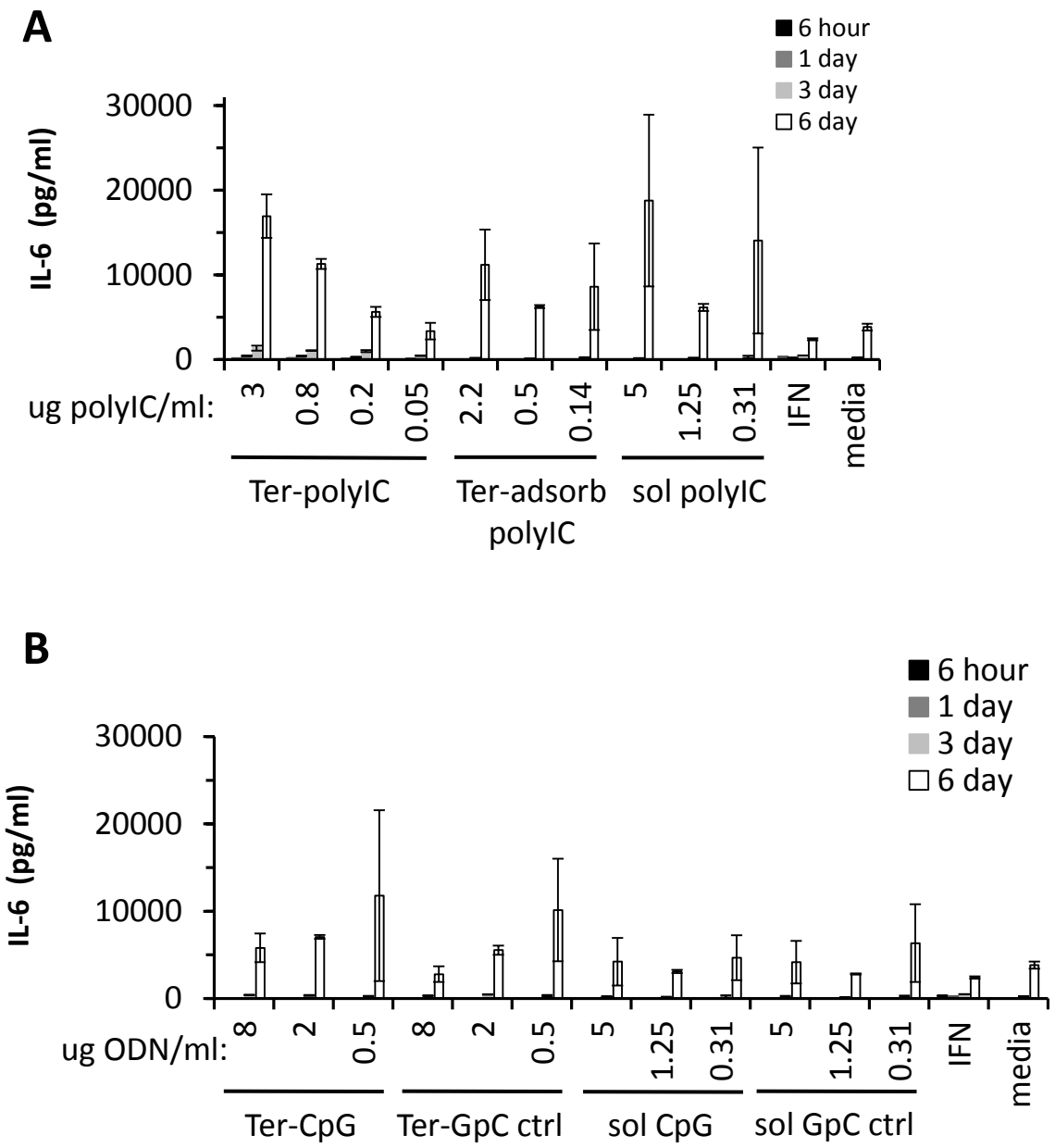

Figure 14. IL-6 secretion from BT-20 cells treated with polymer blend particles. IL-6 secretion induced by (A) Ter-polyIC, Ter-adsorb polyIC, and (B) Ter-CpG and Ter-GpC ctrl. Cells were exposed to stimulants for 4 hours, and then were removed. Type I IFN was prepared at 1,000 units/ml, and was not removed. At the indicated time points, cell supernatants were collected for analysis by ELISA.

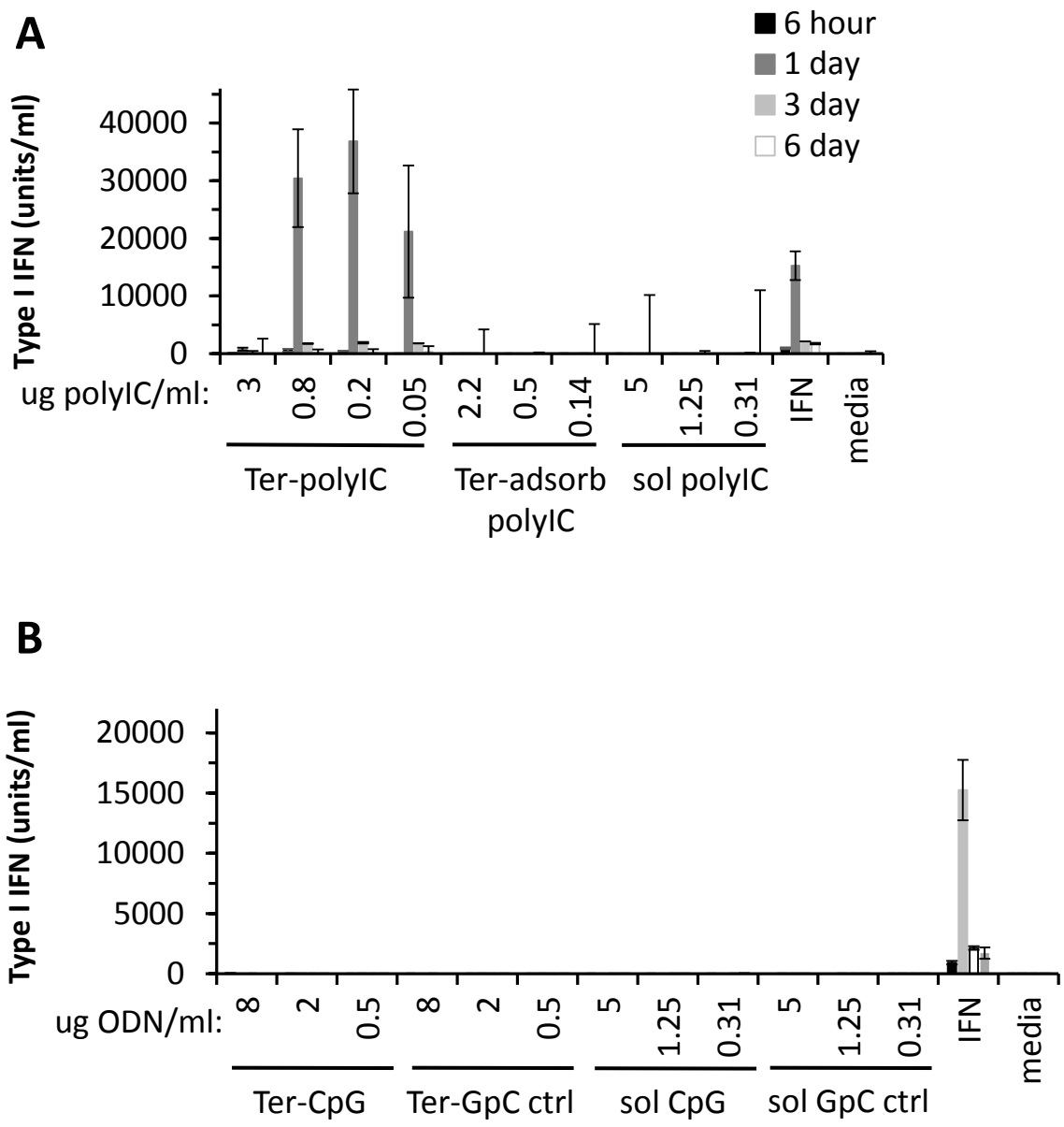

Figure 15. Type I IFN secretion from BT-20 cells treated with polymer blend particles. Type I IFN secretion induced by (A) Ter-polyIC, Ter-adsorb polyIC, and (B) Ter-CpG and Ter-GpC ctrl. Cells were exposed to stimulants for 4 hours, and then were removed. Type I IFN was prepared at 1,000 units/ml, and was not removed. At the indicated time points, cell supernatants were collected. Type I IFNs from BT-20 cell supernatants was assayed by measuring the level of protection of Vero cells from infection by VSV-GFP.

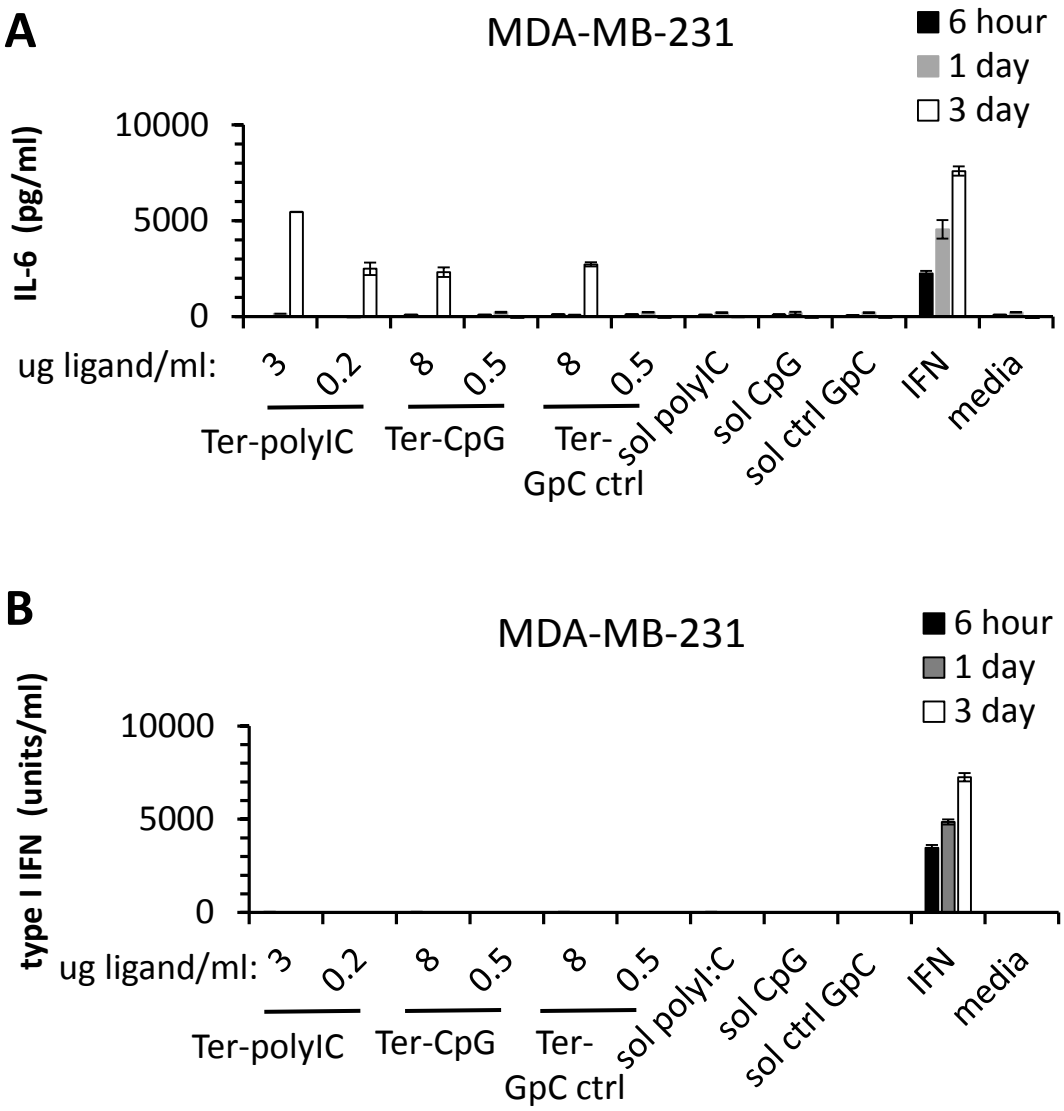

Figure 16. Effect of polymer blend particles on cytokine secretion from MDA-MB-231 cells. Cells were pulsed with stimulants for 4 h, and cell supernatants were collected at the indicated time points for cytokine analysis. Soluble ligands were prepared at 5 µg/ml. Human type I IFN was prepared at 10,000 units/ml and was not removed. Type I IFNs from MDA-MB-231 cell supernatants were assayed by measuring the level of protection of Vero cells from infection by VSV-GFP.

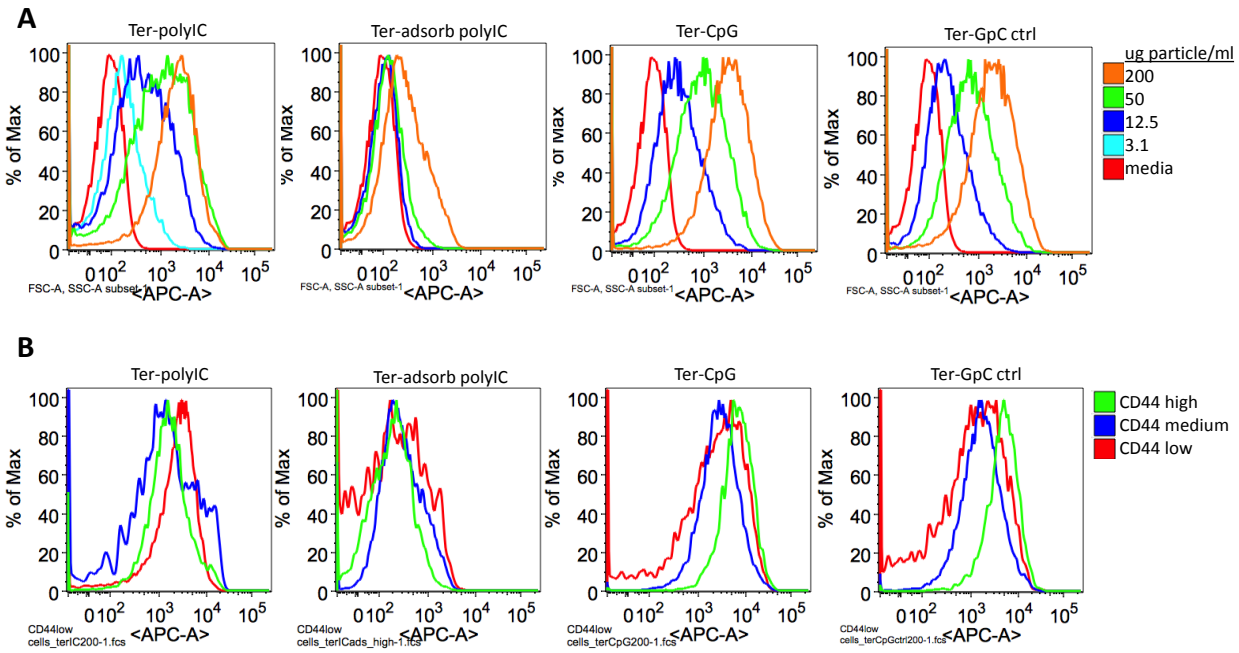

Figure 17. BT-20 cell uptake of polymer blend particles. Cells were pulsed with particles for 4 h. The uptake of particles was assessed after 1 day. The gMFI of APC indicates the level of particle uptake for (A) different particle concentrations and (B) the highest particle concentration tested.

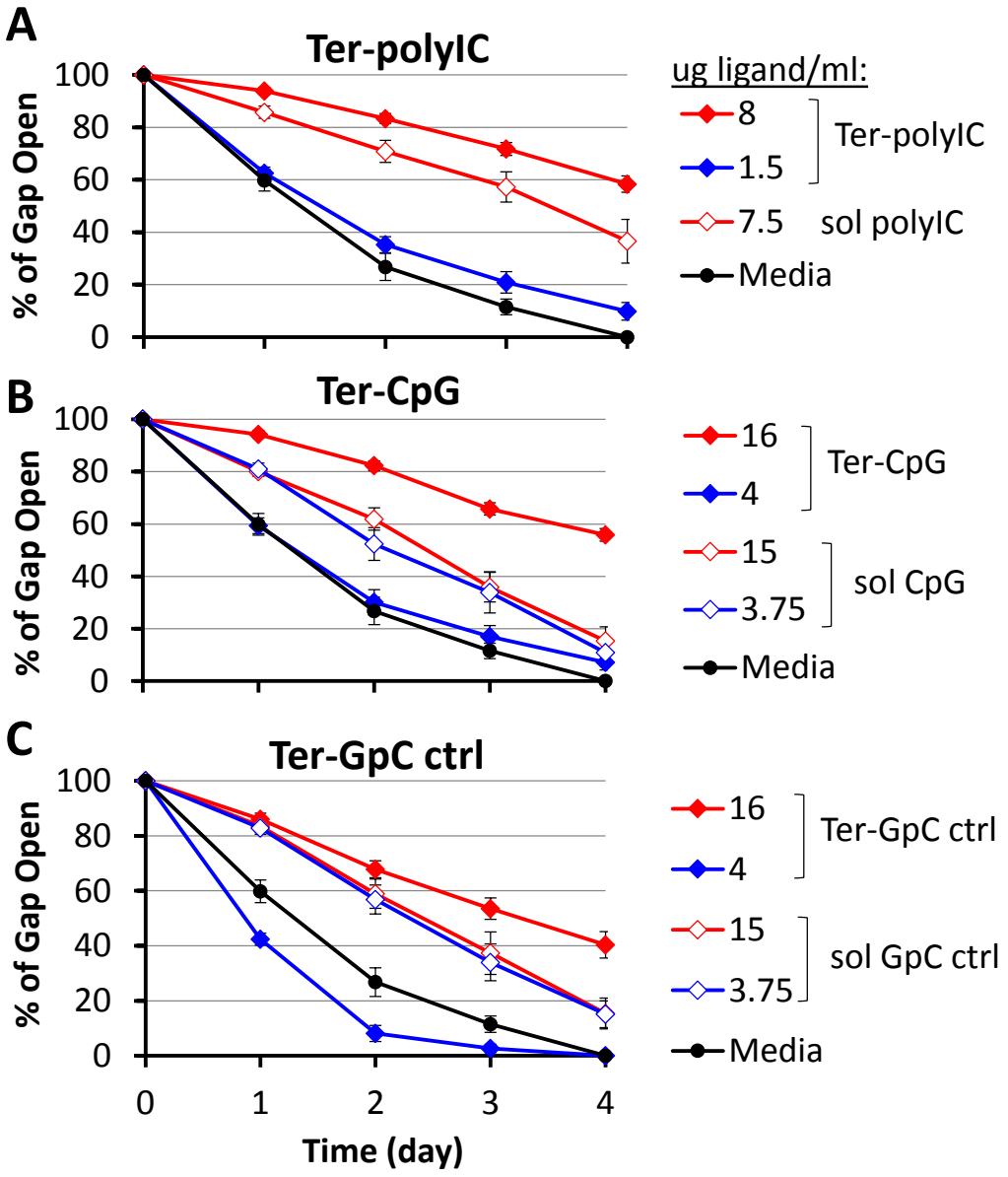

Figure 18. Effect of polymer blend particles on the *in vitro* migration distance of BT-20 cells. Cells were plated in a 6-well plate and pulsed with (A) Ter-polyIC, (B) Ter-CpG, or (C) Ter-GpC ctrl for 4 hours. Stimulants were removed, and a scratch was created in the cell monolayer. Images were acquired to monitor the width of the scratch/gap. The migration distance is expressed as the percentage of the gap that remained open, relative to the initial gap width. Doses of particles and soluble ligands are expressed as μg ligand/ml.

3.5 Conclusion

Of the TLR ligand-encapsulated terpolymer particles tested, Ter-polyIC was the most effective at inducing cell death and preventing cell proliferation and migration. The CD44 medium cells were the only subpopulation sensitive to Ter-polyIC. 6 days after treatment, the majority of the cells which remained viable and had proliferated were CD44 high cells. Our results suggest that the CD44 high cells secrete a relatively high level of IL-6, which may enhance their rate of proliferation.

3.6 References

[1] Merigan TC, Hall TS, Reed SE, Tyrrell DAJ. Inhibition of Respiratory Virus-Infection by Locally Applied Interferon. Lancet. 1973;1:564-7.
[2] Sundmacher R, Neumannhaefelin D, Cantell K. Successful Treatment of Dendritic Keratitis with Human Leukocyte Interferon - Controlled Clinical-Study. A Graef Arch Klin Ex. 1976;201:39-45.
[3] Arvin AM, Feldman S, Merigan TC. Human Leukocyte Interferon in Treatment of Varicella in Children with Cancer - Preliminary Controlled Trial. Antimicrob Agents Ch. 1978;13:605-7.
[4] Greenberg HB, Pollard RB, Lutwick LI, Gregory PB, Robinson WS, Merigan TC. Effect of Human Leukocyte Interferon on Hepatitis B Virus-Infection in Patients with Chronic Active Hepatitis. New Engl J Med. 1976;295:517-22.
[5] Stetson DB, Medzhitov R. Type I interferons in host defense. Immunity. 2006;25:373-81.
[6] Chawla-Sarkar M, Lindner DJ, Liu YF, Williams B, Sen GC, Silverman RH, et al. Apoptosis and interferons: Role of interferon-stimulated genes as mediators of apoptosis. Apoptosis. 2003;8:237-49.
[7] Friedman RM. Clinical uses of interferons. Brit J Clin Pharmaco. 2008;65:158-62.
[8] Caraglia M, Marra M, Pelaia G, Maselli R, Caputi M, Marsico SA, et al. Alpha-interferon and its effects on signal transduction pathways. J Cell Physiol. 2005;202:323-35.
[9] Thyrell L, Erickson S, Zhivotovsky B, Pokrovskaja K, Sangfelt O, Castro J, et al. Mechanisms of Interferon-alpha induced apoptosis in malignant cells. Oncogene. 2002;21:1251-62.
[10] Panaretakis T, Pokrovskaja K, Shoshan MC, Grander D. Interferon-alpha-induced apoptosis in U266 cells is associated with activation of the proapoptotic Bcl-2 family members Bak and Bax. Oncogene. 2003;22:4543-56.
[11] Takaoka A, Hayakawa S, Yanai H, Stoiber D, Negishi H, Kikuchi H, et al. Integration of interferon-alpha/beta signalling to p53 responses in tumour suppression and antiviral defence. Nature. 2003;424:516-23.
[12] Diamond MS, Kinder M, Matsushita H, Mashayekhi M, Dunn GP, Archambault JM, et al. Type I interferon is selectively required by dendritic cells for immune rejection of tumors. J Exp Med. 2011;208:1989-2003.
[13] Dunn GP, Bruce AT, Sheehan KCF, Shankaran V, Uppaluri R, Bui JD, et al. A critical function for type I interferons in cancer immunoediting. Nat Immunol. 2005;6:722-9.

[14] Swann JB, Hayakawa Y, Zerafa N, Sheehan KCF, Scott B, Schreiber RD, et al. Type I IFN contributes to NK cell homeostasis, activation, and antitumor function. J Immunol. 2007;178:7540-9.
[15] Fuertes MB, Kacha AK, Kline J, Woo SR, Kranz DM, Murphy KM, et al. Host type I IFN signals are required for antitumor CD8(+) T cell responses through CD8 alpha(+) dendritic cells. J Exp Med. 2011;208:2005-16.
[16] Gresser I, Maury C, Vignaux F, Haller O, Belardelli F, Tovey MG. Antibody to Mouse Interferon-Alpha/Beta Abrogates Resistance to the Multiplication of Friend-Erythroleukemia Cells in the Livers of Allogeneic Mice. J Exp Med. 1988;168:1271-91.
[17] Bidwell BN, Slaney CY, Withana NP, Forster S, Cao Y, Loi S, et al. Silencing of Irf7 pathways in breast cancer cells promotes bone metastasis through immune escape. Nat Med. 2012;18:1224-+.
[18] Robinson SP, Goldstein D, Witt PL, Borden EC, Jordan VC. Inhibition of Hormone-Dependent and Independent Breast-Cancer Cell-Growth Invivo and Invitro with the Antiestrogen Toremifene and Recombinant Human Interferon-Alpha-2. Breast Cancer Res Tr. 1990;15:95-101.
[19] Taylorpapadimitriou J, Shearer M, Balkwill FR, Fantes KH. Effects of Huifn-Alpha-2 and Huifn-Alpha (Namalwa) on Breast-Cancer Cells Grown in Culture and as Xenografts in the Nude-Mouse. J Interferon Res. 1982;2:479-91.
[20] Balkwill FR, Goldstein L, Stebbing N. Differential Action of 6 Human Interferons against 2 Human Carcinomas Growing in Nude-Mice. Int J Cancer. 1985;35:613-7.
[21] Vandenberg HW, Leahey WJ, Lynch M, Clarke R, Nelson J. Recombinant Human Interferon-Alpha Increases Estrogen-Receptor Expression in Human-Breast Cancer-Cells (Zr-75-1) and Sensitizes Them to the Antiproliferative Effects of Tamoxifen. Brit J Cancer. 1987;55:255-7.
[22] Hervas-Stubbs S, Perez-Gracia JL, Rouzaut A, Sanmamed MF, Le Bon A, Melero I. Direct Effects of Type I Interferons on Cells of the Immune System. Clin Cancer Res. 2011;17:2619-27.
[23] Anders CK, Winer EP, Ford JM, Dent R, Silver DP, Sledge GW, et al. Poly(ADP-Ribose) Polymerase Inhibition: "Targeted" Therapy for Triple-Negative Breast Cancer. Clin Cancer Res. 2010;16:4702-10.
[24] Silver DP, Richardson AL, Eklund AC, Wang ZC, Szallasi Z, Li Q, et al. Efficacy of Neoadjuvant Cisplatin in Triple-Negative Breast Cancer. J Clin Oncol. 2010;28:1145-53.
[25] Berger R, Fiegl H, Goebel G, Obexer P, Ausserlechner M, Doppler W, et al. Toll-like receptor 9 expression in breast and ovarian cancer is associated with poorly differentiated tumors. Cancer Sci. 2010;101:1059-66.
[26] Yang HA, Zhou HQ, Feng P, Zhou XN, Wen HY, Xie XF, et al. Reduced expression of Toll-like receptor 4 inhibits human breast cancer cells proliferation and inflammatory cytokines secretion. J Exp Clin Canc Res. 2010;29.
[27] Merrell MA, Ilvesaro JM, Lehtonen N, Sorsa T, Gehrs B, Rosenthal E, et al. Toll-like receptor 9 agonists promote cellular invasion by increasing matrix metalloproteinase activity. Mol Cancer Res. 2006;4:437-47.
[28] Li SL, Wilkinson M, Xia XQ, David M, Xu LH, Purkel-Sutton A, et al. Induction of IFN-regulated factors and antiturnoral surveillance by transfected placebo plasmid DNA. Mol Ther. 2005;11:112-9.
[29] Huang B, Zhao J, Li HX, He KL, Chen YB, Mayer L, et al. Toll-like receptors on tumor cells facilitate evasion of immune surveillance. Cancer Res. 2005;65:5009-14.

[30] De Sousa CP, Blum CM, Sgroe EP, Crespo AM, Kurt RA. Murine mammary carcinoma cells and CD11c(+) dendritic cells elicit distinct responses to lipopolysaccharide and exhibit differential expression of genes required for TLR4 signaling. Cell Immunol. 2010;266:67-75.
[31] Sandholm J, Kauppila JH, Pressey C, Tuomela J, Jukkola-Vuorinen A, Vaarala M, et al. Estrogen receptor-alpha and sex steroid hormones regulate Toll-like receptor-9 expression and invasive function in human breast cancer cells. Breast Cancer Res Tr. 2012;132:411-9.
[32] Gonzalez-Reyes S, Marin L, Gonzalez L, Gonzalez LO, del Casar JM, Lamelas ML, et al. Study of TLR3, TLR4 and TLR9 in breast carcinomas and their association with metastasis. Bmc Cancer. 2010;10.
[33] El Andaloussi A, Sonabend AM, Han Y, Lesniak MS. Stimulation of TLR9 with CpG ODN enhances apoptosis of glioma and prolongs the survival of mice with experimental brain tumors. Glia. 2006;54:526-35.
[34] Wang C, Cao SQ, Yan Y, Ying QA, Jiang T, Xu K, et al. TLR9 expression in glioma tissues correlated to glioma progression and the prognosis of GBM patients. Bmc Cancer. 2010;10.
[35] Schmausser B, Andrulis M, Endrich S, Muller-Hermelink HK, Eck M. Toll-like receptors TLR4, TLR5 and TLR9 on gastric carcinoma cells: An implication for interaction with Helicobacter pylori. Int J Med Microbiol. 2005;295:179-85.
[36] Droemann D, Albrecht D, Gerdes J, Ulmer AJ, Branscheid D, Vollmer E, et al. Human lung cancer cells express functionally active Toll-like receptor 9. Resp Res. 2005;6.
[37] Nishimura M, Naito S. Tissue-specific mRNA expression profiles of human toll-like receptors and related genes. Biol Pharm Bull. 2005;28:886-92.
[38] Lee JW, Choi JJ, Seo ES, Kim MJ, Kim WY, Choi CH, et al. Increased toll-like receptor 9 expression in cervical neoplasia. Mol Carcinogen. 2007;46:941-7.
[39] Ilvesaro JM, Merrell MA, Swain TM, Davidson J, Zayzafoon M, Harris KW, et al. Toll like receptor-9 agonists stimulate prostate cancer invasion in vitro. Prostate. 2007;67:774-81.
[40] Lund J, Sato A, Akira S, Medzhitov R, Iwasaki A. Toll-like receptor 9-mediated recognition of herpes simplex virus-2 by plasmacytoid dendritic cells. J Exp Med. 2003;198:513-20.
[41] Dalod M, Salazar-Mather TP, Malmgaard L, Lewis C, Asselin-Paturel C, Briere F, et al. Interferon alpha/beta and interleukin 12 responses to viral infections: Pathways regulating dendritic cell cytokine expression in vivo. J Exp Med. 2002;195:517-28.
[42] Rentsch MB, Zimmer G. A Vesicular Stomatitis Virus Replicon-Based Bioassay for the Rapid and Sensitive Determination of Multi-Species Type I Interferon. Plos One. 2011;6.
[43] Liang CC, Park AY, Guan JL. In vitro scratch assay: a convenient and inexpensive method for analysis of cell migration in vitro. Nat Protoc. 2007;2:329-33.
[44] Bensimon J, Altmeyer-Morel S, Benjelloun H, Chevillard S, Lebeau J. CD24(-/low) stem-like breast cancer marker defines the radiation-resistant cells involved in memorization and transmission of radiation-induced genomic instability. Oncogene. 2013;32:251-8.
[45] Hill A, McFarlane S, Mulligan K, Gillespie H, Draffin JE, Trimble A, et al. Cortactin underpins CD44-promoted invasion and adhesion of breast cancer cells to bone marrowendothelial cells. Oncogene. 2006;25:6079-91.
[46] Lopez JI, Camenisch TD, Stevens MV, Sands BJ, McDonald J, Schroeder JA. CD44 attenuates metastatic invasion during breast cancer progression. Cancer Res. 2005;65:6755-63.
[47] Xu Y, Zhao Y, Huang HW, Chen GH, Wu XJ, Wang Y, et al. Expression and function of toll-like receptors in multiple myeloma patients: toll-like receptor ligands promote multiple myeloma cell growth and survival via activation of nuclear factor-kappa B. Brit J Haematol. 2010;150:543-53.

[48] Chiron D, Pellat-Deceunynck C, Amiot M, Bataille R, Jego G. TLR3 Ligand Induces NF-kappa B Activation and Various Fates of Multiple Myeloma Cells Depending on IFN-alpha Production. J Immunol. 2009;182:4471-8.

Supplemental Work

Supplemental 1. Supplemental information for Chapter 1

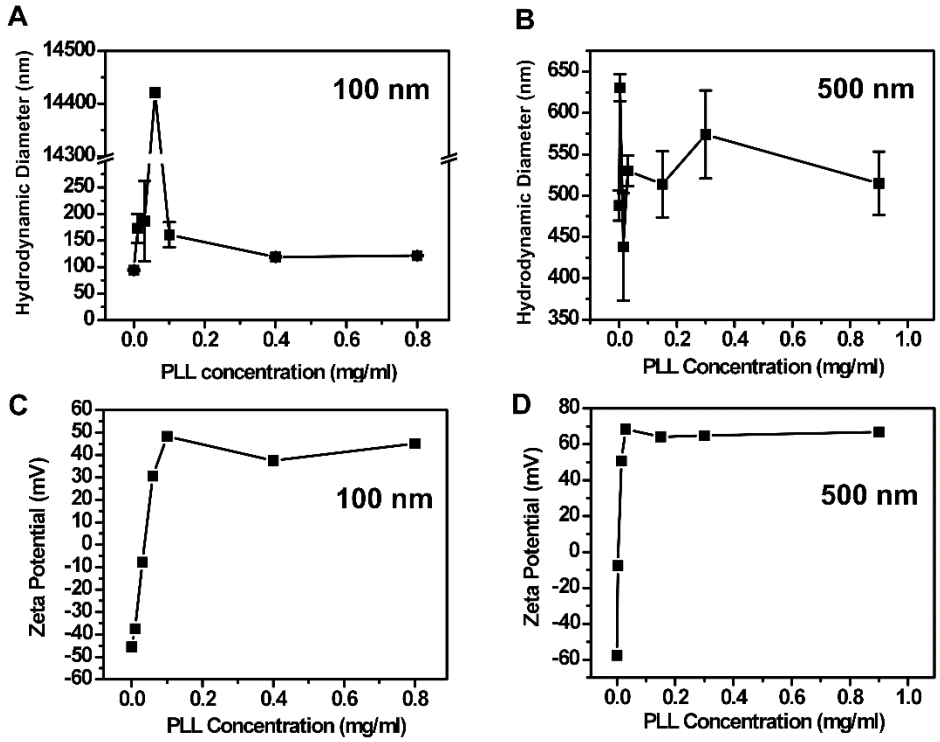

Figure S1. Characterization of PLL-PS. Hydrodynamic diameter of 100 nm (A) and 500 nm (B) PS coated with PLL of a broad range of concentrations. The zeta potential of 100 nm (C) and 500 nm (D) PS coated with PLL of a broad range of concentrations.

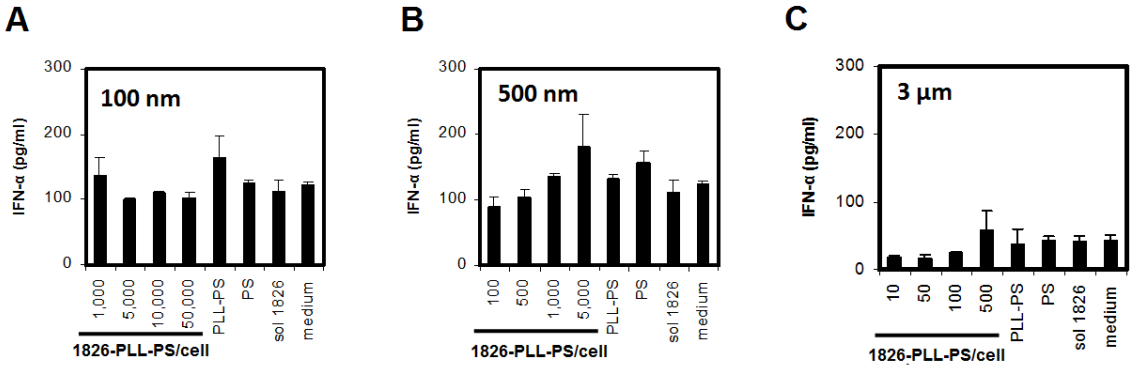

Figure S2. Levels of IFN-α in response to CpG ODN 1826. BC-1 cells were stimulated by (A) 100 nm, (B) 500 nm, and (C) 3 µm 1826-PLL-PS. PLL-PS and PS at the highest particle-to-cell ratio of the corresponding particle size served as negative controls. Soluble ODNs at 0.005 mg/ml served as a positive control. The supernatants of cells were collected after 24 h and analyzed by ELISA for the IFN-α concentration.

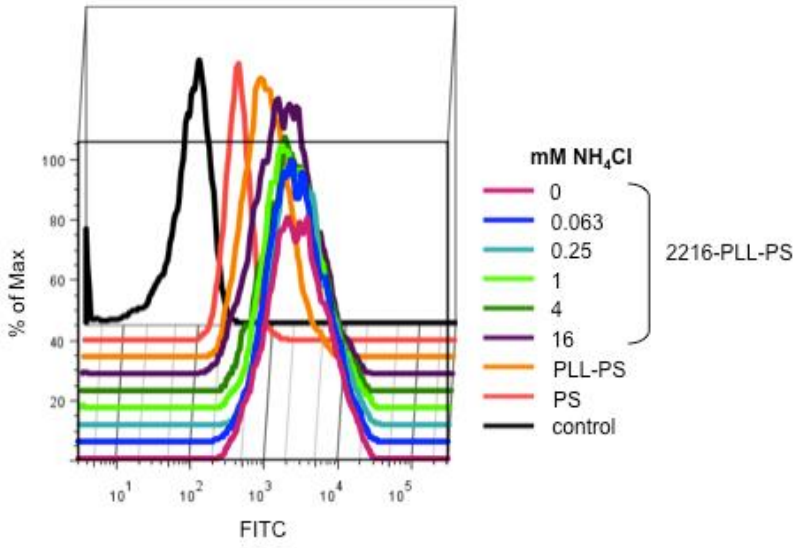

Figure S3. Relative levels of cellular uptake of 2216-PLL-PS in the presence of NH_4Cl. 100 nm 2216-PLL-PS, 100 nm PLL-PS, and 100 nm bare FITC PS were given to cells at 50,000 particles per cell. All of the particles contained FITC which was encapsulated inside particles. The cells were harvested after a 6 h pulse and analyzed by flow cytometry. The fluorescence due to cell surface-associated particles was quenched by using 0.4% Trypan blue. The uptake of 2216-PLL-PS is represented as "% of max," or the normalized cell numbers by using the bin containing maximum number of cells. Within the wide range of NH_4Cl concentrations tested, the uptake of 2216-PLL-PS was not significantly affected ($p > 0.1$).

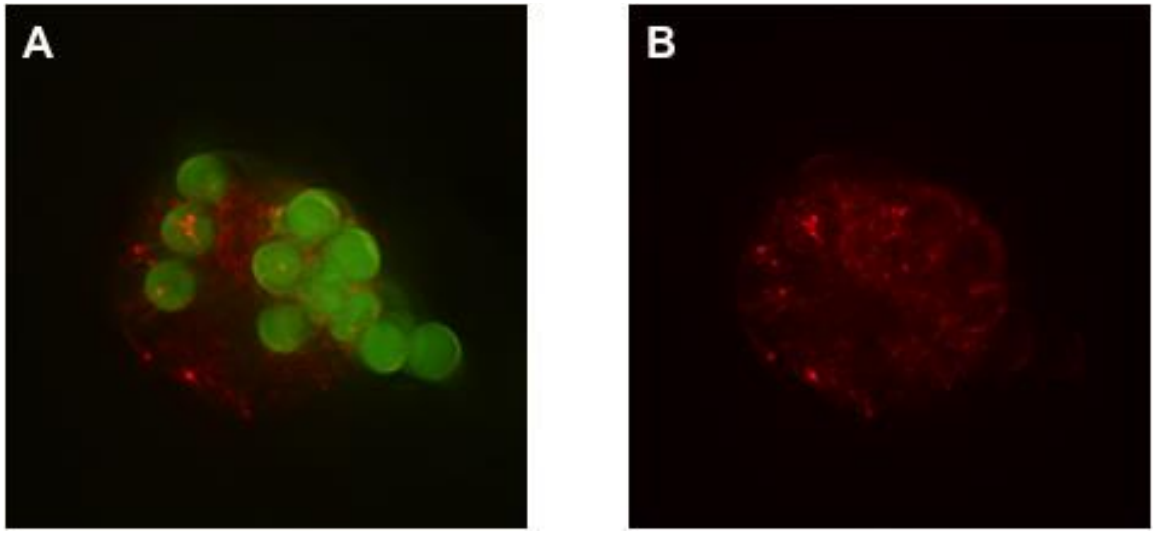

Figure S4. Colocalization of microparticles with early endosomes. (A) A cross-sectional image of BC-1 cells. Early endosomes of cells stained with EEA-1 (red), which colocalized with 3 μm bare FITC PS particles (green). (B) A cross-sectional image of BC-1 cells with only EEA-1 (red) staining.

Materials and Methods

Measurement of uptake levels of 2216-PLL-PS in the presence of NH_4Cl

To determine whether NH_4Cl affected the cell uptake of 2216-PLL-PS, we measured the cellular uptake of 100 nm CpG ODN 2216-bound FITC-PS in the presence and absence of NH_4Cl. First, DCs were seeded in a 24-well plate at a density of 2.5×10^5 cells per well. DCs were pulsed with particles at 50,000 particles per cell for 6 h. Afterward, cells were washed three times with DPBS to remove excess beads. Cells were harvested, washed three times in DPBS containing 1% FBS, and immediately analyzed using a FACsCanto (Cell Analysis Facility, University of Washington). To quench the fluorescence of cell surface-associated particles, 20 μl of Trypan Blue (0.4%) was used to quench the fluorescence due to particles associated with cell surfaces. The distribution of the FITC intensity was examined by using FlowJo (Treestar, Inc.).

Intracellular distribution of PS microparticles

DCs were plated at a density of 2×10^5 cells per well in 500 μl medium onto 12 mm circular glass coverslips (Erie Scientific Co., Portsmouth, NH). To enhance the adherence of cells to coverslips, coverslips were pre-treated with poly-D-lysine (PDL; Sigma-Aldrich, Inc., Saint Louis, MO) by incubating them with 300 μl PDL at 0.01 mg/ml for 5 min at RT. Coverslips were washed three times with 500 μl Milli-Q water and allowed to dry before the seeding of cells. Cells were allowed to adhere for 1 h. Cells were pulsed with 3 μm FITC-PS particles at 10 particles per cell for 4 h. Cells were then washed three times with DPBS to remove excess particles. Afterward, cells were fixed with 4% PFA for 20 min and washed three times with DPBS. Cells were then permeabilized with 0.1% Triton X-100 for 5 min and washed three times with DPBS. Cells were blocked with 500 μl blocking buffer (1% of bovine serum

albumin (BSA) in DPBS) for 30 min at RT. Cells were washed twice with DPBS and labeled with 300 µl of 2 µg/ml rabbit anti-mouse early endosomal antigen-1 (EEA-1; Santa Cruz Biotechnology, Inc., Santa Cruz, CA) in blocking buffer for 30 min at RT. Cells were washed three times, and blocked again with blocking buffer for 15 min. Cells were washed twice and then incubated with 300 µl of 2 µg/ml Cy3-anti rabbit IgG (Abcam, Cambridge, MA) in blocking buffer for 30 min at RT. Lastly, cells were washed three times and stored in DPBS at 4 °C. Coverslips were rinsed with Milli-Q water and then mounted onto Teflon-coated glass slides using DAPI-containing Vectashield Mounting Medium (Vector Laboratories, Inc., Burlingame, CA) for imaging. A DeltaVision Fluorescence Microscope with a 100X oil objective was used to acquire images. The DeltaVision SoftWorx program (Applied Precision, Inc.) was used to deconvolve the raw image. Imaris x64 5.7.2 (Bitplane, Inc.) was used to generate the images and video.

Supplemental 2. Supplemental information for Chapter 2

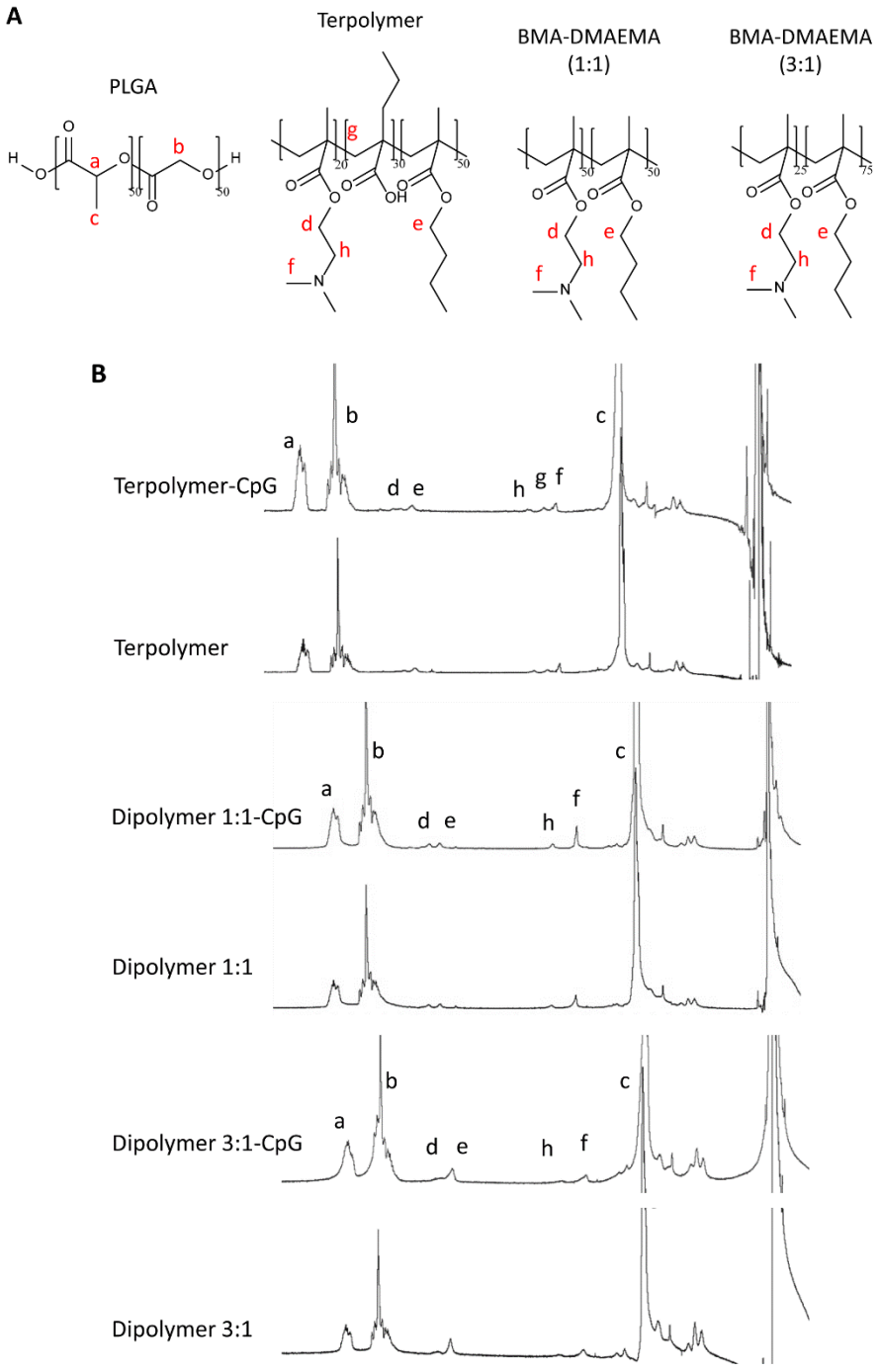

Figure S5. Confirmation of the composition of blend particles by 500 MHz ^{1}H NMR. (A) The chemical structure of PLGA, terpolymer, dipolymer 1:1, and dipolymer 3:1 and the protons observed in (B) ^{1}H NMR spectra of CpG 2216-containing particles and blank particles in $CDCl_3$. PLGA peaks appear in the spectrum of all particle types because all particles were a blend of the PLGA and either the terpolymer or a dipolymer.

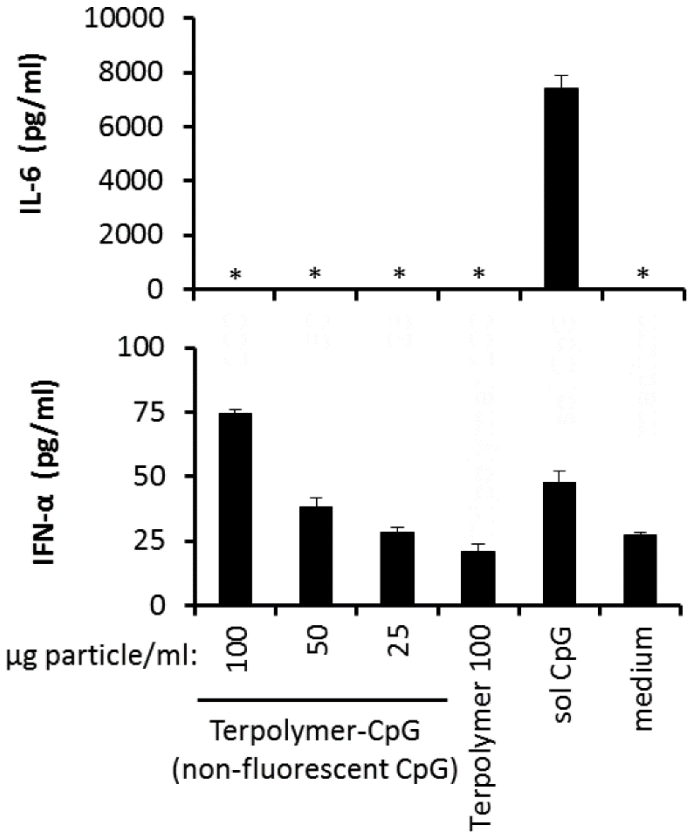

Figure S6. Levels of IL-6 and IFN-α induced by Terpolymer-CpG particles that contain CpG 2216 that is not fluorescently tagged. IL-6 and IFN-α secretions from BC-1 cells after 24 h-incubation with Terpolymer-CpG. 5 µg/ml of soluble CpG was used. The * symbol indicates that the cytokine level was undetectable.

Supplemental 3. The rescue of IL-6 secretion following Ter-CpG 2216 treatment

In Chapter 2, it was shown that NF-κB complexes failed to translocate from the cytoplasm to nuclei in cells treated with Ter-CpG 2216. We next investigated whether Ter-CpG 2216 might activate inhibitors of the NF-κB complex, which would prevent its translocation to nuclei and the transcription of pro-inflammatory genes. To address this issue, cells were pulsed with Ter-CpG 2216 for 4 h, and subsequently treated with soluble CpG 1826, soluble CpG 2216, or LPS, a TLR4 ligand which can induce the pro-inflammatory cytokines such as IL-6 through the NF-κB pathway. The subsequent stimulation by LPS did stimulate IL-6 secretions in cells

pre-treated with Ter-CpG 2216 at the level comparable to cells treated with LPS only. CpG 1826 and CpG 2216 were also able to stimulate IL-6 secretions in cells pre-treated with Ter-CpG 2216, however, the IL-6 secretion was dependent on the initial dose of Ter-CpG 2216. At a higher Ter-CpG 2216 dose, more IL-6 secretion could be obtained by subsequent stimulation with CpG 1826. At a lower dose of Ter-CpG 2216, more IL-6 secretion was obtained with CpG 2216. The same trends were observed for IFN-α secretion. This correlation between the initial Ter-CpG 2216 dose and IL-6 secretion suggest that a synergistic effect occurs between Ter-CpG 2216 and soluble CpG ODNs. Ultimately, these findings suggest that the NF-κB complexes remained functional after Ter-CpG 2216 treatment and could be re-activated by stimuli.

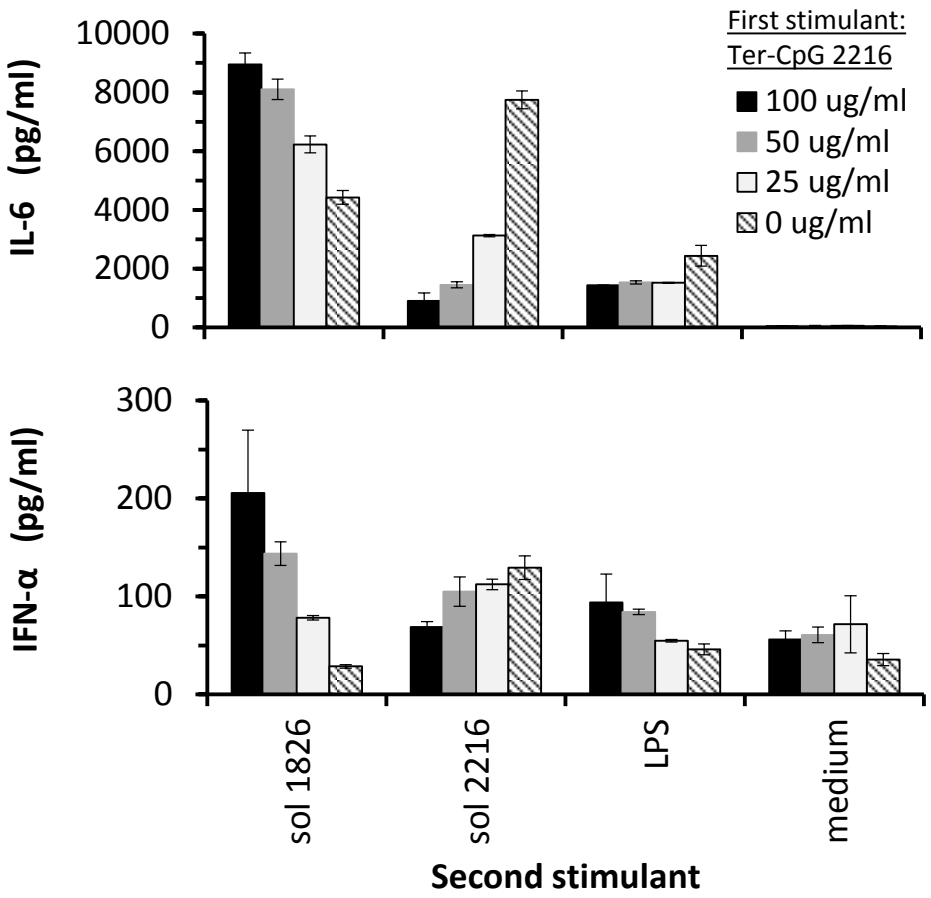

Figure S7. The rescue of IL-6 secretion following Ter-CpG 2216 treatment of BC-1 cells. Cells were pulsed with Ter-CpG 2216 at 100, 50, 25, and 0 μg particle/ml. After 4 h, particles were removed and cells were washed once with DPBS. Cells were incubated in medium for 30 min at 37 °C. Next, the medium was removed, and LPS (1 μg/ml), soluble CpG ODN 1826 (5 μg/ml), soluble CpG 2216 (5 μg/ml), or medium were added to the cells. After 24 h incubation, the IL-6 secretion level was assayed.

Supplemental 4. Ter-CpG 1826 and Ter-CpG 2216 induce distinct cytokine secretion profiles

Two types of commonly used CpG ODNs include type A and type B, such as ODN 2216 and ODN 1826, respectively. Type A ODNs are able to activate both the NF-κB and IRF-7 pathways, whereas type B ODNs activate only the NF-κB pathway. In Chapter 2, it was shown that the natural cytokine secretion profile of CpG ODN 2216 could be tuned by incorporating the ligand into terpolymer blend particles. The incorporation of CpG 1826 into terpolymer blend

particles resulted in both IL-6 and IFN-α production (Figure S8). Although the terpolymer blend did tune the cytokine profile of CpG 1826, it interestingly caused the simultaneous activation of NF-κB and IRF-7 pathways. This particular cytokine profile from type B ODNs has been obtained with CpG 2006 trimers adsorbed onto allylamine-functionalized silica nanoparticles from peripheral blood mononuclear cells (PBMCs) [1], and with CpG 2006 adsorbed to polystyrene particles from pDCs [2]. Altogether, these findings suggest that the manner of presentation of CpG ODNs to TLR9 plays a critical role in the induction of signaling pathways.

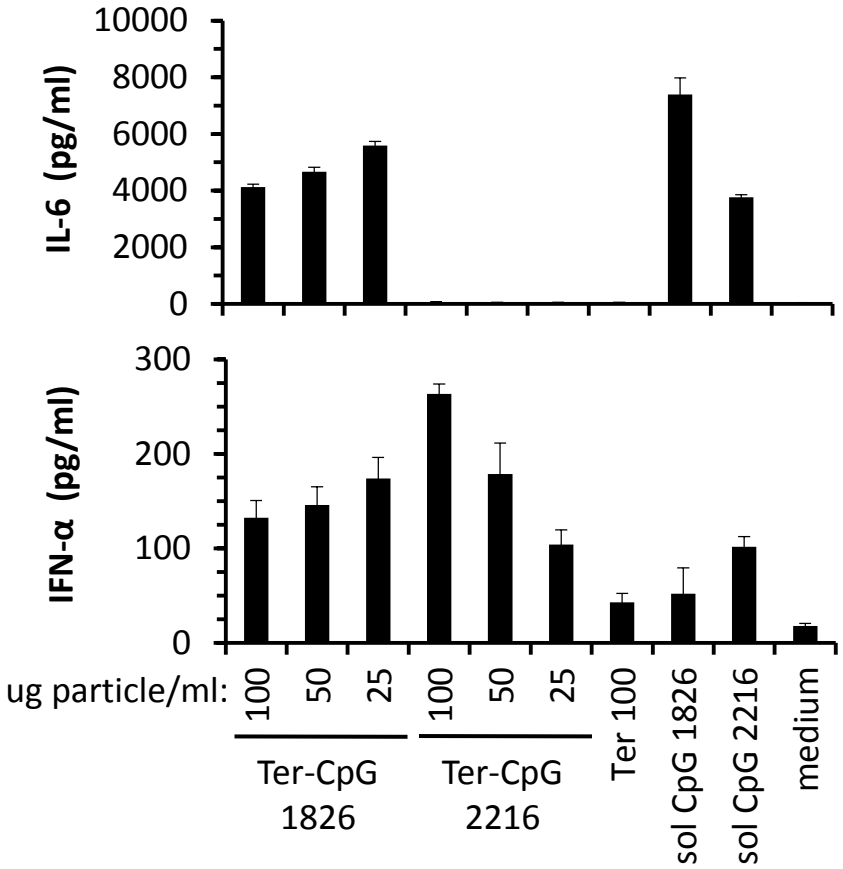

Figure S8. Ter-CpG 1826 and Ter-CpG 2216 induce distinct cytokine secretion profiles from BC-1 cells. Cells were incubated with stimulants for 24 h, and cell supernatants were collected for the analysis of cytokines. Soluble CpG ODNs were prepared at 5 μg/ml.

Supplemental 5. TLR9 signaling regulates the intracellular trafficking of nanoparticles

Introduction

Structurally distinct CpG oligonucleotides (ODNs), type A and type B, induce different immune responses through the activation of toll-like receptor 9 (TLR9). Type A CpG ODN induces both type I IFNs and pro-inflammatory cytokines, whereas type B ODN induces only pro-inflammatory cytokines [3]. Studies suggest that the two TLR9 signaling pathways occur from two distinct endosomal compartments [4, 5]. Type A CpG ODN complexed with N-[1-(2,3-Dioleoyloxy)propyl]-N,N,N-trimethylammonium methyl-sulfate (DOTAP) induced pro-inflammatory cytokines through the NF-κB endosome, and induced type I IFNs through the IRF-7 endosome [4]. The NF-κB endosome was VAMP3-positive, and the IRF-7 endosome was LAMP-2-positive. Because type B CpG activates NF-κB, and type A CpG activates both NF-κB and IRF-7, we hypothesized that these two CpG ODNs accumulate in two distinct intracellular compartments that result in two distinct signaling pathways. In addition, it is unclear whether these two ligands are initially sorted to two distinct compartments or initially sorted to the same type of compartments which then progress into two distinct compartments. Rab5-positive early endosomes are comprised of 2 distinct populations: static early endosomes slowly acquire Rab7, or do not acquire Rab7 at all; dynamic early endosomes quickly acquire Rab7, or already carry Rab7, and have high mobility and directed movement [6].

In this study, we compared the intracellular distributions of types B and A CpG ODN and used single particle tracking (SPT) to examine their trafficking dynamics following their initial endocytosis.

Materials and Methods

Cell culture

A dendritic cell line, BC-1 (a gift from Dr. Yoshiki Yanagawa), was maintained as described previously in Chapter 1.

Immunocytochemistry

DCs were plated at a density of 2.5×10^5 cells per well in 500 µl medium onto the tissue-culture surface of 24 well plates. Cells were allowed to adhere to the surface for 1 h at 37 °C. 100 nm-coated CpG ODN polystyrene particles (1826-PLL-PS or 2216-PLL-PS) were prepared as described previously in Chapter 1. Cells were pulsed with 1826-PLL-PS, 2216-PLL-PS, or PS in 500 µl of 10 vol% medium at 75,000, 50,000, or 100,000 particles per cell respectively for 2 h at 37 °C. To examine cells by fluorescence microscopy, cells were detached from the tissue-culture surface by trypsinization and then plated onto 12 mm circular glass coverslips (Erie Scientific Co., Portsmouth, NH). To enhance the adherence of cells to coverslips, coverslips were first pre-treated with poly-D-lysine (PDL, Sigma-Aldrich, Inc., Saint Louis, MO) by incubating them with 400 µl PDL at 0.025 mg/ml for 15 min at RT. Coverslips were washed four times with 500 µl Milli-Q water and allowed to dry before the seeding of cells. Cells were allowed to adhere for 1 h at 37 °C. Afterward, cells were fixed and permeabilized with 250 µl BD Cytofix/Cytoperm™ (Invitrogen, Frederick, MD) for 20 min at 4 °C. Cells were washed two times with 250 µl BD Perm/Wash Buffer™ (Invitrogen, Frederick, MD). To examine α-tubulin, cells were first labeled with 250 µl rat mAb to tubulin (Abcam, Cambridge, MA) at 1 ug/ml BD Perm/Wash Buffer™ for 1 h at RT. Cells were washed two times with BD Perm/Wash Buffer™. To detect the primary antibody, cells were incubated with 250 µl BD Perm/Wash Buffer™ containing 2 ug/ml Alexa Fluor 647-goat anti-rat IgG (Invitrogen,

Frederick, MD) for 1 h at RT. Lastly, cells were washed two times. Coverslips were rinsed with Milli-Q water and then mounted onto glass slides using DAPI-containing HardSet Vectashield Mounting Medium (Vector Laboratories, Inc., Burlingame, CA) for imaging.

Immunofluorescence Microscopy

Images were acquired with a DeltaVision microscope equipped with a 63× 1.40 numerical aperture (N.A.) oil immersion differential interference contrast objective lens. Images were acquired for single-stained samples to confirm that cross talk between channels did not exist.

Live-Cell Imaging

DCs were added to a well of Lab-Tek II chambered coverglass (ThermoFisher Scientific) at 1.5×10^5 cells per well in 300 μl medium. After overnight incubation at 37 °C, ~ 150 μl medium was removed from the well to reduce the path length that particles would have to travel to reach cells. Particles were added drop-wise to cells in 100 μl of 10 vol% medium. Image acquisition began immediately after the entire particles were added. Time-lapse images were acquired at one plane in which the nucleus of the cell was in focus. A 63× 1.40 N.A. oil immersion differential interference contrast (DIC) objective lens was used. Both DIC and fluorescence images were acquired at 3 seconds per frame for 30 minutes. A humidified environment at 37 °C was maintained inside the live-cell imaging chamber. The ImageJ plugin, Manual Tracking (http://rsbweb.nih.gov/ij/plugins/track/track.html), was used to track the movement of individual particles in a time-lapse series of images.

Results and Discussion

The intracellular location of nanoparticles is CpG sequence-dependent

The different intracellular distributions of CpG ODNs are shown in Figure S9. α-tubulin was labeled to indicate the location of the microtubule-organizing center (MTOC). Endosomes

which have matured along the endocytic pathway are typically near the MTOC. 2216-PLL-PS was concentrated in the perinuclear region and colocalized with the MTOC. In contrast, 1826-PLL-PS and control GpC 2216-PLL-PS were distributed throughout the peripheral cytoplasm and perinuclear region, and were not concentrated near the MTOC. The distinct intracellular distributions of the particles suggests that the ODN type affects the destination of nanoparticles.

Next, single particle tracking (SPT) of ODN-PLL-PS was used to characterize the modes of ODN transport. Within 30 minutes of particle uptake, 2216-PLL-PS was observed to move from the peripheral cytoplasm to the perinuclear region (Figure S10). As shown in Figure S11A, three modes of particle transport were observed: the particle remained in the peripheral region, the particle moved from the peripheral to the perinuclear region, or the particle remained in the perinuclear region during the imaging period. The type of CpG appeared to affect which mode of transport was taken. All 1826-PLL-PS particles and most 2216-PLL-PS particles examined remained in the peripheral region. However, few 2216-PLL-PS particles moved from the peripheral to the perinuclear region or remained in the perinuclear region.

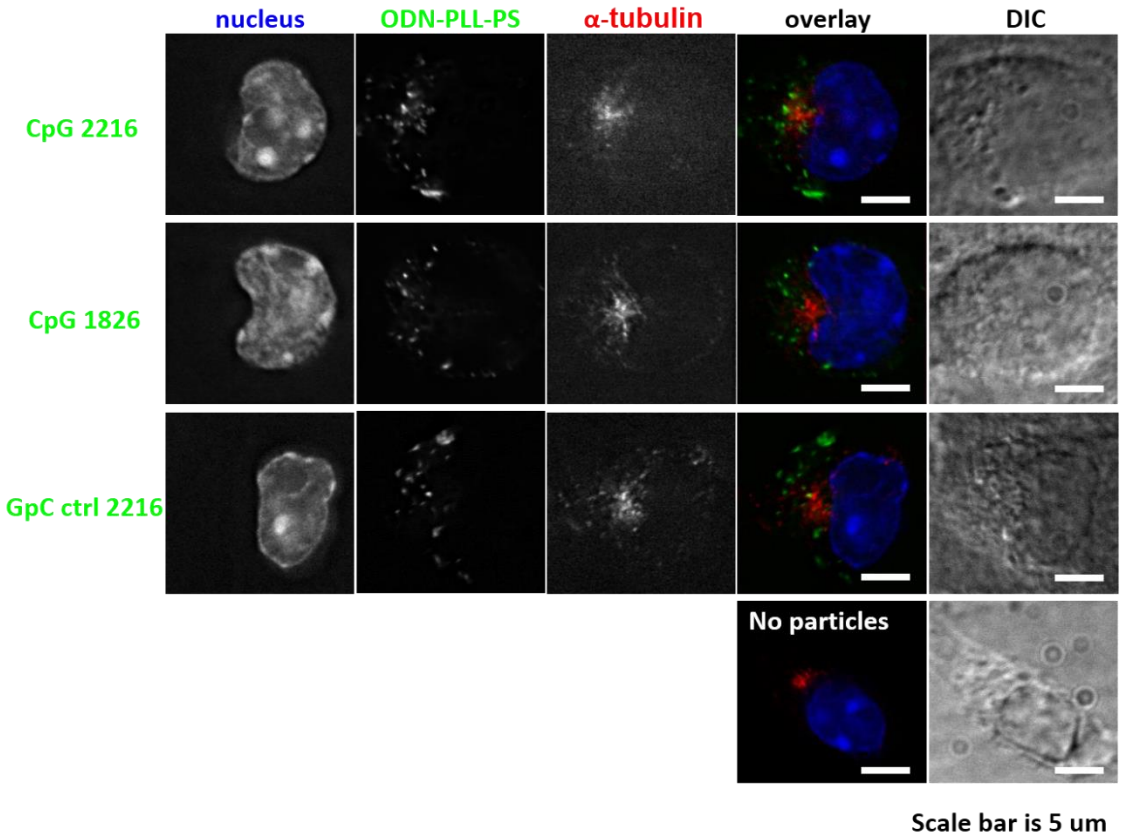

Figure S9. Intracellular distributions of ODN-PLL-PS relative to the microtubule-organizing center. Cells were exposed to particles for 2 h (pulse), and further incubated for 1 h (chase). Nuclei (blue) were stained by DAPI, ODN-PLL-PS (green) contained FITC, α-tubulin (red) was stained with by anti-α-tubulin. Differential interference contrast (DIC) images are shown in the far right column.

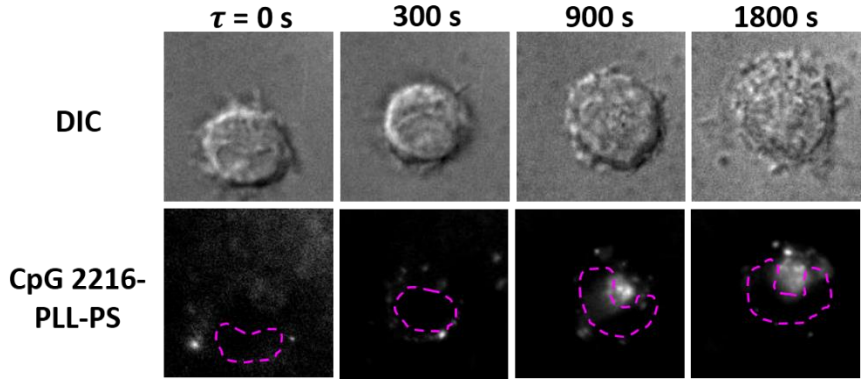

Figure S10. CpG 2216-ODN-PLL-PS traffics to the perinuclear region within 30 min particle uptake. Images were acquired by live-cell imaging at 37 °C. The nuclei appear in differential interference contrast (DIC) images, and the perimeter of each nucleus is outlined by pink dotted lines. CpG 2216-PLL-PS appear as punctate structures and fluoresced because FITC was encapsulated inside PS.

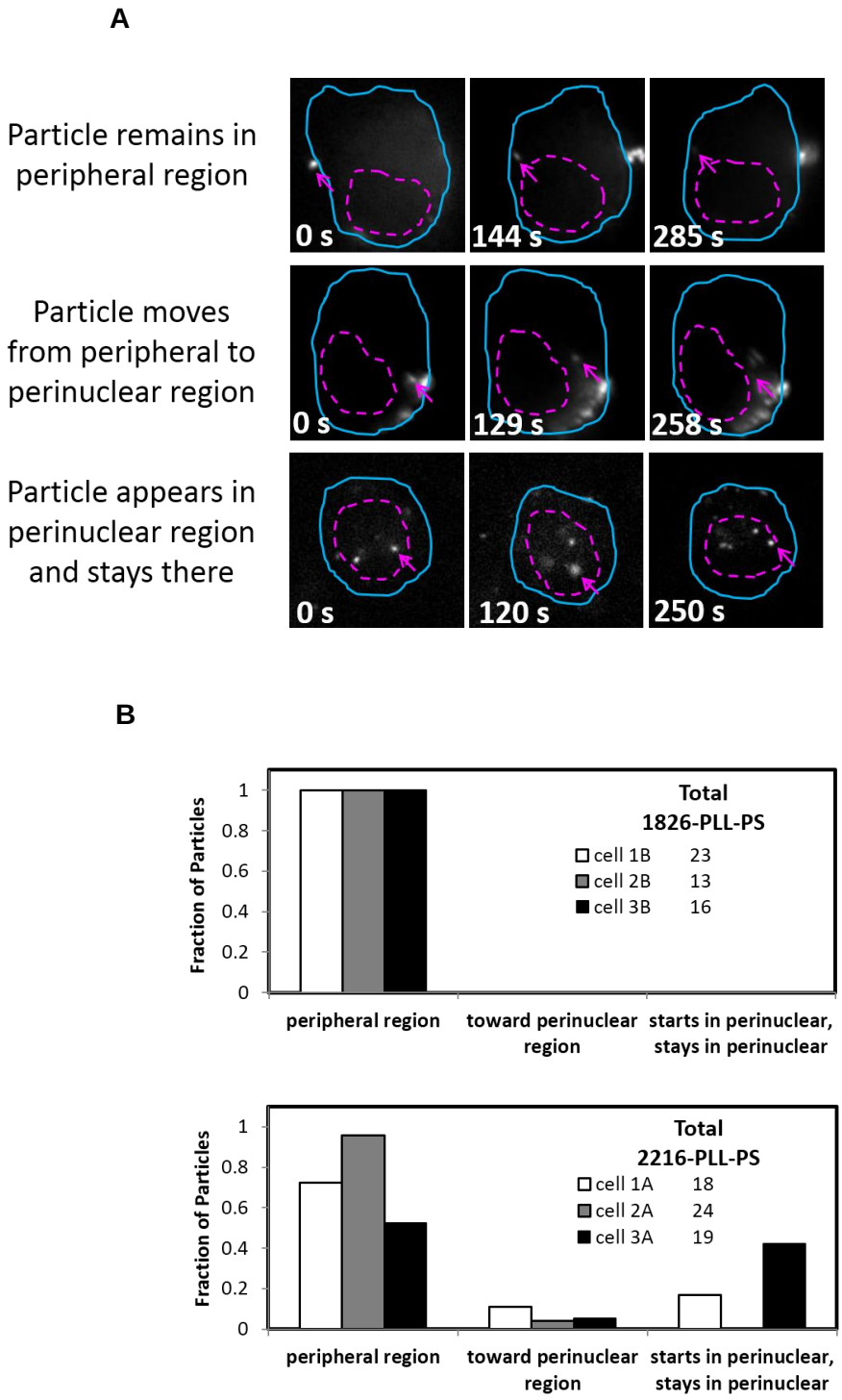

Figure S11. Differences in the mode of particle transport between 1826-PLL-PS and 2216-PLL-PS. (A) All observed cases of particle transport inside cells. The perimeter of the nucleus is outlined in pink; the cell membrane is outlined in blue. (B) The fraction of 1826-PLL-PS and 2216-PLL-PS particles that exhibited each case of particle transport. Three cells were analyzed for each particle type; the number of particles analyzed per cell are indicated.

Next, the dynamic movement of particles was examined. Unfortunately, dendritic cells were highly mobile throughout the imaging period. The particle displacement at each time point was measured as the distance between the particle and the nucleus' center of mass. This measurement is referred to as r_{p-n}. The standard deviation of r_{p-n} over the duration that the particle remained within the focal plane was used to characterize the mobility of the particle relative to the nucleus. A cutoff value of 0.5 for the standard deviation of r_{p-n} was used to compare the population of particles which were mobile (> 0.5) or less mobile (< 0.5). Through this method of analysis, ~ 10% of 1826-PLL-PS particles are less mobile than 2216-PLL-PS. Altogether, these preliminary results suggest that type A CpG is initially transported to dynamic endosomes which eventually mature as the endosomes move toward the perinuclear region.

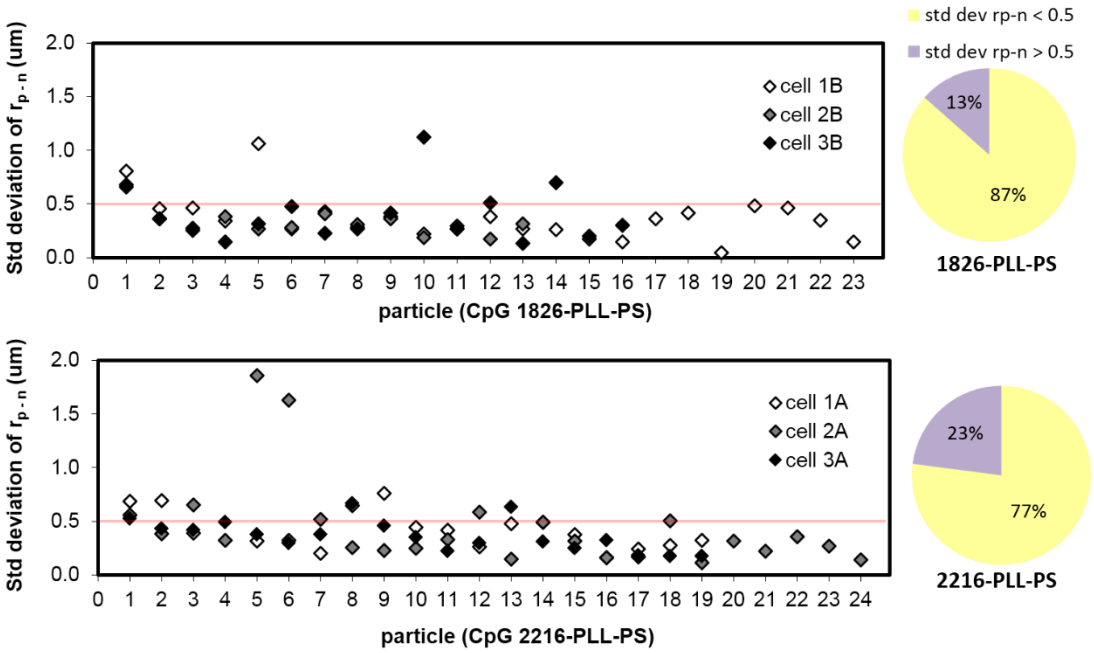

Figure S12. The effect of the type of CpG on the mobility of nanoparticles. The standard deviation of the nanoparticle displacement, r_{p-n}, is used to characterize the particle mobility. Red lines mark the standard deviation of r_{p-n} at 0.5. Pie charts (right) illustrate the relative percentages of the standard deviation of r_{p-n}.

Supplemental 6. The effect of polymer blend particles on the cytokine secretion profile of THP-1 cells

As shown in Chapter 2, the polymer blend particles are able to target the type I IFN pathway in mouse splenocytes and a mouse dendritic cell line, BC-1. We investigated whether the polymer blend particles could also target the type I IFN pathway in human cells. The human monocytic cell line, THP1, was used because it expresses TLR9 and is responsive to CpG ODN [7], and when primed with LPS it upregulates TLR3 expression [8]. THP1 cells were primed with LPS for 20 h, and subsequently were incubated with polymer blend particles for 24 h. Figure S13 indicates that the THP1 cells induced insignificant levels of IL-6 and type I IFN. The type I IFN concentrations for samples containing Ter-adsorb polyIC, soluble polyIC, and soluble CpG appear to be dependent on the ligand dose. However, these sample calculations were made according to the standard curve for plate #2 (Figure S14), which had a lower y-intercept, resulting in artificially higher type I IFN values for those samples.

THP1 cells need to first be LPS primed in order to induce TNF-α in response to polyIC treatment [8]. In our study, the LPS-primed THP1 cells did not respond to polyIC. This could be attributed to the insufficient number of cells remaining in the well of the 96-well plate; many cells were lost due to washing steps after LPS treatment. Similarly, the lack of responsiveness to CpG ODN is also likely due to the insufficient number of cells after washing cells to remove LPS.

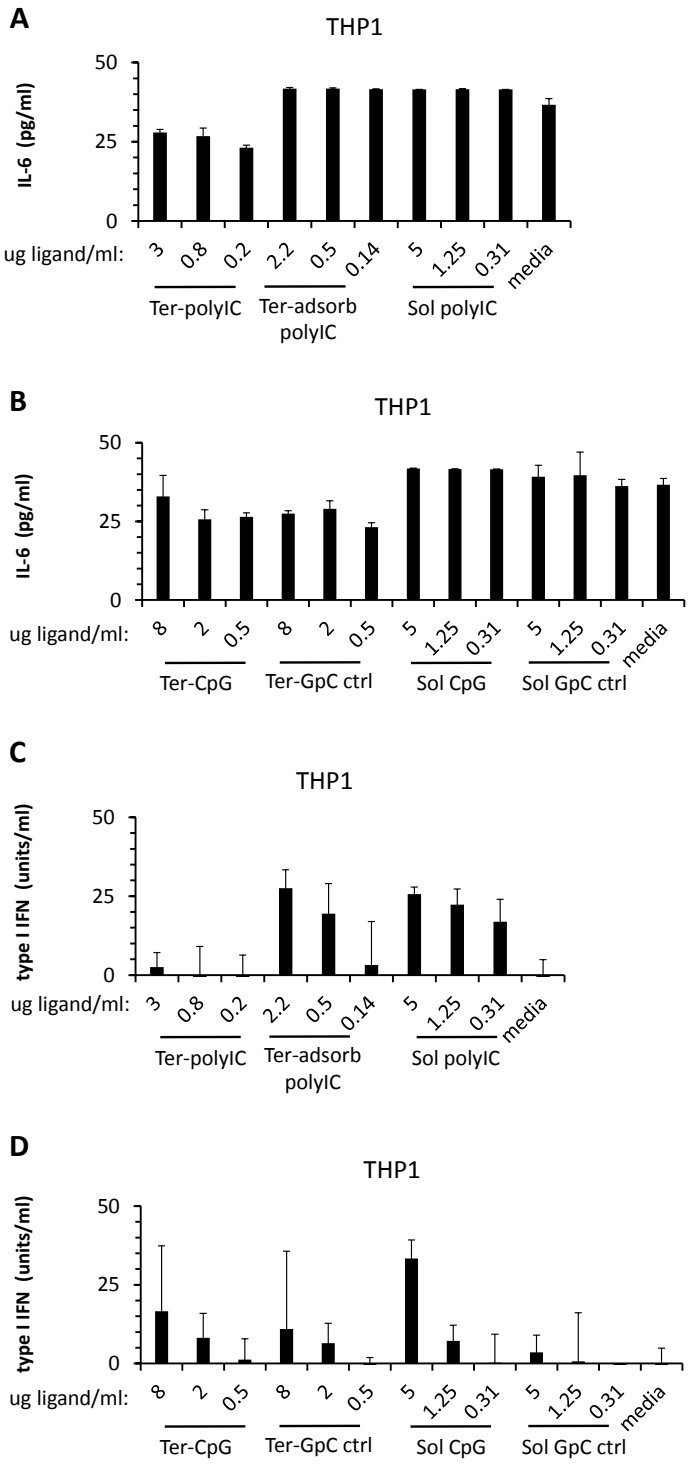

Figure S13. Effect of polymer blend particles on the cytokine secretion from THP1 cells. THP1 cells were differentiated by incubation with lipopolysaccharide (LPS) at 2 μg/ml for 20 h. LPS was removed, and polymer blend particles were incubated with cells for 24 h. The IL-6 and type I IFN secretions were assayed for polymer blend particles containing (A, C) polyIC or (B, D) CpG ODN 2216 and GpC ODN 2216.

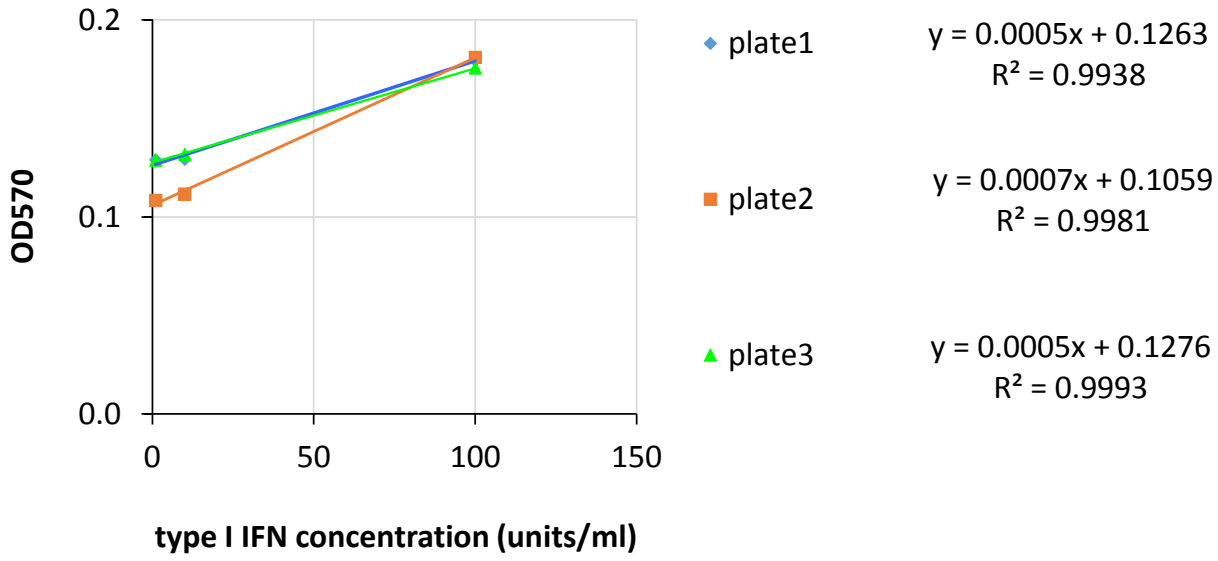

Figure S14. Standard curves used for the quantification of the type I IFN concentration in THP1 cell supernatants. The absorbance measurements of samples from the bioassay ranged between 0.1 to 0.14. Therefore, linear regressions that ranged from an absorbance of 0.1 to 0.18 were used to quantify the type I IFN concentration in THP1 cell supernatants.

Supplemental 7. The effect of polymer blend particles on MDA-MB-231 cells

Ter-CpG particles and blank particles did not affect cell viability within 3 and 6 days of treatment within the wide range of particle concentrations tested (Figure S15). Soluble type B and A CpGs, 2006 and 2216, respectively, and soluble polyIC did not induce cell death either. Positive controls include type I IFN at 10,000 units/ml and camptothecin at 5 µM, which are known to induce MDA-MB-231 cell death [9, 10]. In addition, the proliferation of MDA-MB-231 cells was unaffected by Ter-CpG and soluble ligands within 3 and 6 days of treatment (Figure S16). Since the cytokine, IL-6, is known to affect the proliferation of cells, we next assayed for IL-6 to confirm that it was present in supernatants of proliferating cells. After 3 days of treatment, IL-6 levels showed dependence on the Ter-CpG dose, but after 6 days of treatment, IL-6 levels of TLR ligand-treated cells were similar to that of non-treated cells (Figure S17). Interestingly, type I IFN-treated cells induced the most IL-6 secretion even though cell

proliferation was inhibited. Camptothecin-treated cells induced the least IL-6 secretion. The concentration of camptothecin used for this set of experiments was 5 μM. Lower camptothecin concentrations resulted in higher IL-6 secretion (Figure S18). High camptothecin concentrations likely killed cells which affected the level of IL-6 secretion.

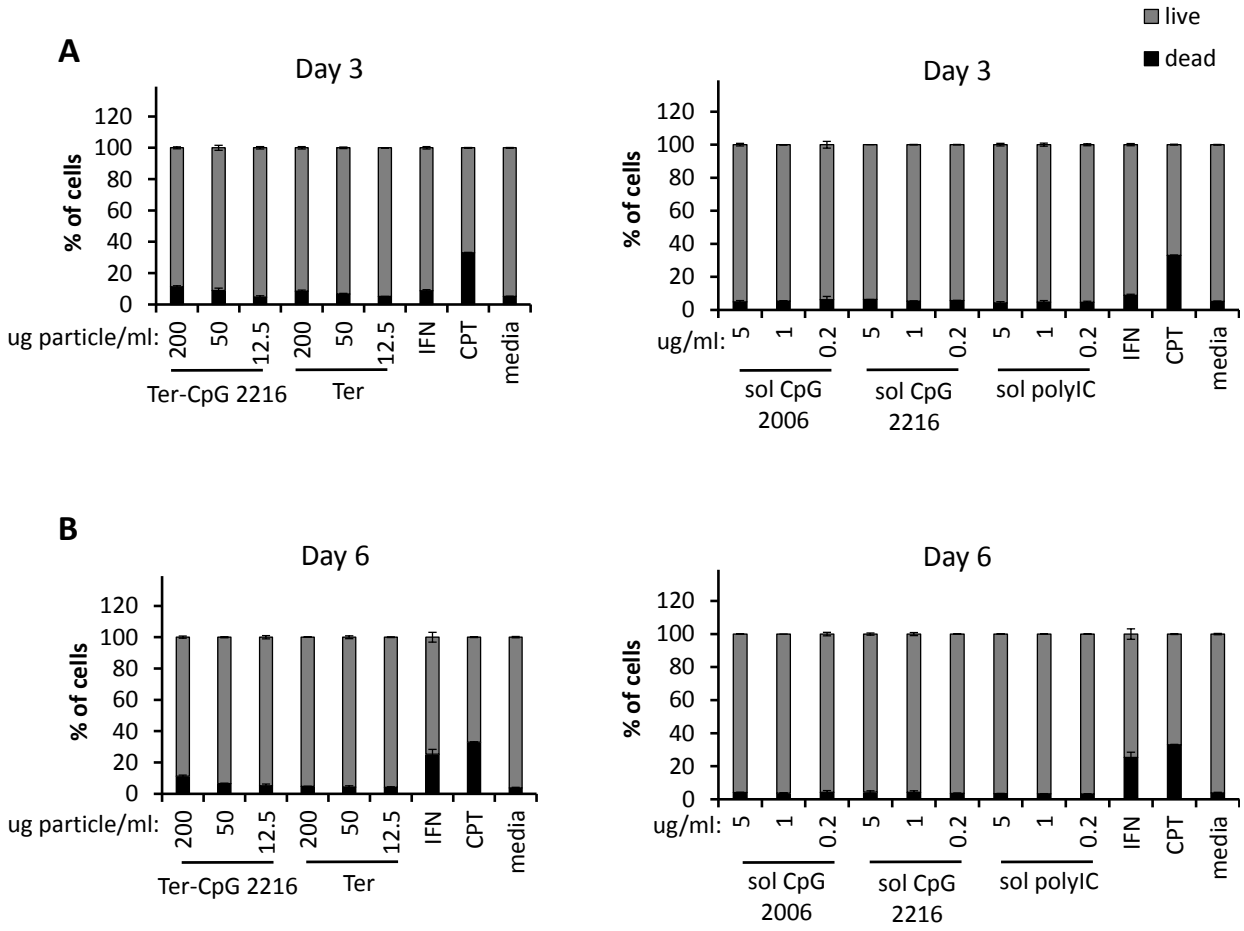

Figure S15. Effect of Ter-CpG on MDA-MB-231 cell viability. Particles and soluble ligands were incubated with cells for (A) 3 days or (B) 6 days, and the cell viability was analyzed by Annexin-V and 7-AAD staining. Positive controls included human leukocyte type I IFN at 10,000 units/ml and camptothecin at 5 μM. Type I IFN was incubated with cells for 3 days or 6 days. Camptothecin was incubated with cells for 3 days only. Both positive controls were more effective treatments than particles. The Ter-CpG particle concentrations (200, 50, and 12.5 μg particle/ml) correspond to ligand concentrations of 8, 2, and 0.5 μg CpG ODN 2216/ml, respectively.

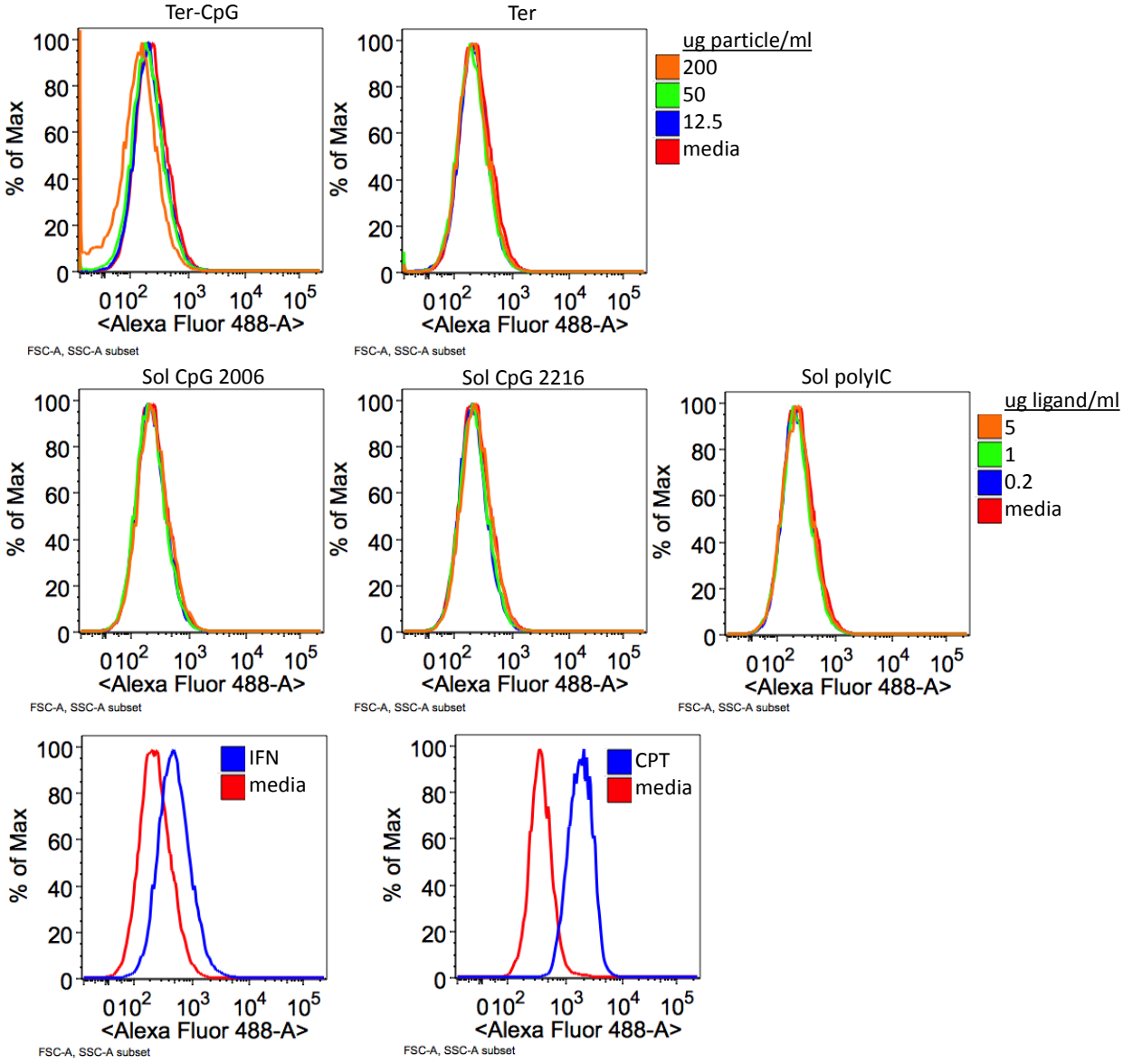

Figure S16. Effect of Ter-CpG on MDA-MB-231 cell proliferation. Particles and soluble ligands were incubated with cells for 6 days and the gMFI of CFSE was analyzed and compared to the gMFI of CFSE of non-treated cells (media control). Positive controls included human leukocyte type I IFN at 10,000 units/ml and camptothecin at 5 μM. Type I IFN was incubated with cells for 3 days or 6 days. Camptothecin was incubated with cells for 3 days only. Positive controls were effective at preventing cell proliferation, but particles and soluble ligands were not effective. The Ter-CpG particle concentrations (200, 50, and 12.5 μg particle/ml) correspond to ligand concentrations of 8, 2, and 0.5 μg CpG ODN 2216/ml, respectively.

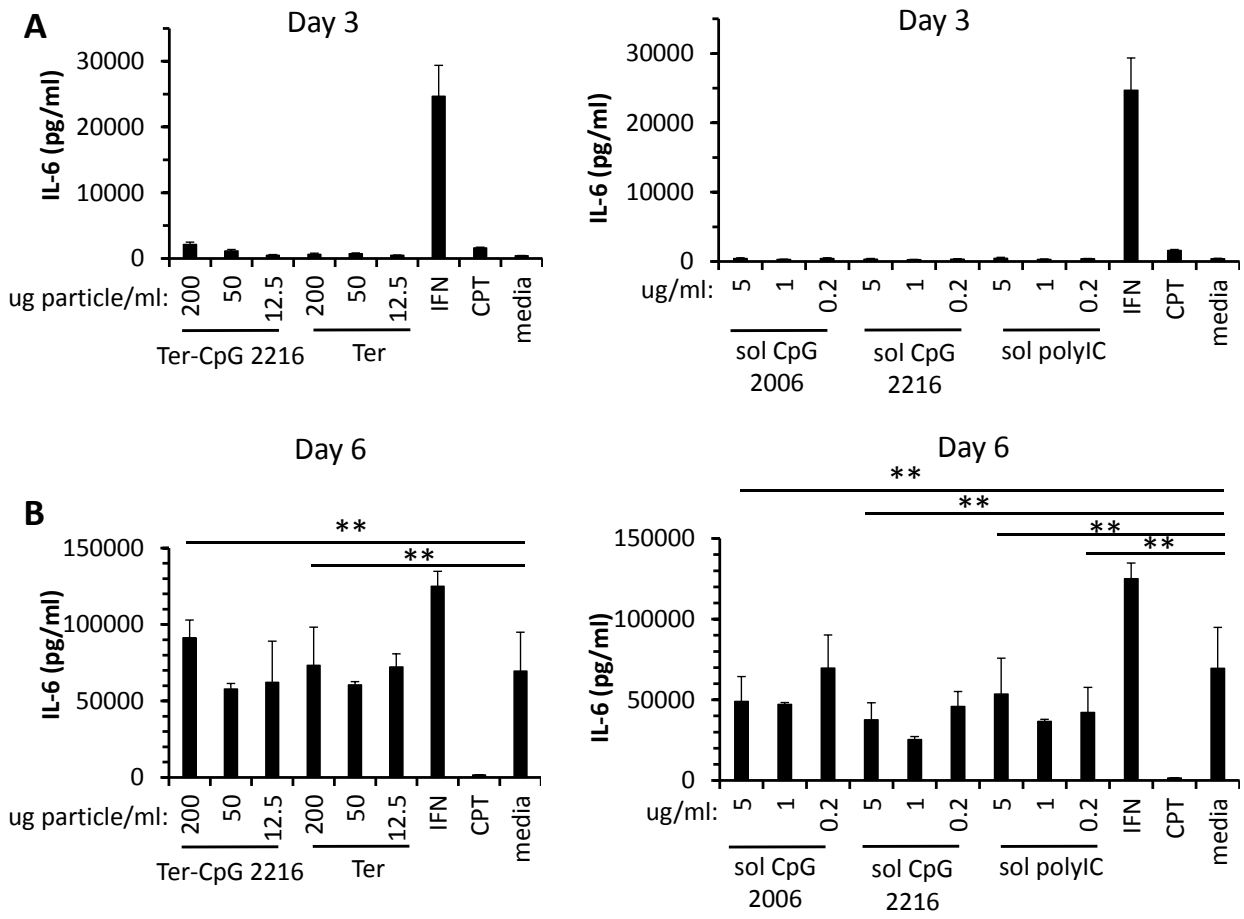

Figure S17. IL-6 secretion from MDA-MB-231 cells treated with Ter-CpG. Particles and soluble ligands were incubated with cells for (A) 3 days or (B) 6 days. Type I IFN at 10,000 units/ml and camptothecin at 5 μM were incubated with cells for 3 days or 6 days. The Ter-CpG particle concentrations (200, 50, and 12.5 μg particle/ml) correspond to ligand concentrations of 8, 2, and 0.5 μg CpG ODN 2216/ml, respectively. A one-tailed and unpaired student t-test was used to analyze the differences between experimental groups. The * symbol indicates $p < 0.05$, and the ** symbol indicates $p > 0.05$.

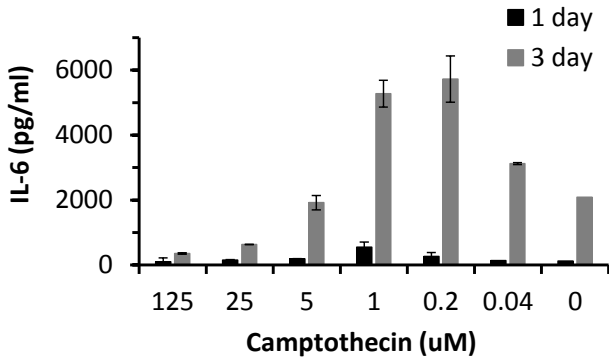

Figure S18. Dose-dependent IL-6 secretion from MDA-MB-231 cells treated with camptothecin. Camptothecin was incubated with cells at the indicated concentrations, and the cell supernatants were collected after 1 or 3 days.

Supplemental 8. The effect of polymer blend particles on purified BT-20 cell subpopulations

Results from Chapter 3 indicated that Ter-polyIC affected the viability of the CD44 medium cell subpopulation, but not the CD44 high cell subpopulation. We found that these two subpopulations could also be distinguished through their level of CD24 expression. CD24(+) BT-20 cells were identified as CD44 medium cells, and CD24(-) BT-20 cells were identified as CD44 high cells. These cell subpopulations were purified and used for experiments to isolate the responses of each subpopulation to Ter-polyIC.

The two subpopulations induced distinct cytokine secretion profiles in response to Ter-polyIC. The CD24(+) cells secreted lower IL-6 levels than CD24(-) cells (Figure S19). However, CD24(+) cells secreted type I IFNs whereas CD24(-) cells did not (data not shown). This suggests that the CD24(+) cells were the source for type I IFNs. We next neutralized IL-6 or the IFN-α/β receptor (IFNAR) to determine whether IL-6 and/or type I IFNs affected cell survival. The differences in cell viability between (1) samples incubated with Ter-polyIC and (2) samples incubated with both Ter-polyIC and neutralization antibody were statistically insignificant ($p > 0.12$) by the unpaired, one-tailed student t-test. Therefore, the roles of IL-6 and

type I IFNs could not be deciphered from the neutralization results. The duration of the incubation with neutralizing antibodies was 3 days. If the stability of the neutralization antibodies was compromised after 1 day of incubation, a difference in cell viability should still be observed between samples incubated with Ter-polyIC and samples incubated with both Ter-polyIC and neutralization antibody. The concentration range of anti-IL-6 was prepared in excess of IL-6 levels (Figure S19) in the cell supernatant. One could determine whether IL-6 signaling is required for cell proliferation by incubating cells with different doses of IL-6. If cell proliferation and survival is not affected by IL-6, it is possible that proliferation occurs through an IL-6-independent pathway. In addition, the concentration range of anti-IFNAR was consistent with that used in the literature [11]. Further investigation of the effect of type I IFNs is needed to determine whether cell proliferation and survival is IFNAR-independent.

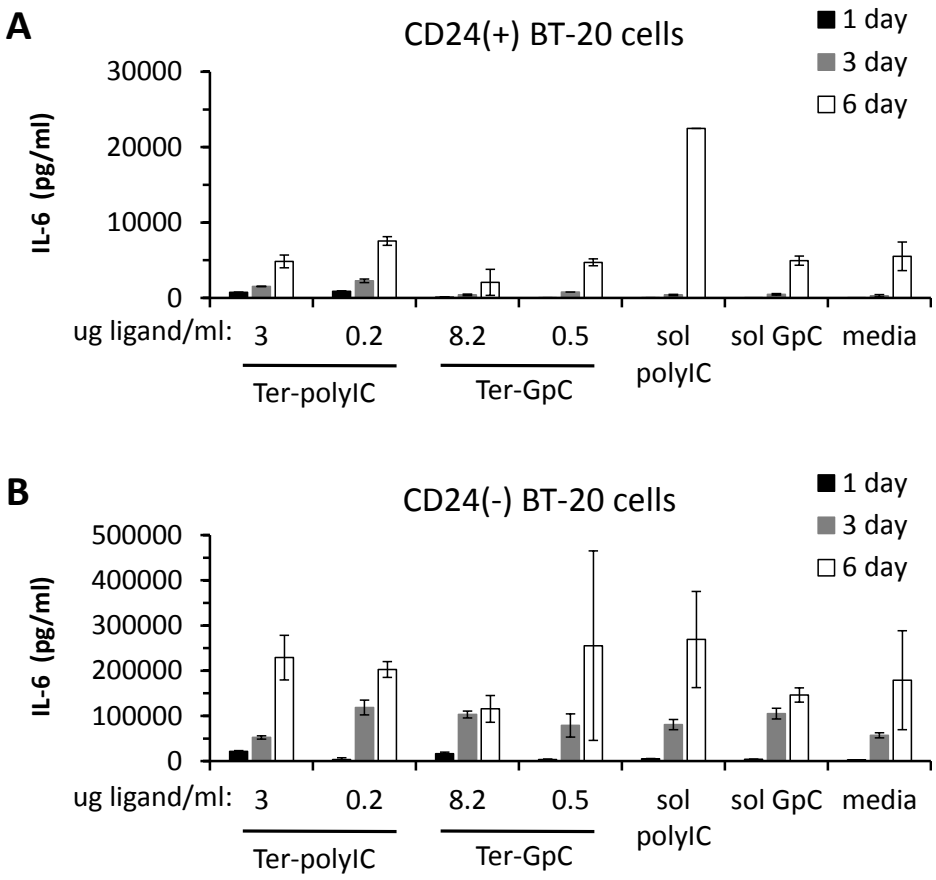

Figure S19. Effect of polyIC on the secretion of IL-6 from BT-20 cell subpopulations. (A) CD24(+) BT-20 cells and (B) CD24(-) BT-20 cells were incubated with stimulants for 1, 3, or 6 days, and cell supernatants were analyzed. Soluble ligands were prepared at 5 µg/ml.

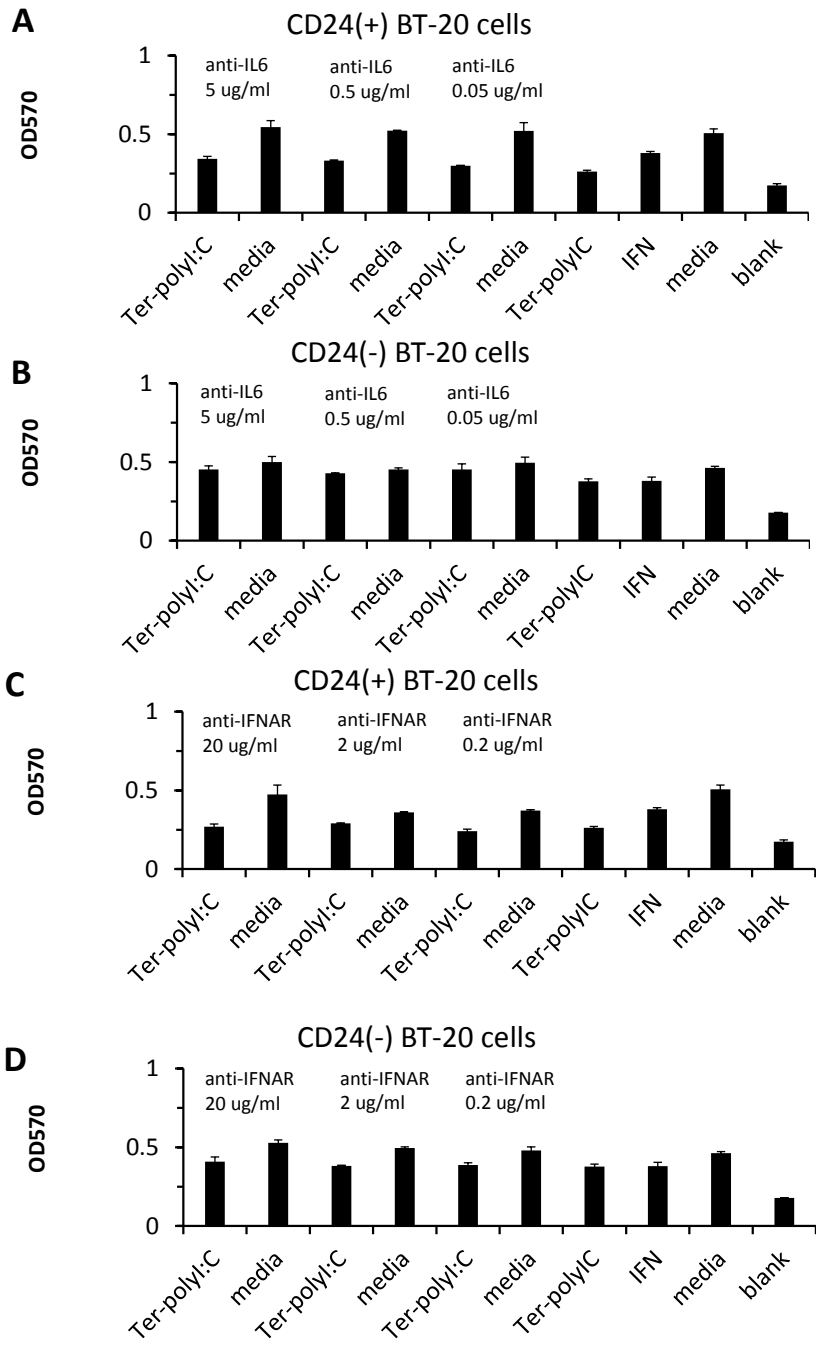

Figure S20. Effect of IL-6 and type I IFN signaling on BT-20 cell subpopulations. CD24(+) BT-20 cells and CD24(-) BT-20 cells were incubated with or without stimulants in the presence of (A, B) anti-IL6 or (C, D) anti-IFNAR. For anti-IL6 samples, cells were first pulsed with stimulants for 4 hours. Then, anti-IL6 was incubated with cells. For anti-IFNAR samples, cells were first incubated with anti-IFNAR for 2 hours; next, cells were pulsed with stimulants in the presence of anti-IFNAR for 4 hours; stimulants were removed, and cells were incubated with anti-IFNAR. After 3 days, cell viability was analyzed by MTT assay. Ter-polyIC was used at a concentration of 0.8 μg/ml polyIC. Type I IFN was prepared at 1,000 units/ml.

A comparison of the zeta potentials between Ter-CpG and blank Ter particles from Chapter 2 suggested that CpG ODN is exposed at the surface of Ter-CpG. Similarly, we hypothesize that polyIC is exposed at the surface of Ter-polyIC. In Chapters 2 and 3, we showed that the adsorption of TLR ligands onto Ter particles resulted in a different cytokine profile from particles that encapsulate the ligands (Ter-polyIC and Ter-CpG). Therefore, we examined whether the manner of presentation of polyIC affected the viability of CD24(+) and CD24(-) BT-20 cells. The amount of polyIC exposed at the surface of Ter-polyIC could not be estimated, but we attempted to mimic this particle surface by adsorbing a small amount of polyIC onto Ter particles (Ter-adsorb polyIC low). In contrast, Ter particles nearly saturated with polyIC on their surface were made by adsorbing a large amount of polyIC onto Ter particles (Ter-adsorb polyIC high). The different effects of Ter-polyIC, Ter-adsorb polyIC high and soluble polyIC on CD24(+) cell viability were statistically insignificant ($p > 0.3$). It is important to note that the morphology of CD24(+) purified cells used for this experiment had changed to a round shape, which was quite different from the elongated shape that was observed shortly after BT-20 cells were sorted. The effect of the amount of polyIC adsorbed onto the surface of Ter particles can be re-examined with a younger generation of purified cells.

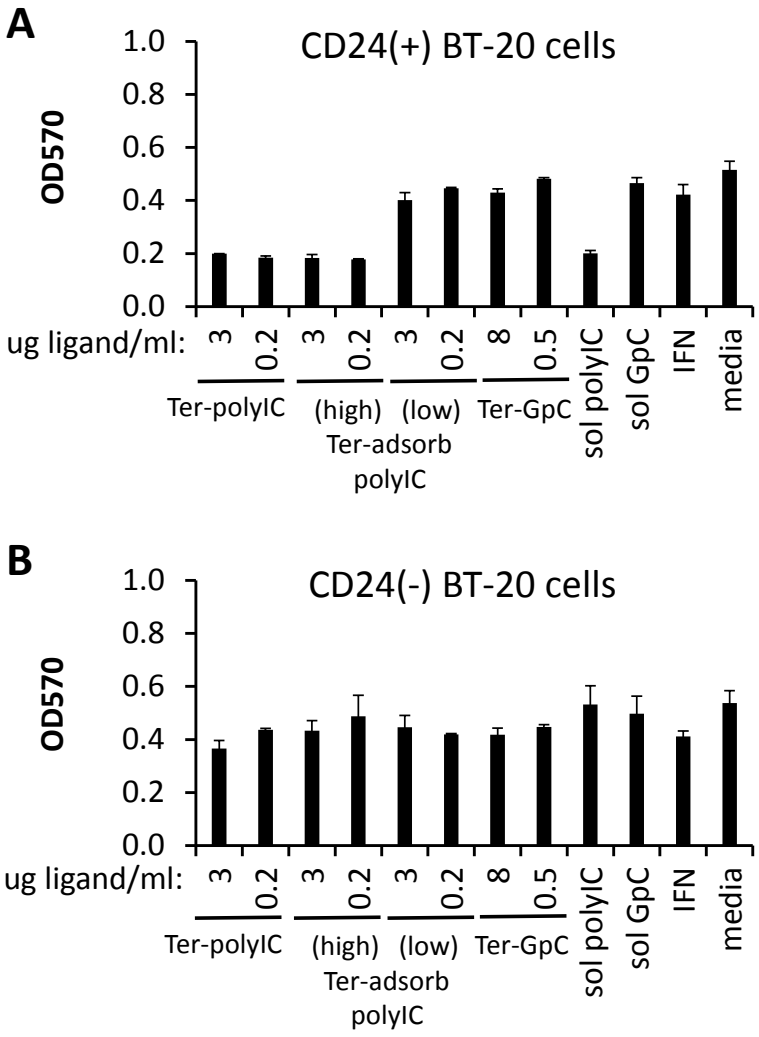

Figure S21. Effect of the mode of presentation of polyIC by polymer blend particles on the viability of BT-20 cell subpopulations. (A) CD24(+) BT-20 cells and (B) CD24(-) BT-20 cells were incubated with stimulants for 3 days, and cells were analyzed for cell viability by MTT assay. Type I IFN was prepared at 1,000 units/ml.

Supplemental 9. The effect of pH on the release of polyIC from Ter-polyIC

In Chapter 2, it was shown that Ter-CpG retained CpG ODN after 24 h incubation at 37°C. The same experiment was performed for Ter-polyIC. Preliminary results indicated that the polyIC was present at low concentrations in the supernatants after incubation at 37°C (Figure S22). Future experiments need to be performed to confirm that polyIC was retained in the

pellets. In Chapter 3, cells were pulsed with particles for 4 hours, so it can be concluded that the particles released negligible amounts of polyIC prior to particle internalization. Within 1 day, approximately 20% of the polyIC was released from particles. By day 6, 40% of the polyIC was released.

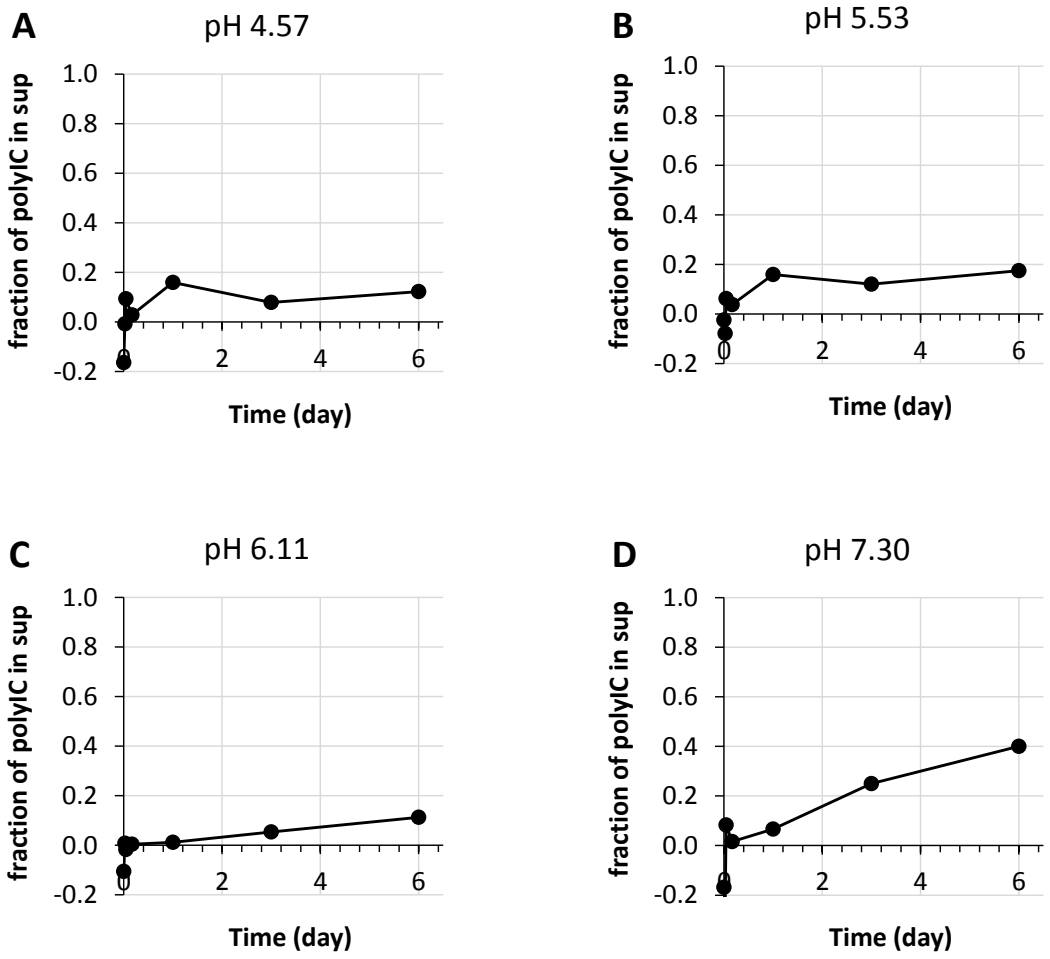

Figure S22. Effect of pH on the release of polyIC from Ter-polyIC particles at 37 °C. Particles were incubated in 10 mM citric acid and 20 mM disodium hydrogen phosphate. The polyIC release profiles are shown as the fraction of polyIC released from particles into the supernatant. The fraction of polyIC was determined by normalizing the amount of polyIC to the amount of polyIC in the pellet at 0 hours.

Supplemental 10. The method of analysis of BT-20 cells by flow cytometry

The initial gating of BT-20 cells in flow cytometry plots

A flow cytometer was used to analyze cells that were pulsed with particles, but these samples contained residual particles. A method for gating cells was established so that the effect of residual particles on analyses was minimized. BT-20 cells and samples containing particles only were stained with anti-CD44-PE-Cy7, AnnexinV-Alexa Fluor 488, and 7-AAD (PerCP-Cy5.5). Flow cytometry plots of stained particles are shown in Figure S23. The gated population in forward scatter versus side scatter plots contains cells and excludes particles (Figure S24). For cell death analysis, this gated cell population was next plotted as AnnexinV versus 7-AAD (Figure S25). Here, a quadrant gate was drawn according to single-stained cell controls. The live cell population comprised the lower left quadrant only, whereas the dead cell population comprised the other three quadrants. For the analysis of CD44 cell subpopulations, the forward scatter versus side scatter gated population was examined as a histogram of anti-CD44-PE-Cy7 fluorescent intensity (Figure S26). This histogram was divided into three subsets according to the three distinct peaks that represented low, medium, and high levels of CD44 staining.

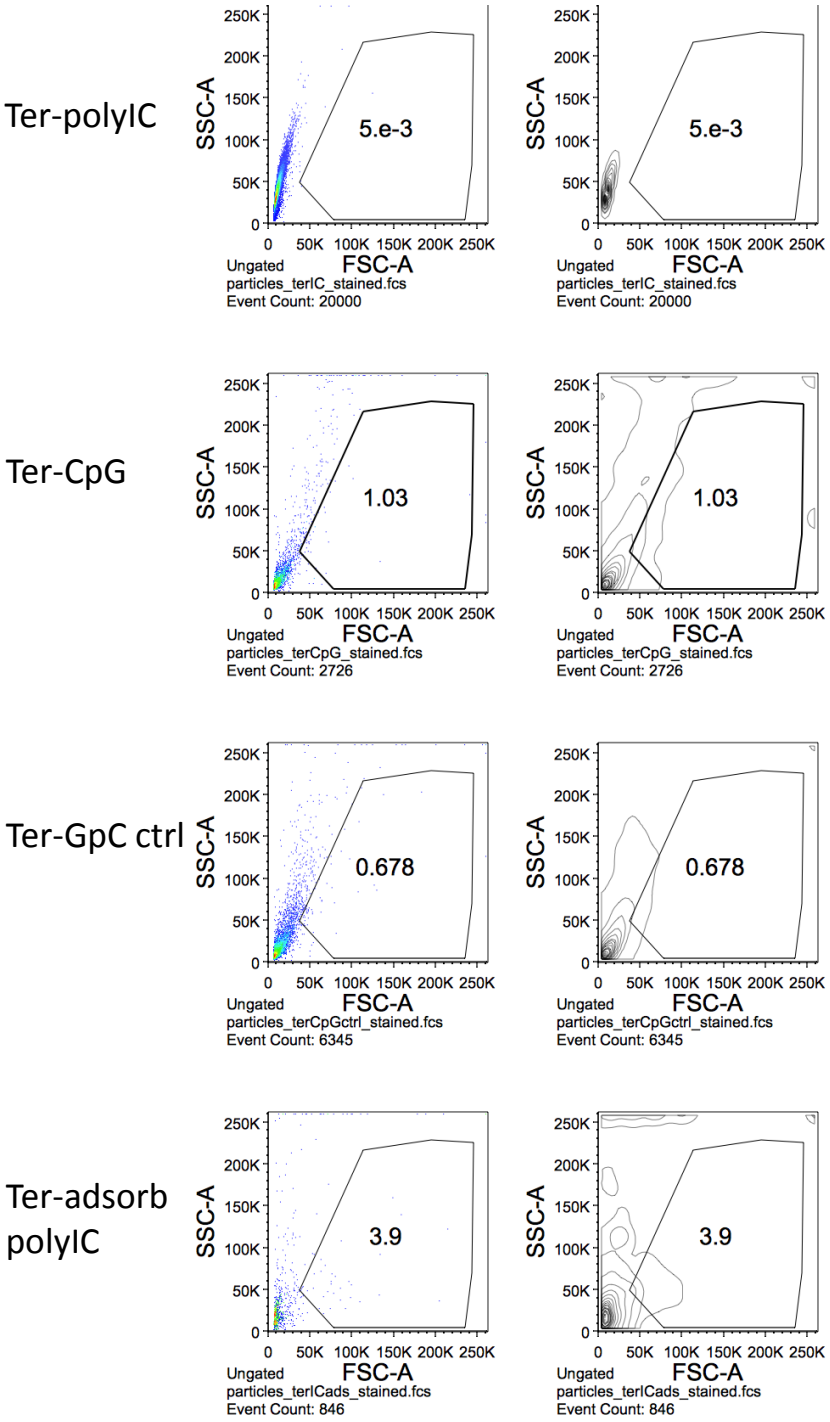

Figure S23. Flow cytometry plots of polymer blend particles stained with anti-CD44, AnnexinV, and 7-AAD. The plots show the forward scatter versus the side scatter of stained particles. Particles were stained using the same protocol for staining cells with anti-CD44-PE-Cy7, AnnexinV-Alexa Fluor 488, and 7-AAD (PerCP-Cy5.5). Gates used for analysis were drawn to exclude the particle population, but to include the cell population. Pseudocolor dot plots are shown in the left column, and contour plots are shown in the right column.

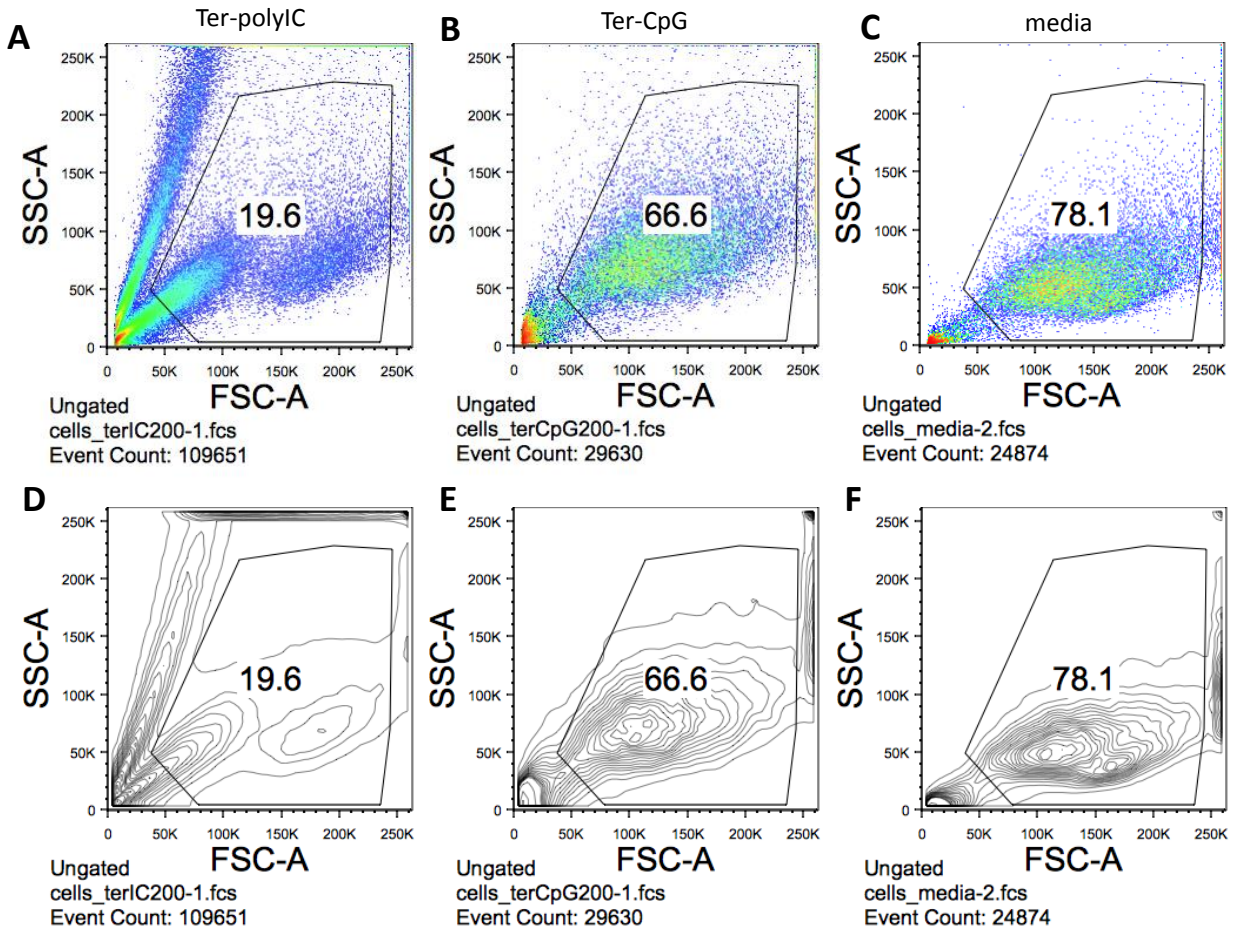

Figure S24. Flow cytometry plots of BT-20 cells pulsed with polymer blend particles and analyzed after 1 day. Cells were stained with anti-CD44-PE-Cy7, AnnexinV-Alexa Fluor 488, and 7-AAD (PerCP-Cy5.5). The plots show the forward scatter versus the side scatter of stained cells. Gates used for analysis were drawn to exclude the particle population, but to include the cell population. (A-C) Pseudocolor dot plots, and (D-F) contour plots of cells incubated with Ter-polyIC (left), Ter-CpG (middle), and media (right). Particle concentrations were prepared at 200 µg particle/ml.

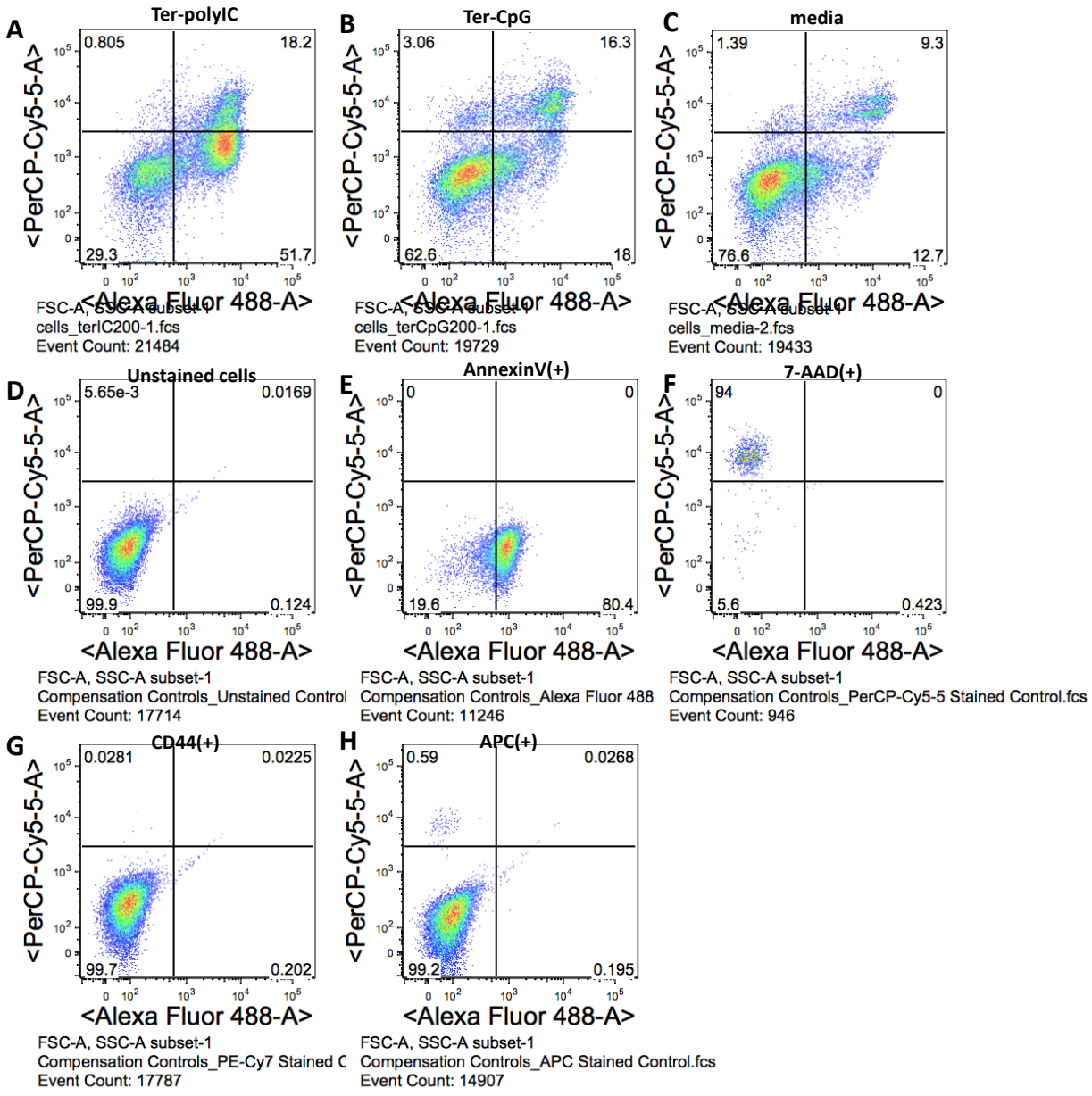

Figure S25. Flow cytometry plots of gated BT-20 cells pulsed with polymer blend particles and analyzed after 1 day. Cells were stained with anti-CD44, AnnexinV, and 7-AAD. The plots show the Alexa Fluor 488 intensity (Annexin V) versus the Per-CP-Cy5.5 intensity (7-AAD) of stained cells. Quadrant gates for (A-C) samples were drawn based on plots for (D) unstained and (E-H) single-color stained cells.

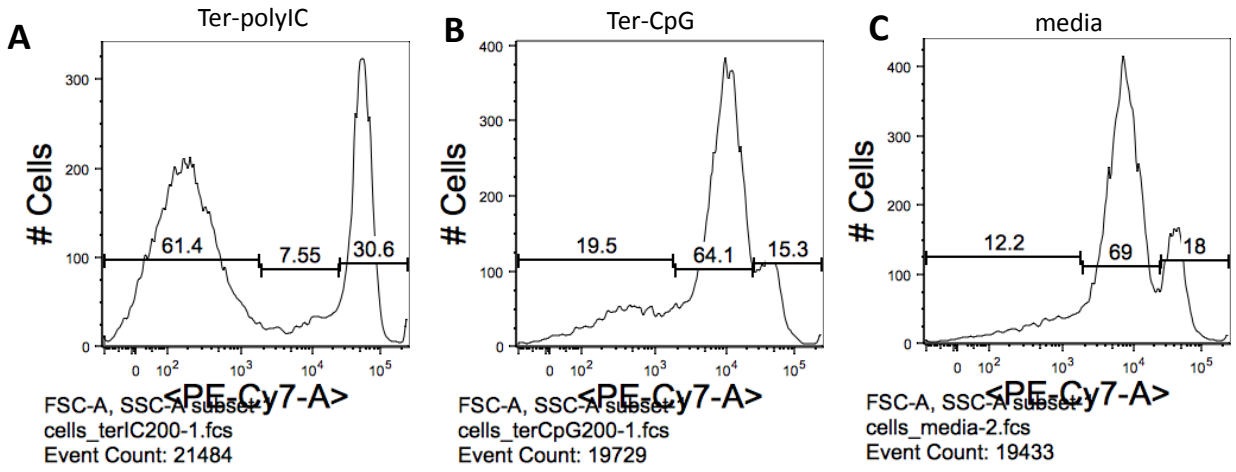

Figure S26. Flow cytometry histograms of gated BT-20 cells pulsed with polymer blend particles and analyzed after 1 day. Cells were stained with anti-CD44-PE-Cy7, AnnexinV-Alexa Fluor 488, and 7-AAD (PerCP-Cy5.5). The histograms show the PE-Cy7 intensity (CD44) distribution of the forward and side scatter subset of BT-20 cells. The three subsets drawn on the histograms were based on the three distinct peaks that represented CD44 low cells, CD44 medium cells, and CD44 high cells.

The method of analysis of live and dead BT-20 cells by flow cytometry

The gated cell population in forward scatter vs. side scatter plots (Figure S24) was plotted as AnnexinV (Alexa Fluor 488) vs. 7-AAD (PerCP-Cy5.5). Next, the boundaries for quadrant gates were determined by examining unstained and single-stained cells (Figure S25). Quadrant gates were drawn to distinguish live cells (Q1: AnnexinV(-), 7-AAD(-)) from early apoptotic cells (Q4: AnnexinV(+), 7-AAD(-)), late apoptotic cells and necrotic cells (Q3: AnnexinV(+), 7-AAD(+)). The percentages of cells in Q1 for BT-20 cells pulsed with a high concentration of Ter-GpC (Figure S27) or a low concentration of Ter-polyIC (Figure S28), and cells incubated with type I IFN (Figure S29), and media (Figure S30) suggest that the majority of cells remain viable after 1 day of treatment. Compared to cells incubated with media, the cells that underwent early apoptosis (Q4) after incubation with Ter-polyIC and type I IFN were CD44 high cells.

Cells that were late apoptotic or necrotic (Q3) were CD44 low cells. Cells which stained for only 7-AAD (Q2) were also categorized as dead cells, but their mechanism of death was not clear. Cells in Q2 should have also stained positively for AnnexinV if they stained positively for 7-AAD. Events in Q2 primarily fall into the CD44 low subpopulation, and could be shriveled cells or cell debris because they have relatively low forward scatter and low side scatter. For BT-20 cells incubated with Ter-GpC, the events in Q2 were APC-positive indicating that they contained particles (Figure S27B). In summary, the live and dead cell populations in Chapter 3 were identified as events in Q1 and events in Q2-4, respectively.

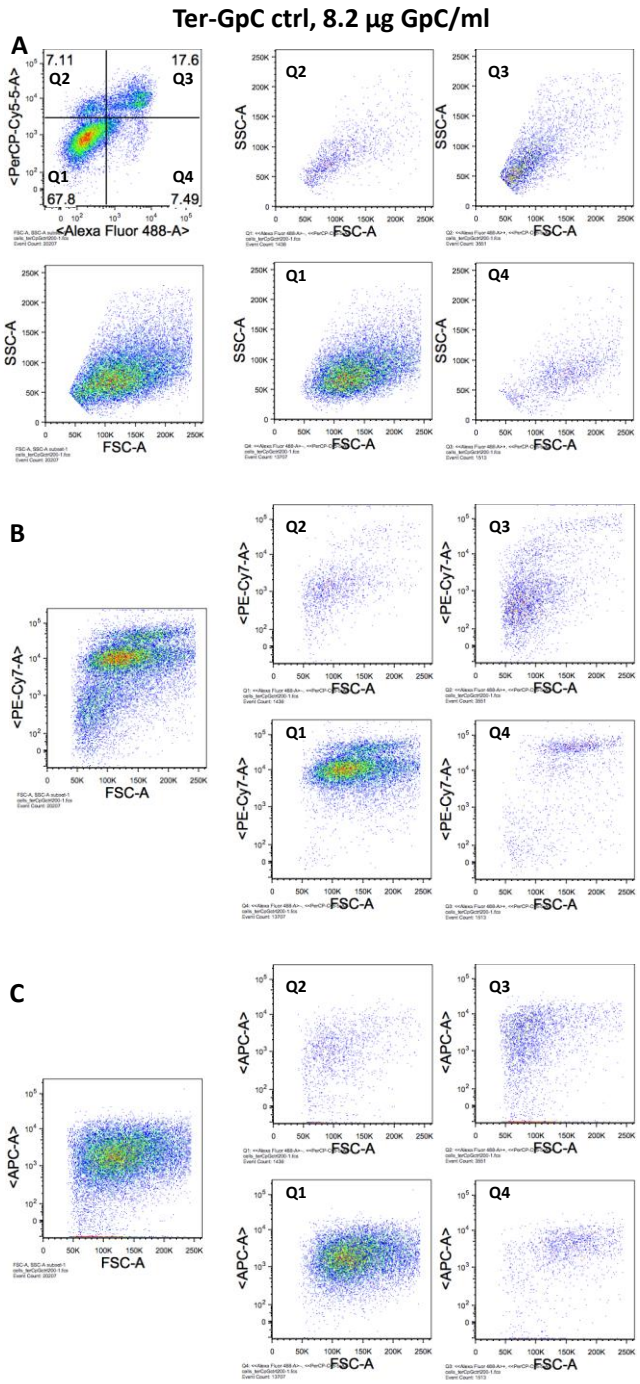

Figure S27. Flow cytometry plots of live and dead BT-20 cells pulsed with Ter-GpC and analyzed after 1 day. Cells were stained with anti-CD44-PE-Cy7, AnnexinV-Alexa Fluor 488, and 7-AAD (PerCP-Cy5.5). Panel (A) shows the quadrant gate, and the forward scatter vs. side scatter plots of cells in each quadrant. Panel (B) shows the forward scatter vs. PE-Cy7 intensity (CD44) plots of each quadrant. Panel (C) shows the forward scatter vs. APC intensity (particle fluorescence) plots of each quadrant.

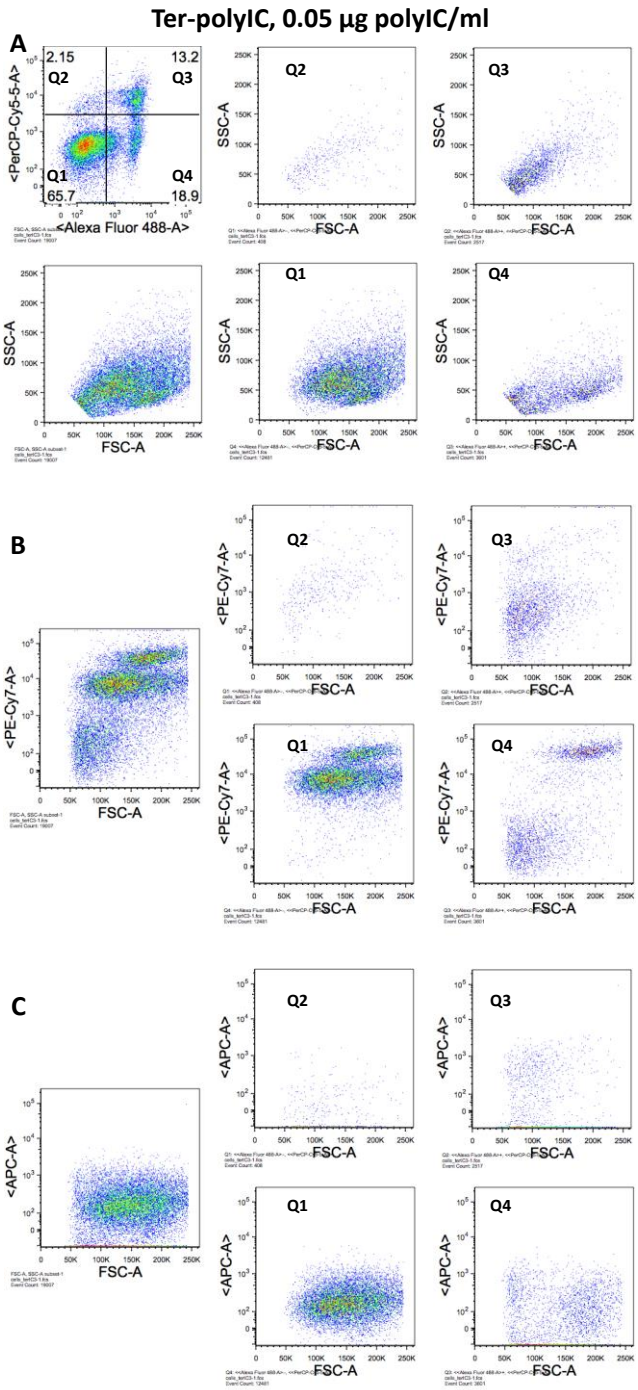

Figure S28. Flow cytometry plots of live and dead BT-20 cells pulsed with Ter-polyIC and analyzed after 1 day. Cells were stained with anti-CD44-PE-Cy7, AnnexinV-Alexa Fluor 488, and 7-AAD (PerC-Cy5.5). Panel (A) shows the quadrant gate, and the forward scatter vs. side scatter plots of cells in each quadrant. Panel (B) shows the forward scatter vs. PE-Cy7 intensity (CD44) plots of each quadrant. Panel (C) shows the forward scatter vs. APC intensity (particle fluorescence) plots of each quadrant.

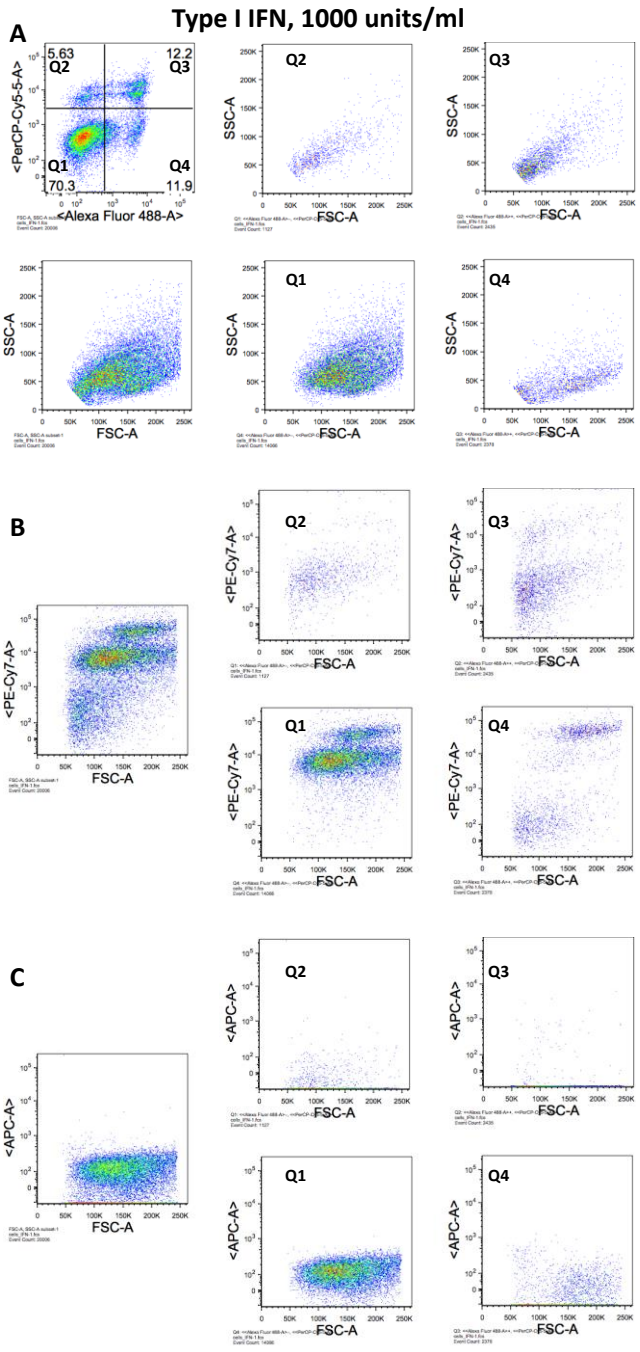

Figure S29. Flow cytometry plots of live and dead BT-20 cells incubated with type I IFN and analyzed after 1 day. Cells were stained with anti-CD44-PE-Cy7, AnnexinV-Alexa Fluor 488, and 7-AAD (PerCP-Cy5.5). Panel (A) shows the quadrant gate, and the forward scatter vs. side scatter plots of cells in each quadrant. Panel (B) shows the forward scatter vs. PE-Cy7 intensity (CD44) plots of each quadrant. Panel (C) shows the forward scatter vs. APC intensity (particle fluorescence) plots of each quadrant. The cells have a low level of APC intensity because they were not incubated with particles.

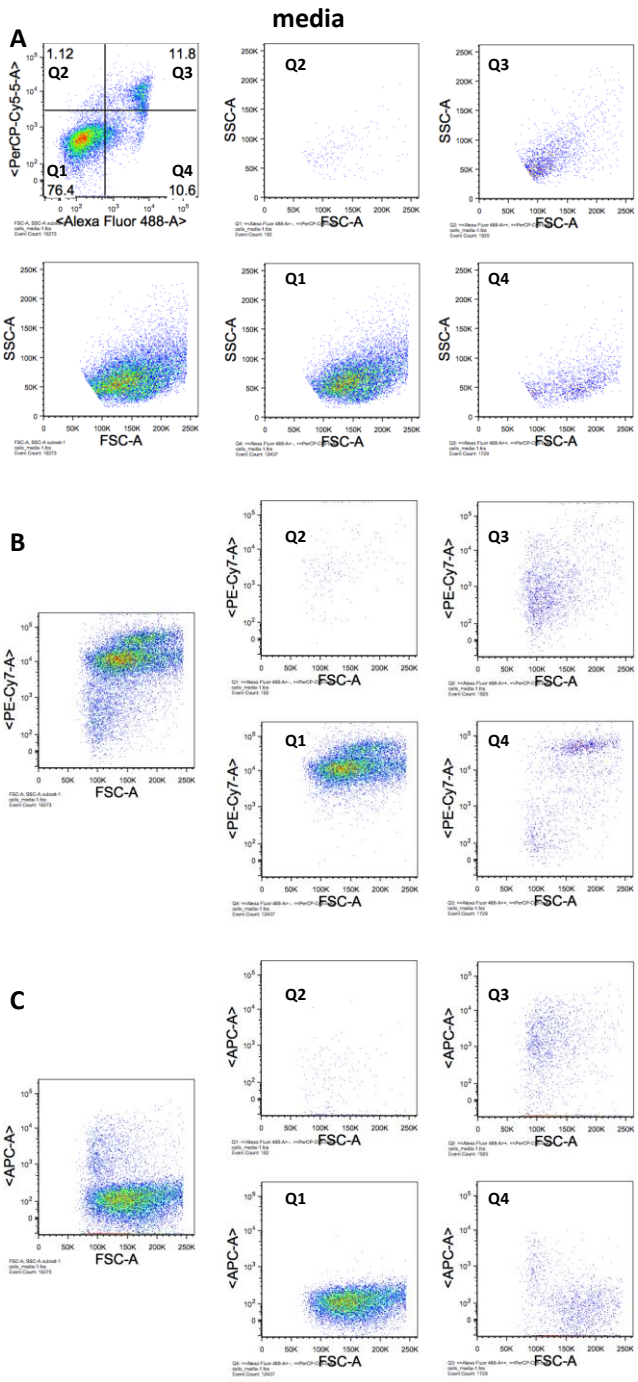

Figure S30. Flow cytometry plots of live and dead BT-20 cells incubated with cell culture medium and analyzed after 1 day. Cells were stained with anti-CD44-PE-Cy7, AnnexinV-Alexa Fluor 488, and 7-AAD (PerCP-Cy5.5). Panel (A) shows the quadrant gate, and the forward scatter vs. side scatter plots of cells in each quadrant. Panel (B) shows the forward scatter vs. PE-Cy7 intensity (CD44) plots of each quadrant. Panel (C) shows the forward scatter vs. APC intensity (particle fluorescence) plots of each quadrant. The cells have a low level of APC intensity because they were not incubated with particles.

Supplemental 11. The method of analysis of hydrodynamic size measurements of polymer blend particles by dynamic light scattering

The number size distribution profile and intensity distribution profile of polymer blend particles by DLS were first examined. Ter-adsorb polyIC low and Ter-adsorb polyIC high at pH 11 and 2.5, respectively, are used as examples. Ter-adsorb polyIC low at pH 11 was monodisperse (polydispersity index, PDI = 0.17). When a minor peak in the large size range of the intensity distribution profile (Figure 31B) did not significantly affect the peak of the number distribution profile (Figure 31A), the number average size was calculated across the entire number size distribution profile. Ter-adsorb polyIC high at pH 2.55 was polydisperse because the PDI = 0.59, and two or more peaks appeared in the intensity distribution profile (Figure 32B). In this case, the number average size was calculated by selecting the peak with the largest area in the number size distribution profile (Figure 32A). The decay of the correlation curve for Ter-adsorb polyIC high (Figure 32C) occurred slower than for Ter-adsorb polyIC low (Figure 31C). This confirmed that Ter-adsorb polyIC high was larger, likely due to aggregation as the PDI was high. The stability of the particles could also be evaluated by their surface charge. Ter-adsorb polyIC high was nearly neutral, and the surface charge of Ter-adsorb polyIC low was highly negatively charged.

Ter-adsorb polyIC low (8 ug/ml), pH 11.06

A

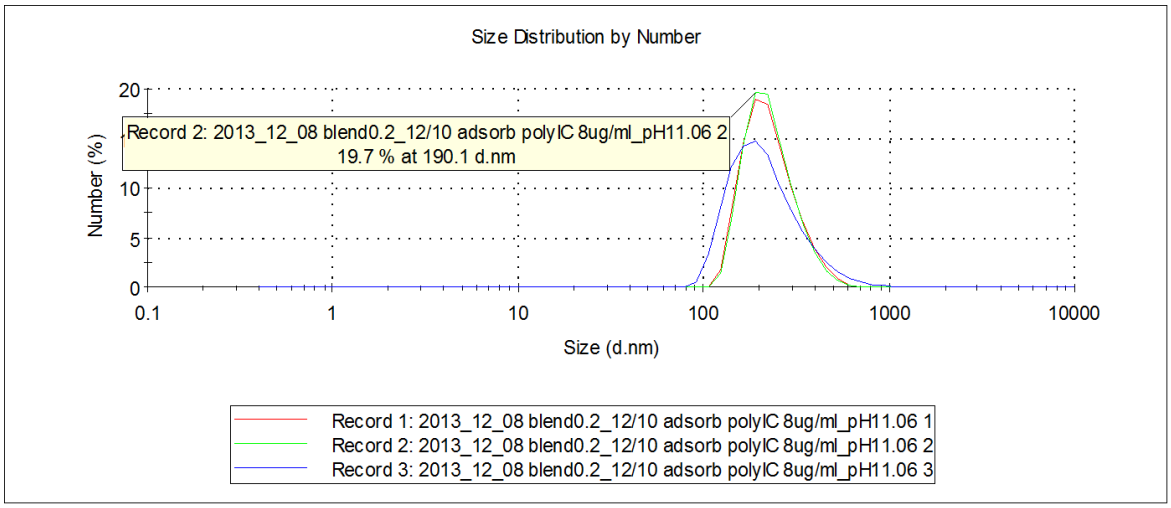

B

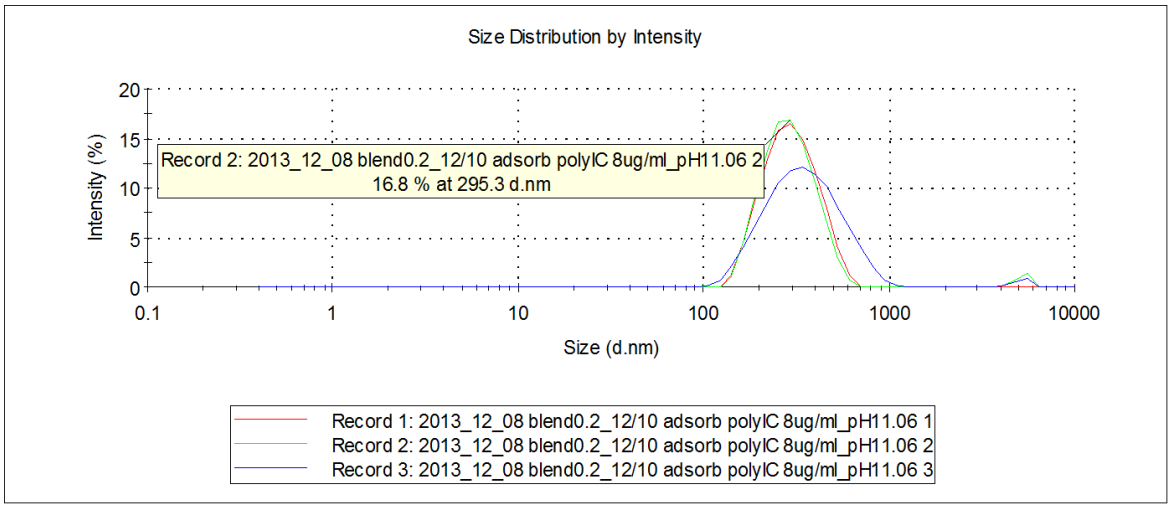

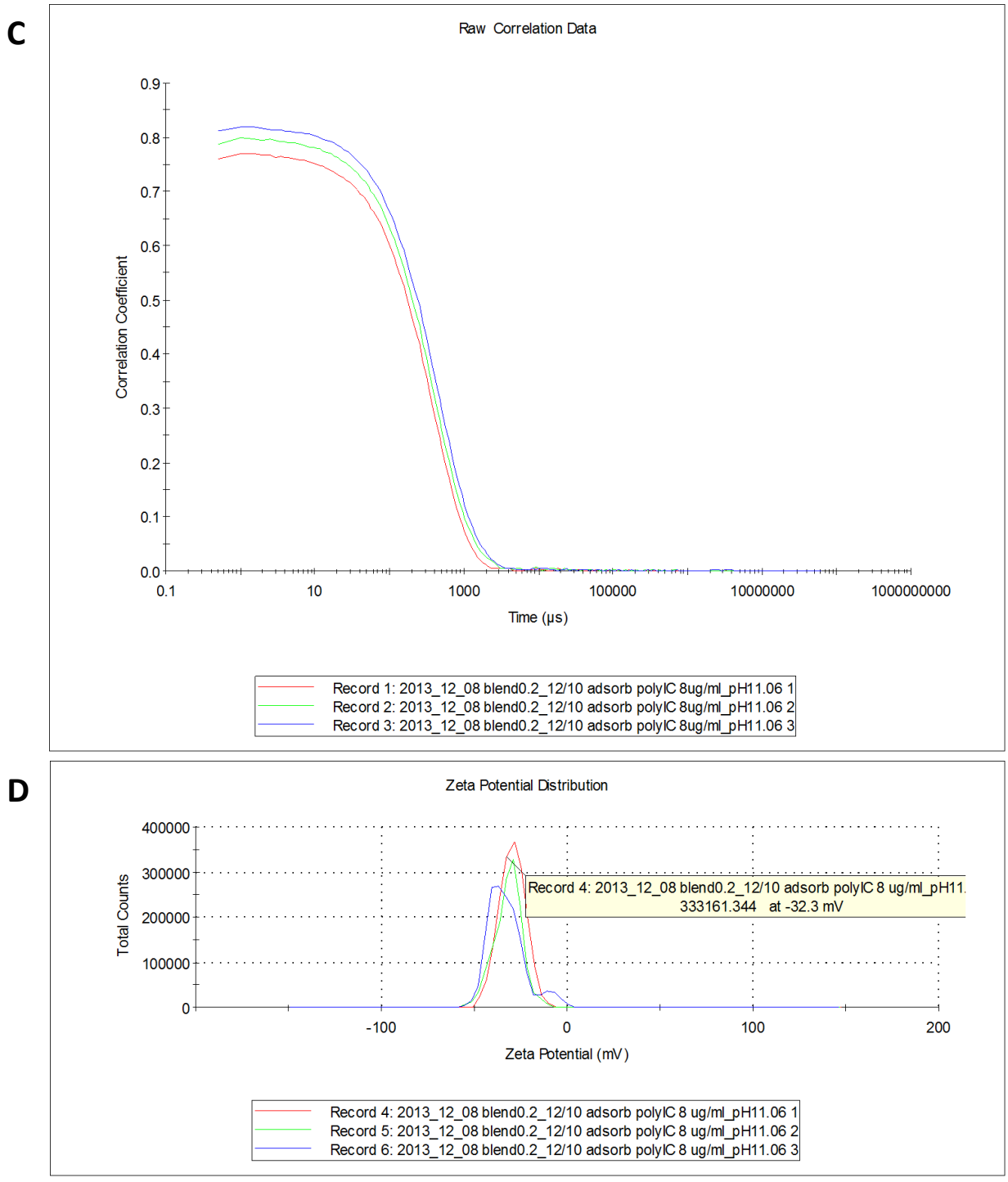

Figure S31. Hydrodynamic size and surface charge measurements of Ter-adsorb polyIC low by dynamic light scattering. The size distribution of particles by (A) number and (B) intensity of scattered light. (C) The correlogram of the sample. (D) The zeta potential distribution of the particles. Three consecutive measurements were taken in 10 mM KNO_3 at pH 11.06 at room temperature. Ter-adsorb polyIC was fabricated by incubating blank Ter particles with polyIC at 8 µg polyIC/ml. The average polydispersity index of the measurements was 0.17.

Ter-adsorb polyIC low (300 ug/ml), pH 2.55

A

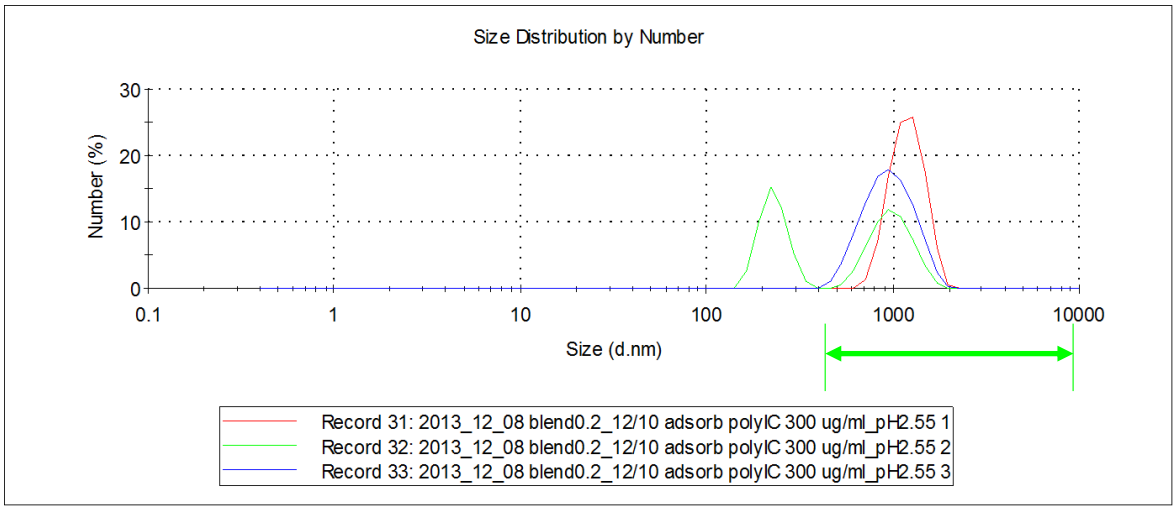

B

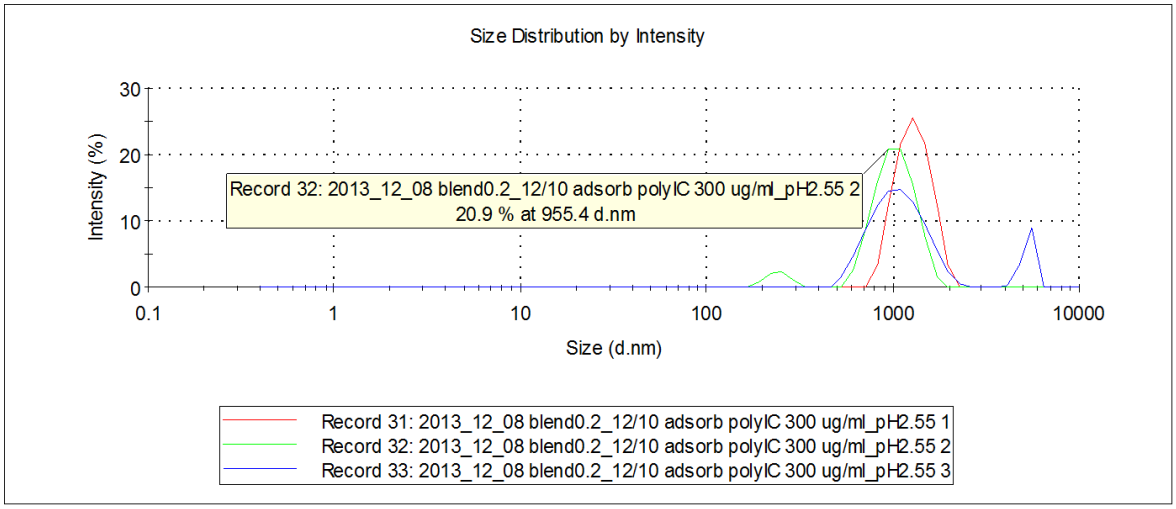

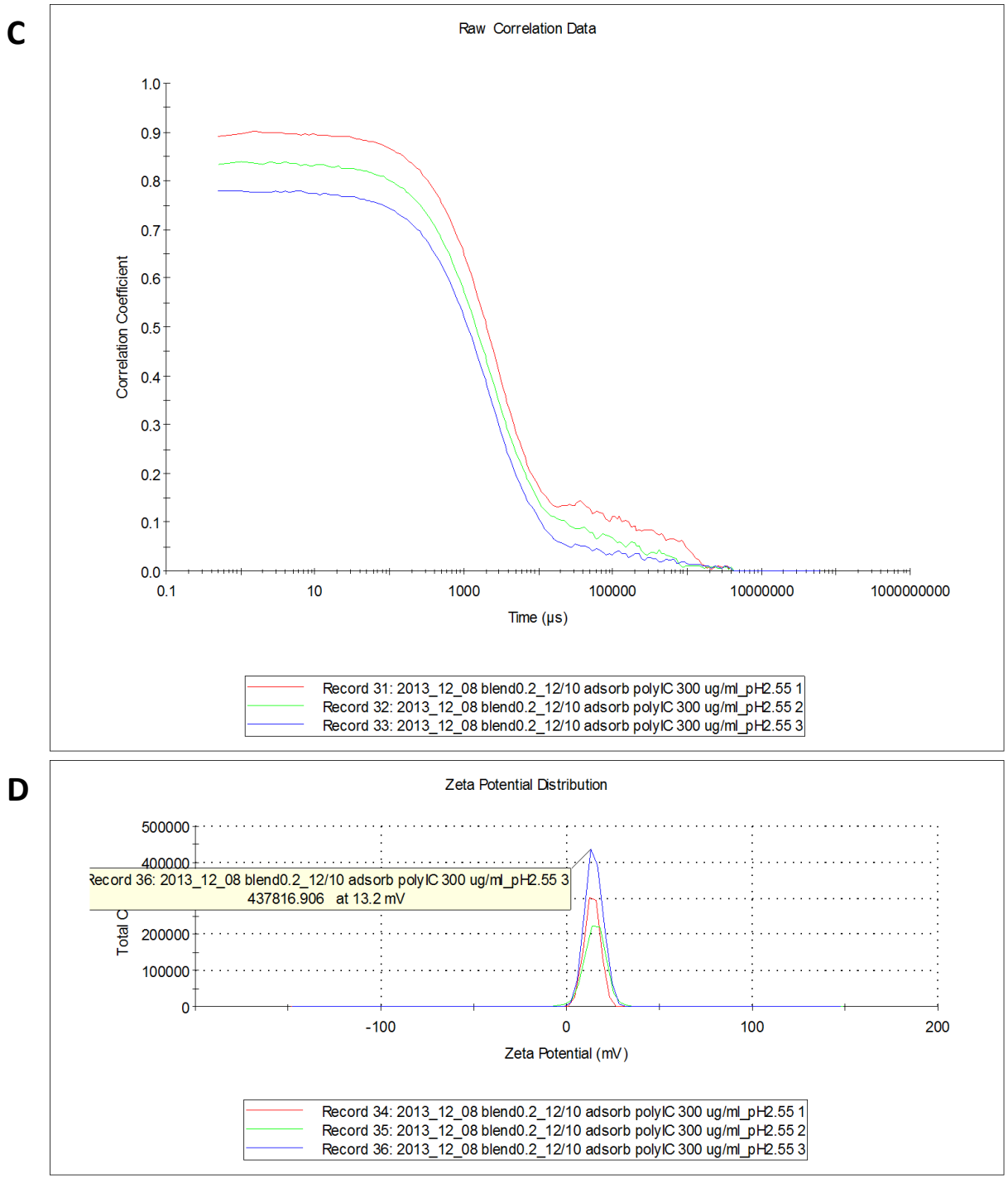

Figure S32. Hydrodynamic size and surface charge measurements of Ter-adsorb polyIC high by dynamic light scattering. The size distribution of particles by (A) number and (B) intensity of scattered light. (C) The correlogram of the sample. (D) The zeta potential distribution of the particles. Three consecutive measurements were taken in 10 mM KNO_3 at pH 2.55 at room temperature. Ter-adsorb polyIC was fabricated by incubating blank Ter particles with polyIC at 300 µg polyIC/ml. The average polydispersity index of the measurements was 0.59.

References

[1] Chinnathambi S, Chen S, Ganesan S, Hanagata N. Binding Mode of CpG Oligodeoxynucleotides to Nanoparticles Regulates Bifurcated Cytokine induction via Toll-like Receptor 9. Sci Rep-Uk. 2012;2.
[2] Kerkmann M, Costa LT, Richter C, Rothenfusser S, Battiany J, Hornung V, et al. Spontaneous formation of nucleic acid-based nanoparticles is responsible for high interferon-alpha induction by CpG-A in plasmacytoid dendritic cells. J Biol Chem. 2005;280:8086-93.
[3] Krieg AM. CpG motifs in bacterial DNA and their immune effects. Annu Rev Immunol. 2002;20:709-60.
[4] Sasai M, Linehan MM, Iwasaki A. Bifurcation of Toll-Like Receptor 9 Signaling by Adaptor Protein 3. Science. 2010;329:1530-4.
[5] Guiducci C, Ghirelli C, Marloie-Provost MA, Matray T, Coffman RL, Liu YJ, et al. PI3K is critical for the nuclear translocation of IRF-7 and type IIFN production by human plasmacytoid predendritic cells in response to TLR activation. J Exp Med. 2008;205:315-22.
[6] Lakadamyali M, Rust MJ, Zhuang XW. Ligands for clathrin-mediated endocytosis are differentially sorted into distinct populations of early endosomes. Cell. 2006;124:997-1009.
[7] Doyle SL, Jefferies CA, Feighery C, O'Neill LAJ. Signaling by Toll-like receptors 8 and 9 requires Bruton's tyrosine kinase. J Biol Chem. 2007;282:36953-60.
[8] Pan ZK, Fisher C, Li JD, Jiang Y, Huang S, Chen LY. Bacterial LPS up-regulated TLR3 expression is critical for antiviral response in human monocytes: evidence for negative regulation by CYLD. Int Immunol. 2011;23:357-64.
[9] Robinson SP, Goldstein D, Witt PL, Borden EC, Jordan VC. Inhibition of Hormone-Dependent and Independent Breast-Cancer Cell-Growth Invivo and Invitro with the Antiestrogen Toremifene and Recombinant Human Interferon-Alpha-2. Breast Cancer Res Tr. 1990;15:95-101.
[10] Beltran A, Parikh S, Liu Y, Cuevas BD, Johnson GL, Futscher BW, et al. Re-activation of a dormant tumor suppressor gene maspin by designed transcription factors. Oncogene. 2007;26:2791-8.
[11] Bernardo AR, Cosgaya JM, Aranda A, Jimenez-Lara AM. Synergy between RA and TLR3 promotes type I IFN-dependent apoptosis through upregulation of TRAIL pathway in breast cancer cells. Cell Death Dis. 2013;4.